THE UNIVERSITY OF READING

Department of Meteorology

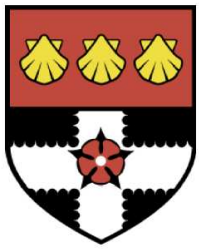

The dynamical impact of the Stratosphere on the Troposphere

Andrew James Charlton

A thesis submitted for the degree of Doctor of Philosophy

October 2003

’Declaration

I confirm that this is my own work and the use of all material from other sources has been properly and fully acknowledged’

Abstract

There has been much recent interest in the atmospheric science community about the impact of the stratosphere on the troposphere. In particular this interest has focussed on a 'mode of variability' in the atmosphere known as the Arctic Oscillation (AO). Recent analysis has suggested that predictability of the tropospheric AO may be obtained from the state of the stratospheric AO. However much of this research has been of a purely qualitative nature. In this thesis a more quantitative basis for the impact of the stratosphere on the troposphere is established.

The first part of the thesis presents a quantitative statistical analysis of a long AO dataset derived from NCEP re-analysis. A relationship between the AO in the lower stratosphere and on the 1000hPa surface on a 10-45 day time scale is revealed. The relationship accounts for $\sim 5\%$ of the variance of the 1000hPa time series and is statistically significant.

The second part of the thesis examines the response of the troposphere to changes to the stratospheric initial conditions in a state-of-the-art numerical weather prediction model. In each case two ensemble forecasts, each with 30 ensemble members, are initialised with different stratospheric initial conditions. In three different case studies the initial conditions in the stratosphere have a statistically significant impact on the tropospheric flow of up to 100-200m in 1000hPa geopotential height.

A mechanism for the impact of the stratosphere on the troposphere is proposed. Long-lived, lower stratospheric Potential Vorticity anomalies cause changes to tropospheric synoptic systems. The aggregated impact of changes to tropospheric synoptic systems maps strongly onto the North Atlantic Oscillation structure and hence onto the AO structure.

Acknowledgements

Doing a PhD at Reading has been a great working and social experience. There are lots of people that I would like to thank for making my time here so much fun.

At work my Supervisors Alan O'Neill and William Lahoz have made my PhD a really enjoyable experience. Alan has shown great enthusiasm for the project throughout and has managed to combine pushing me to my limits with looking after my welfare. William has taught me the benefit of informed criticism. I would also like to thank the members of my thesis committee Brian Hoskins and Ellie Highwood for their help and encouragement throughout. In particular Ellie has been a great friend as well as a fantastic scientific advisor. Also thanks to Anne Pinnock and Jan Fillingham who were at various times the public face of Alan and looked after me throughout. Many other people helped with various technical and scientific parts of this thesis. In particular thanks to David Stephenson, Paul Berrisford, Alexia Massacand,Tim Palmer and Mark Baldwin.

At play there have always been lots of people who have always been keen to take part in whatever madcap scheme I've dreamt up throughout my time in Reading. Firstly, I would like to thank all of my office mates Ian, Ros, Ben, Jo, Graham, Ewan, John and Cyril for making work a really fun place to be and my housemates Pete and Jen for helping me to forget about work when I go home. I'd also like to thank Dave Lawrence for teaching me how to play Basketball and Soccer, Tom Osborne for laughing at my jokes and Marc Stringer for being my longest serving (and possibly suffering) housemate and friend. Finally thanks to Laila for making the last few months very special.

This thesis is dedicated to my family who have provided support and guidance throughout my six years in Reading. To my grandparents Jim and Audrey for teaching me to love what I do and work hard. To my Dad for his truly appalling jokes which kept a smile on my face. To Helen for always keeping my feet on the ground and reminding me I'm just a sad scientist. To my Mum for being my best friend and the best person to talk to when the going was good or bad.

Contents

CHAPTER 1

Introduction

1.1 Introduction and Aims

For much of the past 30 years the accepted view of the stratosphere and troposphere could be summarised by a model of stratospheric dynamics as the “slave” to a tropospheric “master”. This model is best captured by the study of Matsuno (1971) which described stratospheric sudden warmings using a model with a fixed input of planetary waves at the lower boundary near the tropopause. While this model was extremely successful in capturing much of the dynamics of a sudden warming its implicit assumption was that a major change to the dynamical structure of the stratosphere would have no impact on the troposphere and hence the amount of upward propagating tropospheric planetary wave activity.

While a few studies during this period examined the tropospheric response to the stratospheric flow (see later review) it was not until the analysis of Baldwin and Dunkerton (1999) that the slave-master model was brought into question. Baldwin and Dunkerton used a new diagnostic of flow in the stratosphere and troposphere (The Arctic Oscillation (AO,Thompson and Wallace (1998))) to examine variability throughout the depth of the atmosphere. During stratospheric sudden warmings the state of the AO in the stratosphere undergoes large departures from its normal amplitude. The subsequent evolution of the tropospheric AO is biased towards similar departures from its mean amplitude. In this context the model of a passive stratospheric “slave” to the tropospheric “master” may no longer be valid.

The study of Baldwin and Dunkerton provoked much renewed interest in the dynamical relationship between the stratosphere and troposphere. The aim of this thesis is to further investigate the impact of the stratosphere on the troposphere using a sophisticated numerical weather prediction model and a simple statistical model. The thesis seeks to answer the following questions:

- Does the stratospheric state have an influence on the tropospheric flow ?
  - What is the quantitative size of this influence ?
  - By what dynamical mechanism does the influence occur ?
- Are medium, extended and long range[1] forecasts of the tropospheric state improved by considering the stratospheric state ?

1.2 The Stratospheric "Slave", Tropospheric "Master" Model

As mentioned in the introduction, much of the thinking about the stratosphere and troposphere over the past thirty years has been based on the numerical model of stratospheric sudden warming developed by Matsuno (1971). Stratospheric sudden warmings are rapid, major departures of the northern hemisphere stratospheric state from its climatological norm during northern hemisphere winter. A review of observational and dynamical studies of stratospheric sudden warmings can be found in O'Neill (2003).

The Matsuno model of stratospheric sudden warmings is as follows:

- Unusually large amplitudes of upward propagating planetary waves accompany poleward heat transport (Eliassen and Palm, 1961). This leads to an induced southward and westward circulation (in the traditional Eulerian mean framework) which acts to weaken the polar night jet. Eventually the westerly polar night jet becomes easterly.
- Local zonal mean zonal windspeeds which are zero or easterly form a critical layer for planetary waves (Salby, 1996). Critical layers are regions of the atmosphere over which the theory of linear, steady, conservative wave propagation breaks down. In the critical layer wave activity is absorbed.
- The absorption of wave-activity leads to an easterly acceleration below the critical layer. Eventually the zonal mean zonal windspeed beneath the critical layer will become easterly. This leads to a gradual downward progression of the critical layer toward the tropopause.

[1] In this context the standard forecast ranges are defined as, medium-range: 72-240 Hours, extended-range:10-30 days, long-range: greater than 30 days

Notice that in this model there is downward progression of a signal (ie the critical line) from the upper stratosphere to the troposphere even though the forcing of this process is upward from the troposphere to the stratosphere. This process does not involve downward transfer of information because the easterly acceleration below the critical line is dependent upon the amount of upward propagating planetary wave activity and the zonal mean state below and at the critical line (Plumb and Semeniuk, 2002). There are many examples of this process in meteorology including the Plumb (1977) mechanism for the downward descent of the QBO.

Indeed, downward propagating zonal mean zonal wind anomalies in the stratosphere have been observed in a range of different numerical models in response to time varying and time constant lower boundary forcing (Holton and Mass, 1976; Scaife and James, 2000; Christiansen, 2000).

It is clear from the large body of literature which has investigated stratospheric sudden warmings that the troposphere plays an important role in the dynamics of the stratosphere. A number of recent papers have questioned the assumption in many of the studies above that the state of the stratosphere has no impact on the future development of the troposphere. The rest of this thesis investigates this impact.

1.3 The influence of the Stratosphere on the Troposphere

1.3.1 Observational Basis

Soon after the identification of the first stratospheric warming by Scherhag (1952) there was an immediate interest in the relationship between such large dynamical changes to the stratospheric flow during the sudden warming and the tropospheric evolution.

Labitzke (1965) noted that for a particular subset of both major and minor warmings termed 'European' warmings there appeared to be a relationship with the circulation over western Europe. In particular, 10 days after the onset of the stratospheric warming a blocking pattern was set up at the end of the North Atlantic storm track. Another observational study by Quiroz (1986) found that there was a relationship between 500hPa blocking and 10hPa warming, but that blocks led warmings by an average of 3.5 days. However there was one example of a tropospheric block

lagging a stratospheric warming by 15 days.

Kodera et al. (1990) found a longer term relationship between the 1hPa zonal wind in December and the tropospheric winds in the polar region the following February, and Kodera and Chiba (1995) suggested a mechanism for this interaction using a study of the unusually large 1984/85 stratospheric warming.

These early observational studies suggested that there may be a relationship between the stratosphere and troposphere, but generally failed to determine a consistent connection between the stratosphere and troposphere because of:

- The lack of a single diagnostic which could fully represent stratospheric and tropospheric variability.
- The lack of a consistent long record dataset.

1.3.1.1 The Arctic Oscillation

During the early 1990s a series of papers developed the idea of a hemispheric scale mode of variability in the Northern Hemisphere, termed the Arctic Oscillation (AO). This mode encompassed the stratosphere and troposphere and could be used to examine coupled variability of the two systems.

Early attempts to link stratospheric and tropospheric variability in data were made by Baldwin et al. (1994) and Perlwitz and Graf (1995). Both papers used Empirical Orthogonal Function (EOF) analysis techniques on geopotential height fields. This technique aims to 'succinctly describe the joint space/time variability of the many variables in the [geopotential height] data set' (Wilks, 1995). The result of this analysis is a series of eigenvectors or maps of geopotential height. The eigenvectors have associated principal components which describe the amplitude of the eigenvectors at a particular time. The variability of the geopotential height dataset can then be reconstructed by a linear sum of the eigenvectors multiplied by their particular principal components at a given time. The principal components also have the property that their timeseries are uncorrelated.

Baldwin et al. (1994) analysed a set of National Meteorological Center geopotential height data. They showed that zonal mean zonal winds throughout the stratosphere and troposphere were correlated with the second EOF of the northern hemisphere height at 500hPa. The second EOF has a structure similar to the North Atlantic Oscillation (NAO).

Perlwitz and Graf (1995) performed Canonical Correlation Analysis (CCA) of long record 500hPa and 50hPa geopotential height time series. This technique is similar to EOF analysis but looks for patterns in two datasets which maximise the correlation between them. They showed two linked modes of variability in the stratosphere and troposphere. The first of these is a barotropic mode which takes the form of a wavenumber 1 pattern in the stratosphere and the Pacific/North American pattern in the troposphere. The second is a baroclinic mode related to the strength of the polar vortex in the stratosphere and North Atlantic variability in the troposphere.

Both these studies suggested that the large-scale variability in the stratosphere and troposphere could be linked. The two studies also linked the strength of the polar vortex with variability in the North Atlantic storm track.

Thompson and Wallace (1998) extended the use of EOF analysis of geopotential height to the longer NCEP re-analysis dataset. They also made an important change of emphasis by considering the first EOF of the surface pressure dataset. The structure of this mode has one centre of action over the Arctic and two other centres of action over the Pacific and Atlantic ocean basins. This structure is shown in Figure 1.1 (a) for geopotential height on the 1000hPa pressure surface (although this is not the same procedure as adopted by Thompson and Wallace (1998) the structure is similar). This mode was termed the Arctic Oscillation (AO) to distinguish it from the North Atlantic Oscillation (NAO) which is confined to one ocean basin. Regressions of this mode onto the height structure at other levels in the atmosphere produce similar zonally symmetric modes. Thompson and Wallace (1998) claim that this shows the presence of a deep barotropic mode throughout the atmosphere, and that the variability in the stratosphere and troposphere is linked.

Further characterisation of the structure of the AO was made in Thompson and Wallace (2000a). This was achieved by the use of both NCEP reanalysis and other datasets. In these papers Thompson and Wallace linked the first EOF of geopotential height in the Northern and Southern Hemi-

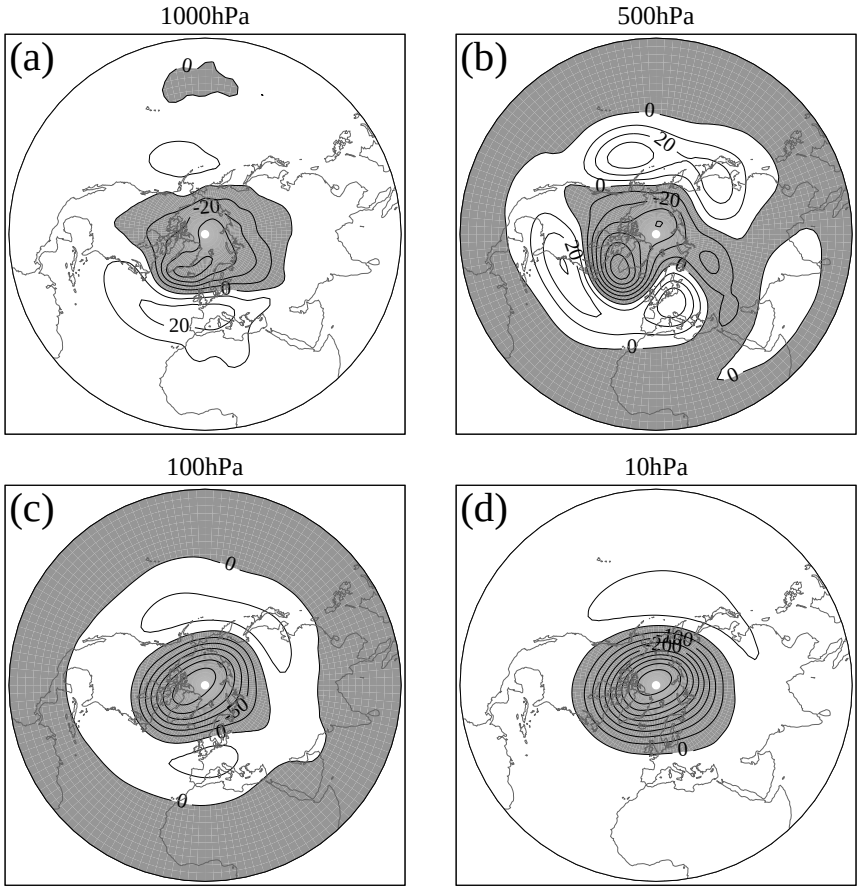

Figure 1.1: *Structure of the Arctic Oscillation reproduced from Baldwin and Dunkerton (1999). Figures show regression of geopotential height against principal components of EOF analysis. Units are metres, shading indicates negative values.(a) shows AO at 1000hPa, (b) shows AO at 500hPa, (c) shows AO at 100hPa and (d) shows AO at 10hPa.*

sphere and called these structures 'Annular Modes'. According to Thompson and Wallace the 'Annular Modes' have the following important features:

- A zonally symmetric structure with high latitude centres of action near 57.5 ° N/S in the lower troposphere, tilted to 65 ° N/S in the upper troposphere-lower stratosphere.
- A two season structure with an active season during which the AO extends in the stratosphere (Southern Hemisphere (November), Northern Hemisphere (January-March)) and an inactive season in which the mode is confined to the troposphere.
- A node line located around 45 ° N/S. This region is associated with an anomalous poleward eddy flux of westerly momentum and a region of positive temperature anomalies at the surface overlaid by negative temperature anomalies aloft.

The most important conclusion of this series of papers is that variability in the Pacific and Atlantic is linked by a hemispheric mode of variability. Some authors have doubted that variability in the two storm track regions is linked. Deser (2000) showed that the correlation between the Atlantic and Pacific centres of action of the AO is very weak. The relationship between SLP and the stratosphere is much larger in an EOF of SLP confined to the Atlantic sector than one confined to the Pacific sector. Deser concluded that the apparent zonally symmetric structure of the AO is due to the dominance of the Arctic centre of action in the variability of both the Pacific and Atlantic sectors. Ambaum et al. (2001) also showed that EOF analysis may not reveal the underlying dynamical structure of Northern hemisphere variability. They used a simple case to show that two same-signed points in an EOF need not necessarily have correlated time series, and that the Pacific and Atlantic centres of action of the AO are only weakly correlated in agreement with Deser (2000). The behaviour of the zonal mean zonal winds in the Atlantic and Pacific basins is vastly different with increasing AO index. Zonal winds in the Atlantic basin form a split tropospheric jet with increasing AO index, there is no such evidence of this in the Pacific sector. However a recent study by Branstator (2002) showed that variations in the Southern Asian waveguide act over a hemispheric scale and are reproduced in correlations of the 300hPa streamfunction with the NAO index.

There is much debate in the literature about the physical relevance of the AO diagnostic and

the links between variability in the Northern Hemisphere Pacific and Atlantic storm track regions. This question is not directly addressed in the thesis due to the wealth of literature already available on the subject. In some sections of the thesis it is assumed that the AO can be used to sufficiently diagnose hemispheric scale variability. The relevance of this mode to connections between the stratosphere and troposphere is addressed in chapter 4.

Baldwin and Dunkerton (1999) extended the analysis of Thompson and Wallace (1998) to all levels in the NCEP reanalysis dataset. The structure of the AO in the middle troposphere and stratosphere is shown in Figure 1.1. In the stratosphere (Figure 1.1 (c) and (d)) the AO has a structure related to the strength of the stratospheric polar vortex. In the middle troposphere (Figure 1.1 (b)) the AO has a more convoluted structure which is harder to interpret.

Baldwin and Dunkerton also defined an Arctic Oscillation Index (AOI). This index measures the amplitude of the Arctic Oscillation at a particular level of the atmosphere at a particular time. Analysis of the Arctic Oscillation Index showed evidence that the phase of the Index propagates from the stratosphere to the troposphere. This is shown in Figure 1.2. The large negative AO amplitudes in the stratosphere during late February 1999 are associated with a wavenumber two stratospheric sudden warming. The AO in the troposphere appears to be biased toward negative values for up to 60 days following the event. However it is also important to note that a similar period of negative stratospheric AO amplitude in December and January does not appear to have a relationship with the troposphere.

Baldwin and Dunkerton (2001) formed composites of the largest amplitude AO events in their dataset. Extreme events are defined in the 10hPa AO index as those which have less than -3.0 AO index for weak vortex composites and greater than +1.5 AO index for strong vortex composites. The two composites are shown in Figure 1.3. The structures of the weak and strong vortex composites are similar. Large magnitude AO index values in the stratosphere are preceded by the same sign AO index values in the troposphere approximately 10 days before the peak of the event. Large magnitude AO index values persist in the middle stratosphere for around 40 days and in the lower stratosphere for around 60 days. During this period the tropospheric AO index has the same sign as the stratospheric part of the AO amplitude but much larger variability in time. The composite structure confirms the suggestion in Baldwin and Dunkerton (1999) that large anomalies in the AO index in the stratosphere precede persistent AO anomalies of the same sign in the

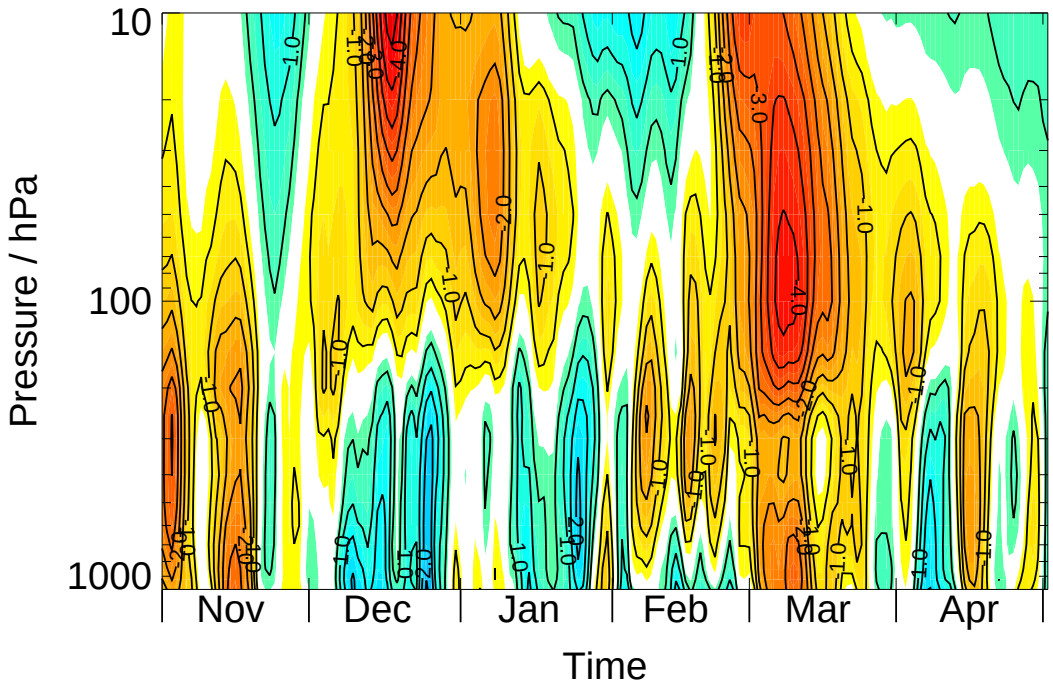

Figure 1.2: *AO Index for Northern Hemisphere 1998/1999. Data from Mark Baldwin. Blue colours show positive values of AO Index and indicate undisturbed zonal flow. Red colours show negative values of AO Index and indicate disturbed zonal flow. Values of AO index greater than -0.5 and less than 0.5 are not shaded.*

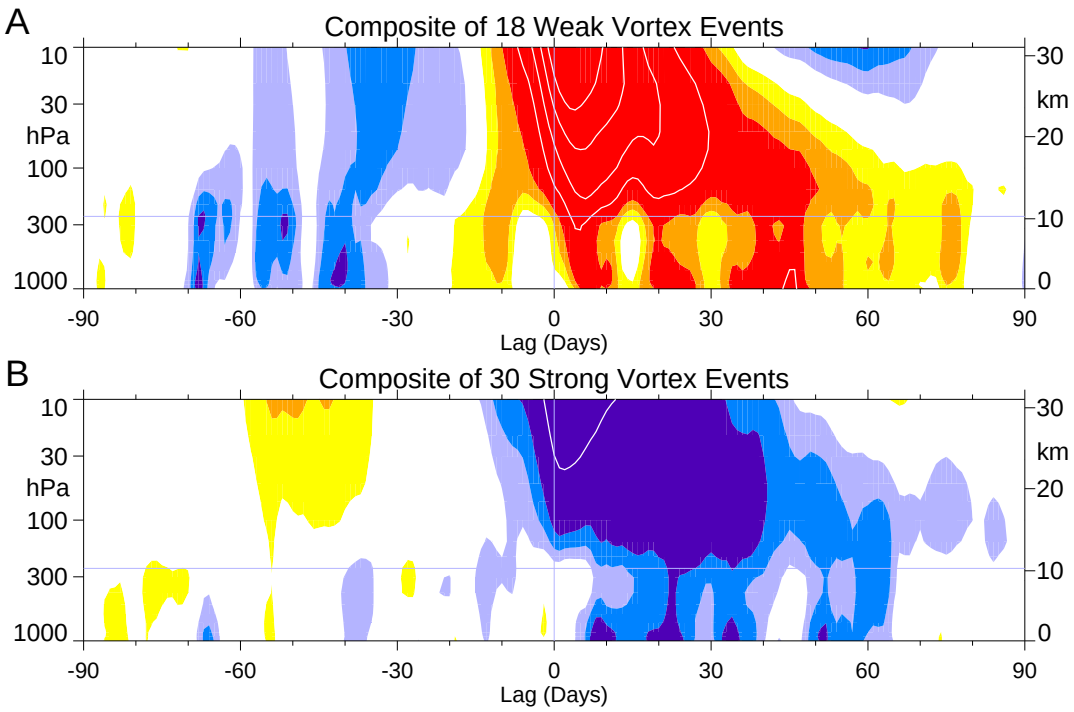

Figure 1.3: *Composite of AO amplitude for (a)18 weak vortex events and (b)30 strong vortex events. Figure taken from Baldwin and Dunkerton (2001) provided by Annular Mode website at http://horizon.atmos.colostate.edu/ao. Red colours show negative values of AO index, Blue colours show positive values of AO index. Contour interval is 0.25 for the shading and 0.5 for the white contours. Values between -0.25 and 0.25 are unshaded.*

troposphere

Gillett et al. (2001) showed that the cross correlation between the 10hPa AO index timeseries and the 1000hPa AO timeseries is significant at the 95 % confidence level when compared to an AR(1) (Wilks, 1995) noise model run as 1000 monte-carlo simulations. This showed that the connections described in Baldwin and Dunkerton (1999) have a statistical basis. The papers by Baldwin and Dunkerton suggested that some predictability of the tropospheric flow could be obtained from the stratospheric flow. This has been investigated more explicitly by a series of recent papers.

Thompson et al. (2002) examined the relationship between tropospheric temperatures and the stratospheric flow using a similar compositing techniques. Composites of surface temperature showed that surface temperature over most of the Northern Hemisphere continents is lower by up to 4 K following weak stratospheric vortex conditions compared to strong stratospheric vortex conditions. Warmer conditions occur over Greenland. This temperature pattern is associated with changes to the strength of the zonal flow over the Northern Hemisphere.

Baldwin et al. (2003a) and Charlton et al. (2003) (Chapter 2 of this thesis) further examined the statistical basis for a relationship between the AO in the stratosphere and troposphere using a simple statistical forecasting model. Both papers found that including stratospheric information in statistical forecasts of the troposphere increased the skill of those forecasts by $\sim 5\%$ for daily forecasts (Charlton et al., 2003) and $\sim 20\%$ for forecasts of the monthly mean (Baldwin et al., 2003a). These studies show that the improvement to forecasting on extended-range timescales gained by using extra, stratospheric information suggested by Thompson et al. (2002) can be seen in AO datasets.

The series of papers by Thompson and Wallace, Baldwin and Dunkerton and others identified a hemispheric mode of variability which encompassed the troposphere-stratosphere system. Moreover they used this mode to suggest that on extended-range and seasonal timescales the stratosphere could be extremely important for tropospheric prediction.

While analysis of atmospheric data suggested that the stratosphere and troposphere are connected it was not possible to determine that there is a causal relationship between the stratosphere and troposphere. It could be suggested that the apparent downward propagation of AO anomalies from the stratosphere to the troposphere is due to the different rate of evolution of tropospherically forced anomalies in the stratosphere and troposphere.

The next section describes numerical modelling experiments which measured the response of the troposphere to a prescribed stratospheric change. The significant tropospheric responses to changes to stratospheric conditions observed in these experiments suggested that the link between the stratosphere and troposphere revealed in the data analysis described above is related to a real impact of the stratospheric state on the tropospheric flow.

1.4 The influence of the Stratosphere on the Troposphere in Numerical Models

This section outlines experiments which investigated the influence of the stratosphere on the troposphere. There is a hierarchy of numerical models of the stratosphere-troposphere system which have been used to investigate this impact. The simplest of these models investigated the propagation of planetary waves in a beta-channel (Holton and Mass, 1976) and the most complicated were high horizontal resolution numerical weather prediction models. The studies described in this section are grouped according to the complexity of the numerical model used in the study.

1.4.1 Mechanistic Models

The term mechanistic models refers to a sub-set of very simple numerical models of the troposphere and stratosphere. Many of the models used in the experiments in this section are variants of the Holton and Mass model (Holton and Mass, 1976). This model is a simple representation of the interaction of the zonal-mean state with planetary wave activity. In itself the model is not suitable for the examination of the impact of the stratosphere on the troposphere, but two of the simple studies described below extend this model to include a basic troposphere.

The model is a quasi-geostrophic, beta-plane channel model. The quasi-geostrophic system neglects terms in the primitive equations which have order greater than the Rossby Number. A beta-plane channel model is a model which has limited horizontal extent in the latitudinal direction. Over this limited range a constant value for the rate of change of planetary vorticity with latitude (beta) can be assumed (Holton, 1992). The Holton and Mass model has a lower boundary at the tropopause. The troposphere is parameterised as a single zonal harmonic at the bottom boundary.

The advantage of models of the Holton and Mass type is that they are very simple and cheap to run. This means that a large number of integrations can be performed at low cost, with the goal of using these integrations to understand the basic dynamics of the real atmosphere and much larger and more complex GCMs.

Plumb and Semeniuk (2002) used a standard stratosphere-only version of the Holton and Mass with a specified tropospheric wave forcing in which the choice of parameters prevents spontaneous oscillation to investigate the downward propagation of zonal mean zonal wind anomalies. By changing the structure of the model to exclude wave-reflection and 'downward control' (Haynes et al., 1991) effects they show that much of the downward propagating signal in the stratosphere is related to the downward descent of critical lines for tropospheric planetary waves. While this study reinforced many of the previous investigations of downward vacillations in the stratosphere it did not examine the impact of these vacillations on the troposphere.

Kodera and Kuroda (2000) made changes to the Holton and Mass model to include meridional propagation of planetary waves and extend the bottom boundary of the model to the surface. Their model showed similar downward vacillations as the Holton and Mass model with constant boundary forcing. Kodera and Kuroda state that downward vacillations in the zonal wind penetrate into the troposphere and affect planetary wave activity here. However their model has a single value of static stability which makes diagnosis of the position of the tropopause difficult. The magnitude of change to the zonal wind in the model in the upper stratosphere is also 2 to 3 times the magnitude of changes to the zonal wind in the real atmosphere. This suggested that the changes to the tropospheric flow observed in this model may be somewhat unrealistic.

Eichelberger and Holton (2002) extended the Kodera and Kuroda model by placing its centre at 45N and making changes to the representation of boundary conditions. This allowed a more direct comparison of the mechanistic model with the AO. The model produced similar downward propagating signals in the second meridional mode which describes the AO variability. The timescale of this variability is around 60 days, significantly shorter than Kodera and Kuroda (2000) and on a similar time scale to that observed by Baldwin and Dunkerton (2001).

Mechanistic model studies showed that downward propagation of zonal wind (and hence AO) anomalies in the stratosphere can be reproduced by the interaction of planetary waves and the zonal flow. However it is not clear that the same mechanism can be used to explain the links between the stratosphere and troposphere in Baldwin and Dunkerton (2001). To understand the links between the stratosphere and troposphere more sophisticated numerical modelling techniques must be used.

1.4.2 General Circulation Model Studies

To understand the impact of the stratosphere on the troposphere it is necessary to use a model which includes a good representation of both the stratosphere and troposphere. This means a General Circulation Model is required. The models used in studies in this section are of varying complexity and horizontal and vertical resolution. The common link between them all is that they solve the primitive equations on a sphere. There are two ways in which experiments can be formulated to examine the relationship between the stratosphere and troposphere.

- **Model Dynamics Problem.** Make changes to the model dynamics of the stratosphere and examine the impact upon the troposphere.
- **Initial Value Problem.** Make changes to the initial conditions in the stratosphere and examine the impact upon the troposphere.

1.4.2.1 Model Dynamics Problem

Model dynamics experiments were first conceived by Boville (1984). Boville made changes to the hyper-diffusion parameterisation in the stratosphere of a simple 9 level GCM. Changes to the diffusion parameterisation had impacts on the mean circulation of troposphere. In a subsequent paper Boville and Cheng (1988) showed that there was similar tropospheric sensitivity to the height of the model lid and the Rayleigh friction parameterisation in a more sophisticated 26 level GCM.

Recently, similar experiments have been conducted with more sophisticated GCMs. Norton (2003) used the Met Office Unified Model to run a series of experiments in which the damping in the stratosphere was increased. This was achieved by increasing the amount of Rayleigh friction in the stratosphere in a similar way to Boville and Cheng (1988). The run with increased Rayleigh friction has a stratospheric state with a permanently warmed polar vortex and much reduced intra-seasonal variability. The changes to the Rayleigh friction parameterisation produced a change to the tropospheric flow which have a structure very similar to the AO.

Polvani and Kushner (2002) produced similar changes to the tropospheric flow in a simple

GCM by making changes to the horizontal gradient of the equilibrium temperature profile in the stratosphere. Weakening the equilibrium temperature profile results in a weaker polar night jet. Changes to the stratospheric polar night jet resulted in changes to the position and intensity of the tropospheric jet. When the polar night jet was strong the tropospheric jet is strengthened and moved further poleward.

These papers showed that making a change to the time-mean stratospheric flow has an impact on the time-mean flow in the troposphere. There are two deficiencies of this approach. Firstly changes made to the stratosphere flow result in an unrealistic stratospheric flow compared to current climatology. This means that while model dynamics experiments show that changes to the stratosphere can influence the troposphere their relevance to the real atmosphere is limited. The stratosphere would never achieve the unrealistic states imposed in model dynamics experiments. Secondly these experiments examine the time mean response of the troposphere to imposed stratospheric changes. This has limited application for forecasting, where the transient response of the troposphere to an imposed stratospheric change is required. Model dynamics experiments are more suited to studies of the response of the troposphere to changes of the stratosphere under climate change (Hartmann et al., 2000).

1.4.2.2 Initial Value Problems

The transient response of the troposphere to an imposed stratospheric change is best examined with initial condition experiments. There have been somewhat fewer of these studies over the past twenty years. Boville and Baumhefner (1990) investigated the growth of tropospheric forecast errors with two different GCMs, one of which had a lower top at 10hPa. Error growth in the troposphere was slightly greater in the model with the low top, suggesting that the better representation of the stratosphere in the control model contributed to an increase in tropospheric predictive skill. Hamilton (1993) suggested that there was increased tropospheric predictability after stratospheric sudden warmings.

The experiments in chapter 3 and 4 of this thesis are most closely related to the study of Kodera et al. (1991). Kodera et al. examined the changes to the tropospheric evolution when changes were made to the initial conditions in the stratosphere. Two runs of the same GCM were compared.

The first, control run had a strong polar vortex in the initial conditions. The second, perturbed run had the same tropospheric initial conditions as the control run but a weak stratospheric vortex in the stratospheric initial conditions. Differences in the tropospheric flow between the control and perturbed runs showed the influence of the stratospheric initial conditions on the troposphere. Kodera et al. showed that the the stratosphere has an influence on the tropospheric zonal flow over timescales of 16-45 days. The size of this influence is $\sim 15ms^{-1}$.

There are a limited number of studies which have investigated the transient respond of the troposphere to imposed stratospheric changes. Chapter 3 and 4 of this thesis will attempt to use a similar methodology to the one used by Kodera et al. (1991) to further investigate this problem and its relevance to medium and extended-range weather forecasts.

1.4.3 Regime Studies

Further to the direct examination of the impact of the stratosphere on the troposphere described above two other studies have examined the coupled relationship between the stratosphere and troposphere in differing regimes of planetary wave activity in a simple GCM. While these studies do not directly examine the impact of the stratosphere on the troposphere their conclusions have some bearing on this issue.

Taguchi et al. (2001) performed a parameter sweep experiment with a simple GCM. The model's temperature response was limited to a Newtonian heating and cooling scheme and all moist processes were excluded. 110, 1000 day integrations of the model were performed, the only difference to each run being the height of a sinusoidal surface topography. This has the effect of altering the amount of planetary wave activity in the system. Four distinct flow regimes are identified.

1. Linear Wave propagation, Strong Polar Vortex
2. Quasi-Linear Wave propagation, small undulations in Vortex Strength
3. Non-Linear Wave propagation, intermittent breakdowns of the polar vortex.
4. Weak or permanently warmed state of the vortex.

Lag correlation analysis of zonal mean zonal wind and temperatures in the model showed that the correlation between stratospheric and tropospheric fields increased as the amount of planetary wave activity increased. A 'downward propagating' structure to the signal is only present in regimes 3 and 4.

Taguchi et al. also emphasised the presence of two different timescales over which anomalies descended through the stratosphere into the upper troposphere. The first timescale was associated with individual stratospheric sudden warming events, and took up to 10 days to propagate from the upper stratosphere to the upper troposphere. The second timescale was slower and related to the propensity of the atmosphere to have stratospheric sudden warmings. This propagation could take over 60 days to move between the upper stratosphere and upper troposphere and is similar to the vacillation cycles in a number of mechanistic model studies (eg Kodera and Kuroda (2000)).

Extension of this work to examine Annular Mode behaviour was described by Taguchi and Yoden (2002). They found that the annularity of tropospheric flow and its relation to the stratosphere is highly dependent upon the regime as described above. In regimes 2 and 3 (quasi-linear wave propagation and non-linear wave propagation) the tropospheric flow shows evidence of a wave one structure. Only in the non-linear wave propagation regime was there any significant evidence of a relationship between the stratosphere and troposphere. The timescale for downward propagation of zonal wind anomalies to the lower troposphere was around 10-30 days.

These studies suggested that the relationship between the stratosphere and troposphere is highly dependent on the amount of planetary wave activity present in the model. This reinforces the point made by Baldwin and Dunkerton (2001) that connections between the stratosphere and troposphere may be associated with large magnitude changes to the stratospheric polar vortex. These changes would be unlikely to occur in the low planetary wave activity regimes in Taguchi et al. (2001).

1.5 Mechanisms for the impact of the stratosphere on the troposphere

Although there is a large body of literature which suggests that the stratospheric state has an impact on the troposphere, there is little agreement in the literature about the mechanism for this link. Mechanisms proposed to explain the impact of the stratosphere on the troposphere can be broadly divided into three categories.

1. **Reflection of Tropospheric planetary waves in the Stratosphere**

   One proposed theory for the influence of the stratosphere on the troposphere is that the stratosphere can form reflecting surfaces for tropospheric planetary waves which are then directed back toward the troposphere and interfere with planetary wave activity there.

   Perlwitz and Harnik (2003) discussed the possibility that reflecting surfaces for planetary waves can form in the northern hemisphere stratosphere. The reflection of planetary wave activity back into the troposphere would change the tropospheric flow substantially. Perlwitz and Harnik showed evidence that a reflecting surface for tropospheric planetary waves forms in the upper stratosphere during some winters and that associated with this a waveguide for planetary waves in the middle and lower stratosphere channels this wave activity to the high latitude troposphere.

   One of the problems of this mechanism is that although Perlwitz and Harnik (2003) present evidence that there is some reflection of waves in the stratosphere back toward the troposphere, the quantitative size of the impact of these reflected waves in the troposphere is unclear. Also, current studies of this mechanism have only noted a correlation between a reflecting zonal mean zonal wind structure and changes to the tropospheric flow. It need not be the case that the presence of a reflecting zonal mean zonal wind structure leads to significant reflection of planetary waves in the upper stratosphere or that such a reflection is the cause of the changes to the tropospheric flow.

2. **Downward descent of critical lines from the stratosphere into the troposphere**

   Many authors have attempted to understand the impact of the stratosphere on the troposphere in terms of a downward progression of critical lines similar to that of the mechanism

of Matsuno (1971). While it is clear that much of the downward progression of zonal mean zonal wind and temperature anomalies in the stratosphere can be understood in terms of this mechanism (Plumb and Semeniuk, 2002) it is not clear how this mechanism could be generalised to include an impact on the troposphere.

Zhou et al. (2002) examined a 22 year subset of NCEP/NCAR re-analysis data. They made composites of events in which there is a large temperature anomaly at 10hPa. They then compared events in which this is followed by a large temperature anomaly in the lower stratosphere (200hPa) and those in which it is not. They found that during downward propagating events there are two pulses of planetary wave activity. The first of these occurs prior to the warming event and is followed by downward descent of a critical line. This results in a positive feedback on the zonal wind and hence refractive index which allows wave activity to be refracted poleward further down in the atmosphere causing a shift in the tropospheric jets around 20 days after the peak of the warming event.

This study highlights one of the problems of this mechanism. In many cases, including the composites shown in this study, critical lines for planetary waves do not descend into the troposphere. This means that a further mechanism must be invoked to describe the way in which the descending critical line interacts with the troposphere.

3. **Balanced, hydrostatic and geostrophic adjustment of the troposphere to the stratospheric PV distribution**

   A further mechanism by which the troposphere and stratosphere can interact is the balanced geostrophic and hydrostatic adjustment of the tropospheric flow to the stratospheric PV distribution. This mechanism differs from those described above in that the balanced geostrophic and hydrostatic adjustment described here would be effectively instantaneous. A theory of the influence of the stratosphere and troposphere which invokes this mechanism must also explain why the impact of large amplitude changes to the stratospheric flow in the troposphere tends to occur some time after the peak of stratospheric event.

   Ambaum and Hoskins (2002) developed a simple dynamical theory of relationships between the stratosphere and the troposphere over the North Atlantic Sector. This theory is summarised in figure 1.4. A deeper Icelandic Low (IC) lowers the tropopause over the Icelandic region. This results in enhanced equatorward refraction of Rossby wave activity and

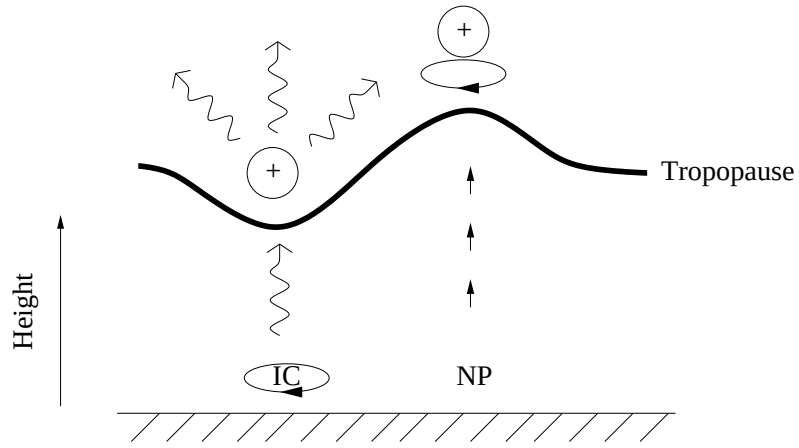

Figure 1.4: *Ambaum and Hoskins theory of NAO stratosphere-troposphere links (after Ambaum and Hoskins (2002)). See text for details.*

less wave breaking in the stratospheric jet. The strong stratospheric jet can be regarded as a positive PV anomaly in the polar lower stratosphere. This PV anomaly causes the polar tropopause to rise. This results in vortex stretching in the polar region and a consequent increase in positive vorticity over the pole and associated low pressure signal. Both Hartley et al. (1998) and Black (2002) have shown that stratospheric PV anomalies could induce differences to the tropospheric flow of similar order, using piecewise, quasi-geostrophic PV inversion techniques. Ambaum and Hoskins (2002) supported their theory both with observational evidence from the ERA-15 dataset and a simple model of the interaction between the stratosphere and troposphere. Their simple model suggests that a 1/6 change to the stratospheric Potential Vorticity causes a 1/12 change to the tropopause pressure. The typical changes to the height of the tropopause associated with this change are between 300 and 500m. Regressions of a stratospheric PV index with the height of the tropopause produce changes of similar size.

1.6 The importance of understanding the impact of the stratosphere on the troposphere.

There are two main reasons why the study of links between the stratosphere and troposphere are important.

Firstly extended-range and seasonal forecasting is currently an area of interest for many of the major numerical weather prediction centres around the world. Palmer and Anderson (1994) discussed the scientific, economic and social benefits of skillful seasonal predictions. If a connection exists between the stratosphere and troposphere and provides extra skill on extended-range and seasonal timescales then the representation of the stratosphere in seasonal forecasting models may be extremely important. The representation of the stratosphere required to simulate these effects in seasonal forecasting models cannot be determined until the coupling between the stratosphere and troposphere is fully understood.

Secondly, changes to the stratospheric flow associated with climate change may have a significant impact on the troposphere (Hartmann et al., 2000). Current observations show a negative trend in Arctic Sea Level Pressure (SLP) (Walsh et al., 1996). A similar trend toward the positive phase of the AO is reported by Thompson et al. (2000b). A trend to a particular phase of the AO would produce changes to the mean temperature of the Northern Hemisphere and affect the distribution of extreme temperature events (Thompson and Wallace, 2001). It has been suggested that these trends may be related to similar trends in the stratosphere. There has been a general downward trend in stratospheric zonal mean zonal temperatures (Shine et al., 2003) over the past twenty years which is well simulated by numerical models, either in response to imposed greenhouse gas and ozone changes or with coupled chemistry simulations. This also represents a trend toward the positive phase of the AO in the stratosphere.

If the stratosphere does have a significant impact on tropospheric climate then it would be important to understand how this impact took place. There are, however a number of other issues, not necessarily related to the impact of the stratosphere on the troposphere which remain unresolved. The future response of the stratosphere under climate change is the subject of some debate in the literature. Shindell et al. (1999) showed that in the low horizontal resolution GISS model in-

creasing greenhouse gas concentrations caused a deepening of the stratospheric polar vortex and a strengthening of the polar night jet. On the contrary many other authors (eg Gillett et al. (2003) and references therein) have shown a warming of the polar vortex under climate change associated with a large increase in tropospheric planetary wave activity. The impact of ozone depletion on the polar vortex is thought to be to cool the vortex (Kindem and Christiansen, 2001), however because of the uncertainty of future ozone changes over the arctic (Austin and Butchart, 1994) the impact of ozone changes on the future stratospheric state is also unknown.

There is also some evidence that stratospheric climate change trends do not have a significant impact on the troposphere. The link between the stratospheric and tropospheric responses to climate change is also unclear. Gillett et al. (2002) compared the response of the surface AO to doubled CO_2 conditions in a model with its top boundary at 30km and a model with a well-resolved stratosphere and a top boundary at 80km. The response of the tropospheric AO in the two models was spatially similar. There was also no evidence in the two models of a significant tropospheric response to stratospheric ozone depletion.

To understand the influence of the stratosphere on the troposphere under climate change a much better understanding of the mechanism and character of the stratospheric influence on the troposphere in the current climate is required.

1.7 Summary

There is a broad literature which covers the impact of the stratosphere on the troposphere, much of which was motivated by the original studies of Baldwin and Dunkerton and Thompson and Wallace. Current knowledge of the impact of the stratosphere on the troposphere can be summarised as

- Large-scale atmospheric variability in the stratosphere and troposphere can be characterised by the first empirical orthogonal function of geopotential height, the Arctic Oscillation (Thompson and Wallace, 1998)
- Large variations in the amplitude of stratospheric AO appear to proceed similar variations

in the tropospheric AO (Baldwin and Dunkerton, 1999) on timescales of 10-60 days.

- Composite pictures of the tropospheric flow following large departures of the stratospheric AO (Baldwin and Dunkerton, 2001) or the polar night jet (Thompson et al., 2002) from its climatological state show significant changes to a number of tropospheric parameters such as mean air temperature and the position of the mean storm track as well as the tropospheric AO.
- Numerical modelling studies which make changes to the model dynamics of the stratosphere show an equilibrium tropospheric response to the structure of the stratospheric polar vortex (Norton, 2003; Polvani and Kushner, 2002). The tropospheric change has hemispheric scale and a similar structure to the AO.
- The mechanism for the impact of the stratosphere on the troposphere is uncertain and may be different on differing timescales.

1.8 Plan of the Thesis

In this thesis we investigate the influence of the stratosphere on the troposphere with particular emphasis on the quantitative size of this link and its usefulness for tropospheric extended-range and seasonal forecasting.

A number of techniques are used to investigate the problem

- Chapter 2 looks at the links between the stratosphere and troposphere in a long AO index dataset. A statistical forecasting model is used to evaluate the improvement of skill for forecasts which use stratospheric information over those which do not.
- Chapters 3 and 4 use a medium-range numerical weather prediction model to examine the links between the stratosphere and troposphere in three case studies. Chapter 3 outlines the experimental methodology used. Chapter 4 describes the results.
- Chapter 5 uses a hemispheric Potential Vorticity inverter to diagnose the non-local geostrophic and hydrostatic adjustment of the troposphere to the stratospheric PV distribution in one of the case studies of chapter 4.

- The conclusions of the thesis are presented in chapter 6.

CHAPTER 2

Statistical Modelling

2.1 Introduction

Chapter 1 introduced the concept of a statistical relationship between the stratosphere and troposphere. Much of the previous work in this area has used descriptive statistical techniques, such as the thresholding analysis of Baldwin and Dunkerton (2001). This analysis is purely qualitative.

The purpose of this chapter is to evaluate quantitatively the relationship between the stratosphere and troposphere and its statistical robustness. The approach developed in this chapter is to examine the predictive capability of the stratosphere to forecast the troposphere in terms of the AO pattern, using multiple linear regression techniques. This should be seen as the next logical step in the level of complexity of statistical techniques applied to AO datasets.

The method differs from the thresholding methods used previously in a number of important ways. First it uses all of the data available, rather than pre-selecting only large events. Second, it also allows us to quantify the size of any potential relationship. Third it allows quantitative comparison of the size of relationships between the troposphere and itself and the stratosphere and troposphere.

This chapter is based on the paper Charlton et al. (2003) which has been published in the Quarterly Journal of the Royal Meteorological Society.

2.2 Datasets and Methodology

2.2.1 Datasets

The datasets used in the study are summarised in Table 2.1. The daily AO amplitude time series used is described in Baldwin and Dunkerton (1999). It contains the amplitude of the AO on 17 pressure levels extracted from NCAR/NCEP Re-Analysis geopotential height data between 1958 and 2000. For technical details see Baldwin and Dunkerton (1999) .

We also examine connections between the stratosphere and troposphere in other datasets. This provides a test of relationships found in the AO dataset which could be a product of the AO diagnostic. These data sets are zonal mean diagnostics traditionally used in stratospheric analysis. They consider the variability around one latitude circle and may be less representative of the variability over the northern hemisphere as a whole. If any relationship between the variables can be found in non-AO diagnostics it would suggest the relationship is robust and not a product of the AO diagnostic. These extra diagnostics were extracted from ECMWF Re-Analysis (ERA-15, Gibson et al. (1997)) and ECMWF Operational Analysis datasets held at the British Atmospheric Data Centre (BADC). Before any analysis is performed the mean annual cycle is removed from the ERA-15 datasets. This prevents the annual cycle from contaminating the results. All datasets are then standardised to have a mean of zero and standard deviation of one. This allows us to

Name	Description	Levels	Time Range	Source
AO	Daily Amplitude of AO	17	1958-2000	Baldwin and Dunkerton (1999)
$\overline{u}$	Zonal Mean Zonal Wind at 60N	17	1979-2000	ERA-15 and ECMWF Operational Analysis
Filtered $\Phi\prime$	Geopotential Height RMS error from zonal mean at 60N	17	1979-2000	ERA-15 and ECMWF Operational Analysis

Table 2.1: *Datasets used in the study*

simplify some of the equations describing the relationships between variables in the statistical model.

In this study we focus on the use of daily data. It has been suggested that the signal to noise ratio could be reduced by smoothing data in some way. In this chapter we focus on daily data as this is the simplest way of addressing the problem.

2.2.2 Methodology

To investigate the relationship between the stratospheric and tropospheric parts of the AO we construct a linear statistical model. This model attempts to quantify the effect of relationships between the stratospheric AO and the tropospheric AO and the tropospheric AO and itself. This is the next logical step from the work of Baldwin and Dunkerton. It attempts to quantitatively test ideas that are implicit in the compositing techniques employed by both Baldwin and Dunkerton (2001) and Thompson et al. (2002).

By fitting the model for a variety of lags between different time series we are able to examine the time scales on which each of these relationships is important and how large the relationships are.

The statistical model is given by:

$$y_z(t+\tau) = \beta_0(\tau)y_z(t) + \beta_1(\tau)x_z(t) + \epsilon(t) \tag{2.1}$$

where :

$y_z(t)$ - is the AO index on a pressure surface z at time t (in days)

$x_z(t)$ - is the AO index on a different pressure surface at time t

τ - is the lag

$\epsilon(t)$ - is a residual error

$\beta_0(\tau)$ and $\beta_1(\tau)$ - are parameters of the model to be determined by least squares regression and are both functions of lag.

The statistical properties of the error determine the suitability of the model to the dataset. If the model is a good fit, that is to say it is a good representation of the dataset, the residual time series should be serially independent and normally distributed. Our criteria for a good model fit do not depend on the size of the error, that is to say a model may be a 'good fit' to the data even if the error term is very large.

Fitting the model involves estimating parameters $\beta_0(\tau)$ and $\beta_1(\tau)$ of the model using ordinary least squares. Repeating this for a range of values of the lag parameter τ produces a set of model parameter estimates as a function of lag.

When using a multiple regression model with two predictors and standardised data, the autocorrelation $\rho(y_z(t+\tau), y_z(t))$ in the tropospheric time series can be decomposed into the sum of a *direct relationship* ($\beta_0(\tau)$) and an *indirect relationship* ($\rho(y_z(t), x_z(t))\ \beta_1(\tau)$). Further details of this approach are given in Junge and Stephenson (2002).

$$\rho(y_z(t+\tau), y_z(t)) = \beta_0(\tau) + \rho(y_z(t), x_z(t))\ \beta_1(\tau) \tag{2.2}$$

The series of relationships represented by the model is shown in Fig. 2.1. The "path" from the troposphere at some given time to the troposphere at some later time represents the direct relationship ($\beta_0(\tau)$). The "path" from the stratosphere to the troposphere, taking into account the mutual correlation between the stratosphere and the troposphere, represents the indirect relationship ($\rho(y_z(t), x_z(t))\ \beta_1(\tau)$).

The parameters $\beta_0(\tau)$ and $\beta_1(\tau)$ represent correlations between the time series. While correlations give no information about causality, a statistically significant correlation between a value at some time t and a value at time t+τ can be exploited for predictive purposes.

We do not suggest that this is the best method of understanding the links in the AO, since the statistical method relies on linear statistical relationships between variables. The question we are asking is: Can we apply a statistical model to AO variables to gain useful predictive skill?

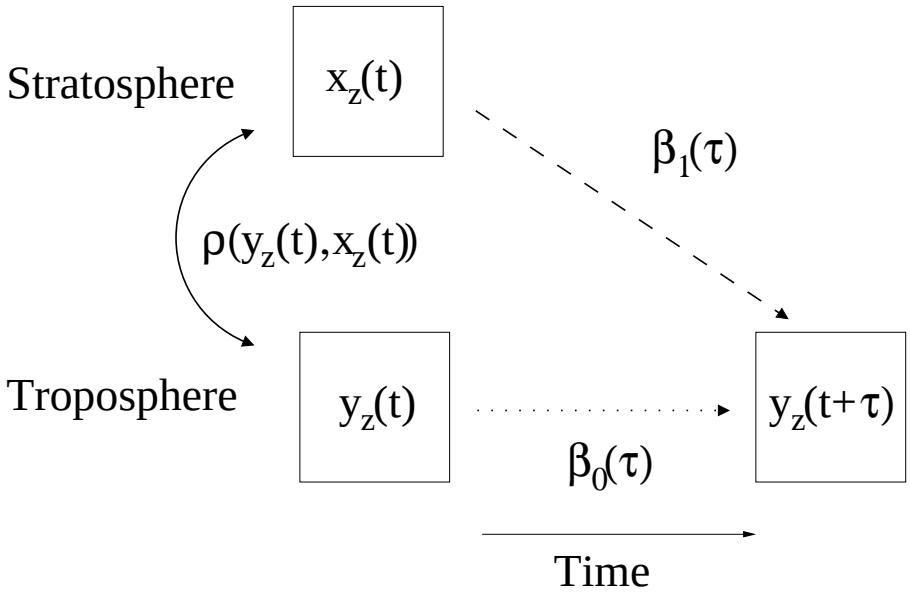

Figure 2.1: *Idealised view of regression relationships. Squares represent state of atmosphere at some time. Dotted arrow indicates direct influence of troposphere on itself, dashed arrow indicates influence of stratosphere on troposphere, solid, curved arrow indicates instantaneous correlation between troposphere and stratosphere.*

2.3 Validity of Model

2.3.1 Evidence for non-linearity of relationship between variables

Baldwin and Dunkerton use thresholding techniques to determine the relationship between the stratosphere and troposphere in the case of large amplitude stratospheric AO events. These techniques use only the end-points of the AO dataset. An issue that arises from this analysis is whether the statistical relationship between the stratosphere and troposphere is the same for small magnitude AO indices in the stratosphere as is is for the large magnitude AO indices examined by Baldwin and Dunkerton. In other words, is there a non-linear relationship between the stratosphere and the troposphere present in the data? We try to answer this question by examining scatter plots of the AO dataset.

Figure 2.2 (a) shows scatter plots of the AO amplitude at 1000hPa plotted against the AO amplitude at 70hPa. 70hPa is chosen as an illustrative level, the conclusions in this section are true for

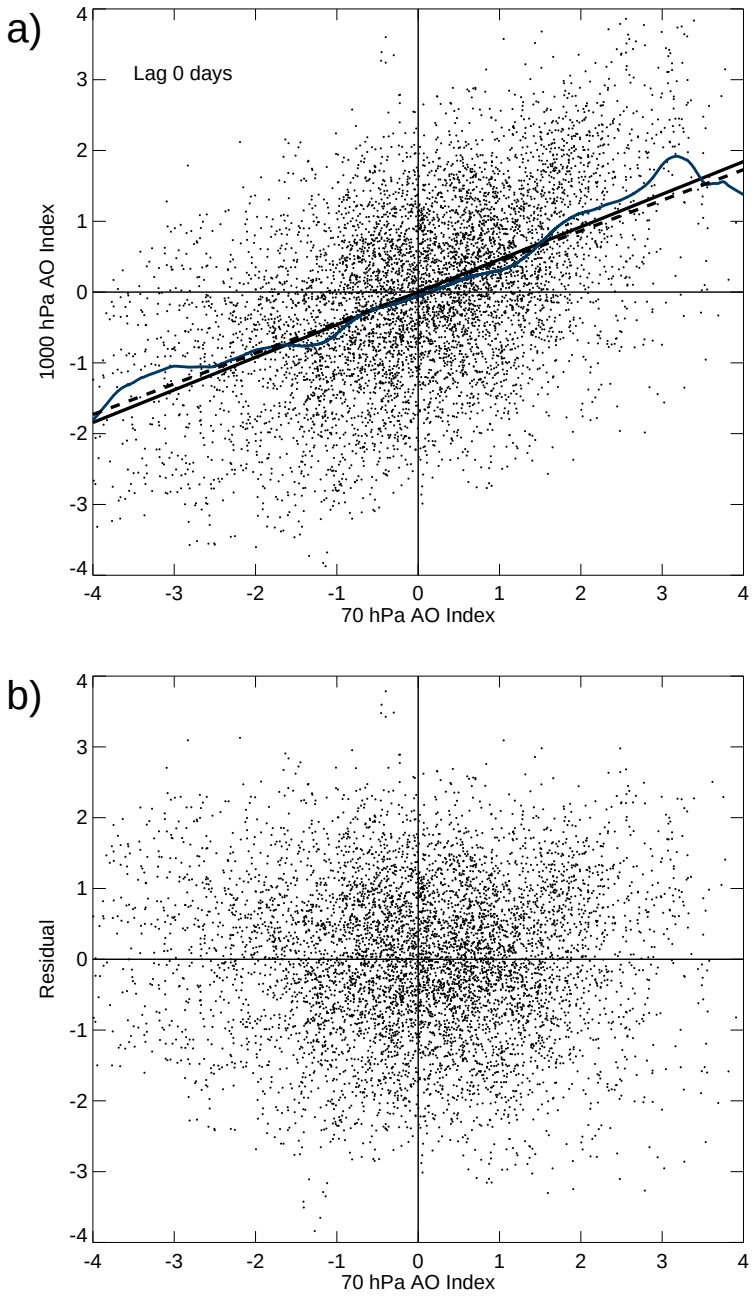

Figure 2.2: *(a) Scatter plot showing 1000hPa AO Index plotted against 70hPa AO index for lag=0 days. Solid line shows fit with all of the data. Dashed line shows fit for data with an AO amplitude of magnitude 1 or less at 70hPa. Blue line shows lowess fit to the data with width 0.5 and a triangular weighting function (b) Scatter plot showing residuals from fit with all data plotted against 70hPa AO Index.*

other levels in the upper troposphere and lower stratosphere (50hPa-250hPa)

In these plots we use only winter (NDJFM) data. The variance of the 70hPa AO in the summer months is much less than in the winter. There is also a much weaker correlation between the 70hPa and 1000hPa AO during the summer months (this is discussed in section 2.4.3). To determine if the relationship between the 70hPa and 1000hPa AO is linear we have to consider data which is not affected by this seasonal change in correlation. For this reason we only consider winter data in the following analysis.

Figure 2.2 (a) shows a general ellipsoidal shape. If the relationship between the variables were non-linear and dependent upon the value of the 70hPa AO, a scatter plot of the two variables would show a general random cloud of points in the centre of the diagram and an ellipsoidal shape at one or both ends of the distribution.

A simple test of the linearity of the relationship between the stratosphere and troposphere can be performed by making a linear fit to different parts of the data. A linear fit to all the data is shown as a solid line in Fig. 2.2. Data is then sub-sampled to include only points at 70hPa which have a magnitude less than 1 non-dimensional AO amplitude. This is shown in the dashed line. In Fig. 2.2 the slope of both of the lines is very similar. This shows that the correlation between the 70hPa and 1000hPa AO amplitude for small values of 70hPa AO is very similar to the correlation when using all of the data. This suggests that the relationship between the AO at 70hPa and 1000hPa does not depend on the amplitude of the AO at 70hPa.

An alternative technique to test for non-linearity in the relationship between the 70hPa and 1000hPa AO is to use lowess smoothing (Chambers et al., 1983). Lowess smoothing is a locally weighted regression. At each point in the dataset a linear fit is made to a subset of the data (in this case with all data $x - 0.5 \leq x \leq x + 0.5$ where x is the point in question). Points further away from the centre of the fit are given less weight. If the change to the lowess fit parameter is approximately linear then this suggests that the same relationship exists in all parts of the data

A fit to the data using this technique is shown in Fig. 2.2 (a) in the blue line. The lowess fit lies close to the linear fit to the model for most of the range of values of the AO at 70hPa (there is some evidence of non-linearity for large positive values of the 70hPa AO but this may be related to the relatively few number of data points here). This fit also suggests that the relationship between the

70hPa and 1000hPa AO does not depend on the amplitude of the AO at 70hPa.

Figure 2.2 (b) shows a scatter plot of the residuals about the linear fit to all of the data plotted against the 70hPa AO amplitude. These show little dependence on the value of the 70hPa AO. If there were a non-linear relationship between the 70hPa and 1000hPa AO then we would expect to see a dependency of these residuals on the AO amplitude at 70hPa.

2.3.2 Residual Diagnostics

It is important to establish the suitability of the statistical model to the datasets investigated. The criteria we use to judge if the model is a good fit to the dataset is that the residuals should be serially uncorrelated and normally distributed.

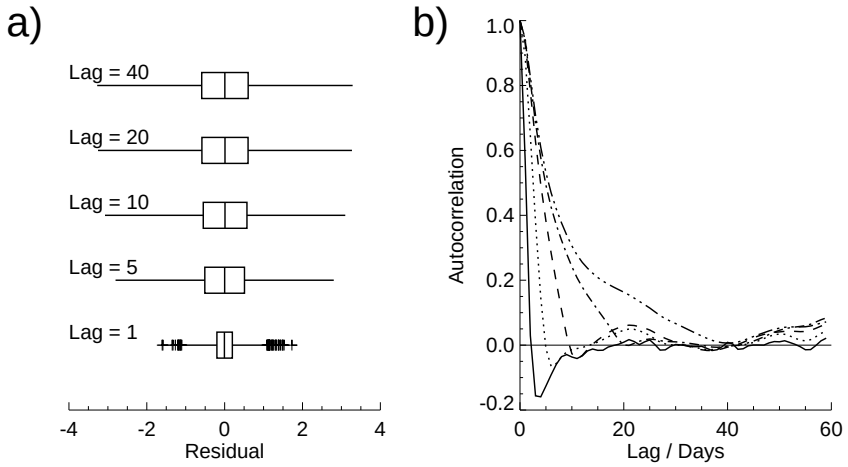

Figure 2.3: *Figures showing distribution of residuals of model fit. Panel a) shows box plots of the distribution of residuals from the same model fit. Central line of box shows median residual, outer lines of box shows upper and lower quartile. Whiskers are plotted at 1.5 times the inter-quartile range. Crosses show data points outside 1.5 times the inter-quartile range. Panel b) shows autocorrelation function of residuals when model is fitted using 1000hPa as the predictand series and 70hPa as the predictor series. Autocorrelation is shown for 1 day model lag (solid line), 5 days model lag (dotted line), 10 days model lag (dashed line), 20 days model lag (dot-dash) and 40 days lag (triple-dot dash).*

Figure 2.3 shows some diagnostics of the residuals for a fit of the model where the predictand

series, $(y_z(t+\tau))$,is the 1000hPa AO time series and the predictor series, $(x_z(t))$,is the 70hPa AO time series. Figure 2.3 (a) shows box plots for a number of different model lags between one and forty days. We define a good model to have normally distributed residuals. The box plots show that the residuals have a median value close to zero and are symmetrically distributed about this median. This indicates that there is no bias in the model and the residuals left over from the model fit are approximately Gaussian noise.

Figure 2.3 (b) shows the autocorrelation of residuals for a number of different model lags between one and forty days. A good model fit is defined as one in which the residuals are independent. In this case, the autocorrelation of residuals should decay rapidly with increasing lag. At small model lags (solid,dotted and dashed lines) this is the case; but for larger model lags (dot-dash and triple-dot dash lines) the residual autocorrelation remains large beyond 10 days. This is common in atmospheric data (Wilks (1995),section 5.2.3) and is a product of time dependence in the data used to construct the model.

Ignoring serial correlation in the data can lead to an underestimate of the variance of the sampling distribution and hence to over confidence in the significance of a hypothesis test. In order to account for the time dependence of the data when calculating the significance of the model correlations we reduce the degrees of freedom in our hypothesis test by a factor proportional to the typical time between uncorrelated points in the input dataset (Wilks (1995),section 5.2.3).

The largest autocorrelation in the AO time series is found at 10hPa. This time series has a decorrelation time of approximately 10 days. We reduce the number of degrees of freedom in all our significance testing calculations by a factor of 10 in line with this result. Although this technique is not ideal it provides a good indication of the significance of the model correlations.

The diagnostics presented in this section show that the linear model used in this chapter is a good fit to the AO dataset used in the study. The rest of the chapter assumes that the methodology described in the previous sections is adequate to investigate the relationship between the stratospheric and tropospheric datasets.

2.4 Examining connections between the lower stratosphere and lower troposphere

In the following section the model is fitted using the 1000hPa time series as the y time series in our model (see Eq. 2.1) and the 70hPa time series as the x time series in our model. We chose 70hPa to illustrate points which are generalised to include a range of levels in the Upper Troposphere Lower Stratosphere (UTLS) region (which we define here as between 50hPa and 250hPa) in Section 2.5.

Statistical testing of many of the results is conducted. This testing uses a student t-test. Results referred to as "significant at the 5 $\%$ level" refer to the test being conducted at 95 $\%$ confidence. That is to say there will be a 5 $\%$ chance of a false-positive result.

2.4.1 Whole year behaviour

The model described by Eq. 2.1 was fitted to the AO dataset (Table 2.1) for a range of lags.The parameters of the fit are shown in Fig. 2.4(a).

If the time series at 1000hPa were dependent only upon itself then we could model the AO time series at 1000hPa as an AR(1) or red-noise process (Chatfield, 1996):

$$y(t+1) = \alpha y(t) + \epsilon(t+1). \tag{2.3}$$

The autocorrelation of the time series at lag one is equal to α and is less than one for a stationary time series.

Substituting shows that, $y(t+2) = \alpha(\alpha y(t) + \epsilon(t)) + \epsilon(t+1)$.

And so in general,

$$y(t+\tau) = \alpha^{\tau} y(t) + \sum_{l=0}^{\tau} \alpha^{\tau-l} \epsilon(t+l) \tag{2.4}$$

There is an exponential decay of the autocorrelation with lag.$\rho(\tau) = e^{\tau ln\alpha}$.

Parameters from the fit of the model show that over the medium-range time scale (1-10 days lag) the decay of the autocorrelation function is near to exponential. Exponential decay of the autocorrelation with increasing lag over these time scales means the 1000hPa AO time series could be modelled as an autoregressive process. The direct relationship ($\beta_0(\tau)$,dotted line) is much larger than the indirect relationship ($\rho(y_z(t), x_z(t))\ \beta_1(\tau)$,dashed line). This suggests that only the direct relationship ($\beta_0(\tau)$) is important on 1-10 day time-scales.

On extended range (10-30 days lag) and slightly longer (30-45 days lag) time scales, the decay of the autocorrelation function (solid line) is less than exponential. This reduction of the decay rate of the autocorrelation function of the 1000hPa AO has been noted by several authors. For example Ambaum et al. (2001) referred to the reduction of the decay rate of the autocorrelation as "shouldering" and hypothesised that it was indicative of a relationship between the stratospheric and tropospheric parts of the AO.

The direct relationship ($\beta_0(\tau)$) is much smaller than the autocorrelation and is not significant at the 5 $\%$ level. The indirect relationship($\rho(y_z(t), x_z(t))\ \beta_1(\tau)$) increases in magnitude and is significant at the 5 $\%$ level. On 10-45 day time-scales the direct relationship accounts for ≤ 1 $\%$ of the variance of the 1000hPa time series. In contrast the indirect relationship accounts for $\sim 5\%$ of the variance of the 1000hPa time series. Although both the direct relationship and the indirect relationship account for very small amounts of the variance of the 1000hPa time series, the indirect relationship accounts for a larger proportion of the variance than the direct relationship. It can be inferred from these results that a significant though small statistical relationship between the AO at 70hPa and 1000hPa is seen on time scales of 10-45 days.

On much longer time scales (45-100 days lag) the autocorrelation of the 1000hPa time series becomes smaller. The indirect relationship ($\rho(y_z(t), x_z(t))\ \beta_1(\tau)$) is much reduced and is not significant at the 5 $\%$ level. The direct relationship ($\beta_0(\tau)$) accounts for most of the autocorrela-

tion of the 1000hPa dataset.

These results suggest a small statistically significant relationship between the 70hPa AO and 1000hPa AO exists on 10-45 day time scales. The autocorrelation of the 1000hPa dataset on these time scales is accounted for mainly by the indirect relationship ($\rho(y_z(t), x_z(t))\ \beta_1(\tau)$).

Attribution of the "shoulder" of the tropospheric AO autocorrelation distribution to stratosphere-troposphere coupling is consistent with the hypothesis of Ambaum and Hoskins (2002). The GCM study of Norton (2003) also suggested that the stratosphere could have an impact on the autocorrelation of the 1000hPa AO.

2.4.2 Time Order Dependence

There is a large difference in the statistical properties of the AO Amplitude at 70hPa and 1000hPa. In particular the autocorrelation of the AO at 70hPa is substantially larger than the autocorrelation of the AO at 1000hPa for the same lag. It could be suggested that the statistical relationship between the 70hPa and 1000hPa AO highlighted in section 2.4.1 is due to the difference in autocorrelation of the 70hPa and 1000hPa time series.

A simple way to test this hypothesis is to fit the model with the same 70hPa time series and a time reversed copy of the 1000hPa time series. The autocorrelation of the new reversed 1000hPa time series is identical to the normal 1000hPa time series. If the statistical relationship highlighted in section 2.4.1 is due to the difference in autocorrelation of the 70hPa and 1000hPa time series, then a fit with the 70hPa and reversed 1000hPa time series will show identical correlations as the fit with the 70hPa and normal 1000hPa time series.

The parameters of the model fit with the 70hPa AO time series and the time reversed 1000hPa AO time series are shown in Fig. 2.4(b). There is no evidence of a similar increase in the value of the indirect relationship ($\rho(y_z(t), x_z(t))\ \beta_1(\tau)$) on 10-45 day time scales as is seen in Fig. 2.4(a). Therefore it can be inferred that the small, statistical relationship between the 70hPa and 1000hPa AO amplitude on 10-45 days is a product of the particular time orientation of the 1000hPa AO time series.

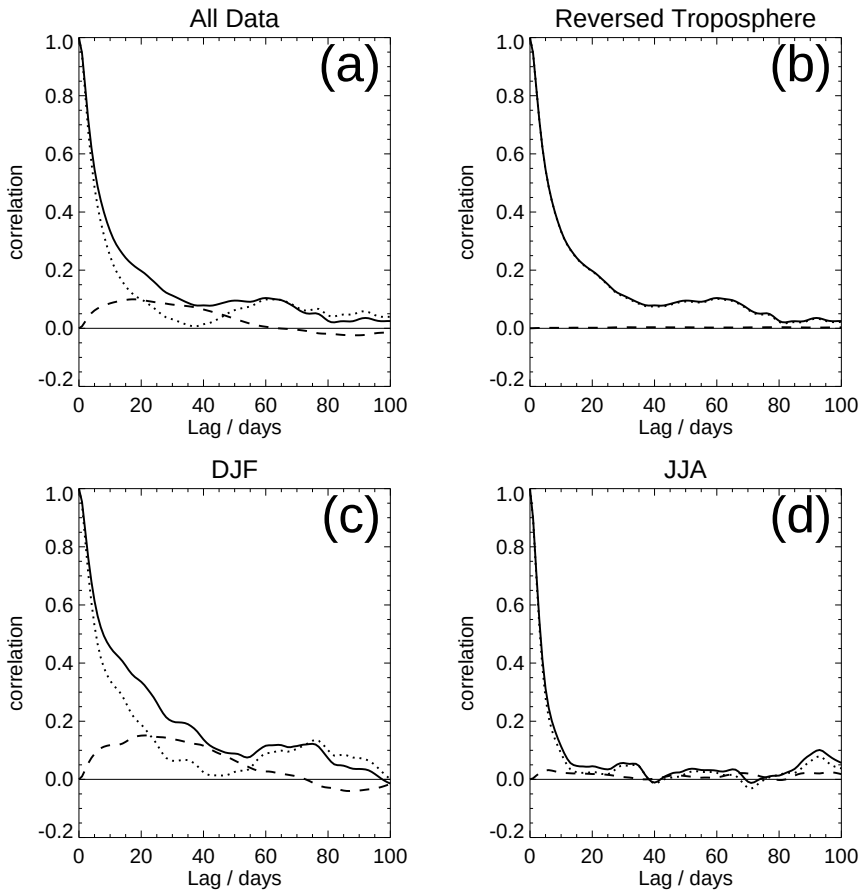

Figure 2.4: *Decomposition of autocorrelation of 1000hPa AO using the model in Eq. 1, where 70hPa is the x_z series and 1000hPa the y_z series. Autocorrelation of 1000hPa series $\rho(y_{1000}(t+\tau), y_{1000}(t))$ shown in solid line, $\beta_0(\tau)$ shown in dotted line and the product $\beta_1(\tau)\rho(y_{1000}(t), x_{70}(t))$ shown in dashed. Panel (a) shows results using all of the data, panel (b) shows results when the y_{1000} time series is reversed in time, panel (c) shows results for DJF data only and panel (d) shows results for JJA data only.*

2.4.3 Winter and summer behaviour

Baldwin and Dunkerton (1999) found that connections between the stratospheric and tropospheric parts of the AO only occur during the winter season. To quantitatively investigate this seasonal dependence the model was fitted to subsets of the AO dataset which only included winter (DJF) and summer (JJA) data. In order to keep a constant data size between fits at different lags, the data for the predictor ($x_{70}(t)$ and $y_{1000}(t)$) series included all of that particular season (eg DJF) and

the predictand ($y_{1000}(t+\tau)$) series is taken to be a slice of data of the same size displaced by the lag in question. For example the data for the DJF fit at 31 days lag would be DJF for the predictor (70hPa AO) series and JFM for the predictand (1000hPa AO) series. The model parameters are shown in Fig. 2.4(c) (DJF) and Fig. 2.4(d) (JJA) .

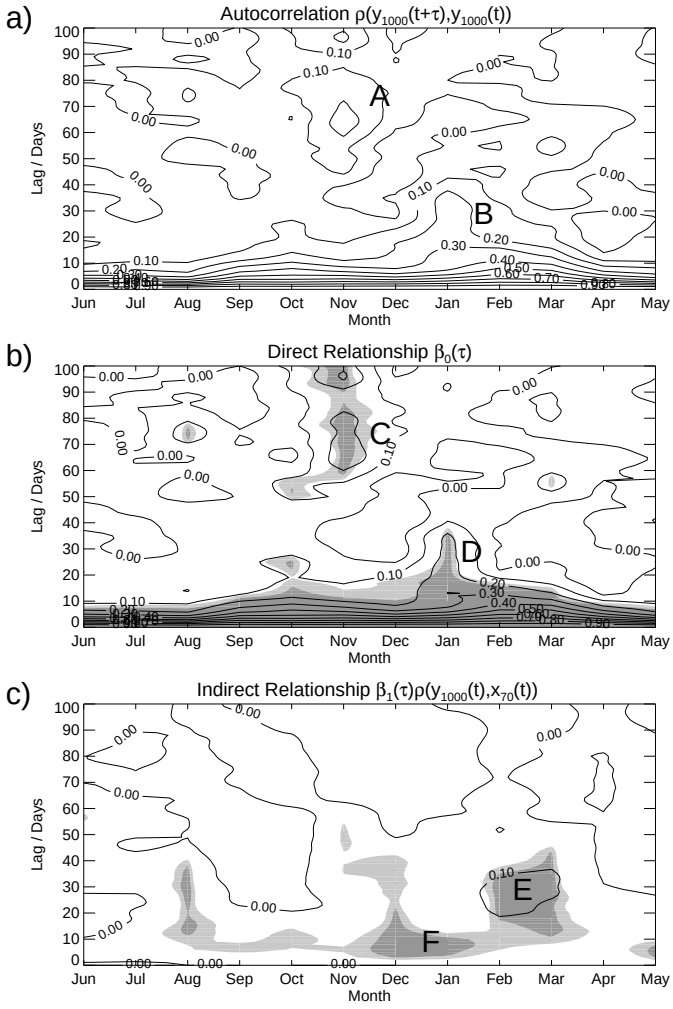

Figure 2.5: *Contour plots of decomposition of 1000hPa AO autocorrelation. a) shows autocorrelation of 1000hPa AO as a function of month and lag. b) shows direct effect ($\beta_0(\tau)$) as a function of month and lag. c) shows indirect effect ($\rho(y_{1000}(t), x_{70}(t))\ \beta_1(\tau)$) as a function of month and lag. Contour interval is 0.1. Dark shading shows correlation is significant at the 5 $\%$ level , light shading shows correlation is significant at the 10 $\%$ level. A-F mark salient features see text for details.*

In DJF (Fig. 2.4 c)) the correlation structure of the model is very similar to the model fit with

all of the data included (Fig. 2.4 a)). The DJF fit shows a peak in the indirect relationship ((($\rho(y_z(t), x_z(t))\ \beta_1(\tau)$,dotted line) over the 10-45 day range. The magnitude of the indirect relationship is larger than in the fit with all the data, suggesting that the main contribution to the relationship between the AO at 70hPa and 1000hPa is in the winter season.In contrast no such structures are seen in the JJA fit. The indirect relationship remains very small at all lags and is not significant at the 5 $\%$ level.

This confirms the suggestion that any connection between the stratosphere and troposphere is only likely to occur during the winter season. Baldwin and Dunkerton (1999) suggested that connections between the stratospheric and tropospheric parts of the AO were linked to stratospheric sudden warming events in the stratosphere. These events occur between December and March and are not present in JJA.

2.4.4 Month by Month Behaviour

A further examination of the seasonality of the relationship is shown in Fig. 2.5. In this analysis we fit the model for subsets of the AO dataset which include data from each calendar month. As in the seasonal analysis care is taken to preserve the data size for each regression.

Figure 2.5 (a) shows the autocorrelation for each calendar month plotted against lag. Figure 2.5 (b) shows the value of the direct, tropospheric correlation for each calendar month. Figure 2.5 (c) shows the indirect, stratospheric correlation for each calendar month. Shading in Fig. 2.5 (b) and (c) shows significance at the 10 $\%$ (light shading) and 5 $\%$ (dark shading) levels. It is important to remember that although the plots are shown with contours they represent 12 independent sets of 100 model fits and values between the marked months are artificial. Contouring is used as it makes the plots easier to read and interpret.

Figure 2.5 (a) shows the autocorrelation of the 1000hPa AO. In general this autocorrelation increases during the winter months. During January, February and March the autocorrelation decays slowly with lag, having values larger than 0.1 beyond 30 days lag (B).The increase in the autocorrelation of the 1000hPa AO in January (B) is attributable to the increase in the direct relationship ($\beta_0(\tau)$) seen in January (D). A similar increase in the direct relationship is not seen in February and March. The increase in autocorrelation in February and March is due to an increase in the

indirect relationship ($\rho(y_{1000}(t), x_{70}(t))\ \beta_1(\tau)$) E.

The dynamics of the stratosphere in February and March are dominated by the break up of the weakening stratospheric vortex. There is large variability in the timing of the breakup of the vortex (O'Neill, 1995). In some years the vortex breaks down in late February with an early final warming. It is plausible that the larger values of the indirect relationship (E) in February and March are associated with the timing of the final warming. A final warming involves a reversal of the jet from winter westerly values to summer easterly values. Such a wind reversal is a major dynamical event in the stratosphere and as such might have a significant effect on the lower stratospheric PV distribution and hence the evolution of the troposphere.

There is also evidence of a relationship between the 70hPa AO and the 1000hPa AO during December and January (F) but the magnitude of the correlation is much smaller and on shorter (5-10 day) time scales. On these time scales the direct effect is much larger.

Figure 2.5 (a) also shows large autocorrelation at a lag of 60 days and greater during November (A). Feature A is accounted for by the large direct relationship in November (C). This suggests that the state of the tropospheric AO in early autumn has some influence on the evolution of the AO throughout the winter.

Fitting the model to monthly sub-sets of the AO datasets shows that the relationship between 70hPa and 1000hPa identified in section 2.4.1 is confined to February and March. This might suggest that the relationship between 70hPa and 1000hPa might be linked to the timing of the final warming of the stratospheric vortex.

2.4.5 Relationship in simple diagnostics

There are many questions about the suitability of the AO to fully represent the variability of the Northern Hemisphere (see section 1.3.1.1). As a partial check of the robustness of the relationships between 70hPa and 1000hPa established in section 2.4.1 using the AO dataset we repeat the analysis using three other simple zonal mean diagnostics. A relationship between 70hPa and 1000hPa in these datasets would suggest the relationship found in the AO dataset is not a product of the AO diagnostic.

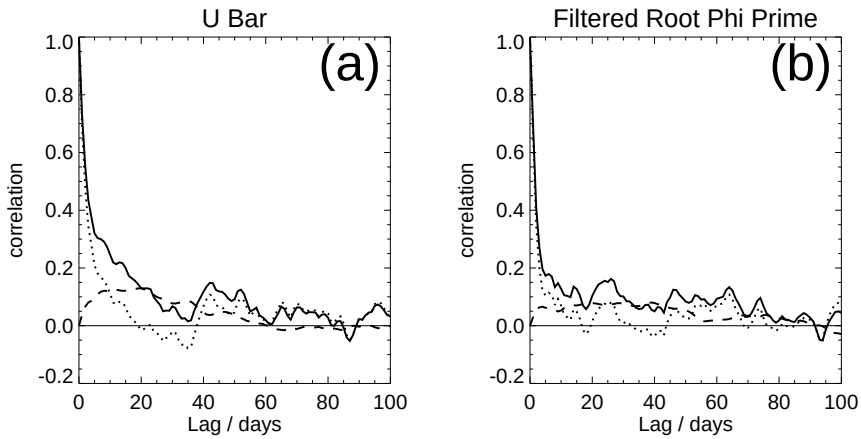

Figure 2.6: *Decomposition of autocorrelation of 1000hPa dataset as figure 2.4 but for (a) $\overline{u}$ time series at 60N and (b) filtered $\Phi\prime$ time series at 60N (right column). For more details of datasets see Table 1.*

The datasets used are outlined in Table 1. Figure 2.6(a) shows correlations from a zonal mean zonal wind dataset. Figure 2.6(b) shows correlations from a filtered Φ' dataset. This quantity is defined as follows.

$$\Phi' = \sqrt{\overline{(\Phi - \overline{\Phi})^2}} \tag{2.5}$$

Where Φ represents geopotential height and the overbar represents a zonal mean. Before calculating this diagnostic we filter the geopotential height analysis to only include zonal wavenumbers up to and including zonal wavenumber two. The stratosphere exhibits primarily low wavenumber variability and it is reasonable to expect that any relationship between the stratosphere and troposphere is likely to occur through these wavenumbers. The Φ' diagnostic would include higher zonal wavenumber variability in the troposphere which may confuse any relationship between the stratosphere and troposphere.

Parameters from the model fit using the two ERA-15 datasets are shown in Fig. 2.6. Both the $\overline{u}$ and filtered Φ' datasets have qualitatively similar correlation series to the AO data set. The indirect relationship ($\rho(y_{1000}(t), x_{70}(t))\ \beta_1(\tau)$) has larger values over the 10-45 day lag as in the

AO dataset. Over a similar time scale there is also a reduction in the size of the direct relationship ($\beta_0(\tau)$) as in the AO dataset. This indicates that the effect observed in the AO data is robust.

By fitting the same statistical model to $\overline{u}$ and filtered Φ' datasets it is possible to determine a similar connection between the lower stratosphere and troposphere without using an AO diagnostic. While the relationship in other diagnostics has a smaller correlation, its presence suggests that the relationship is robust and not a product of the AO diagnostic. Even if the AO provides the best way of revealing a link between the stratosphere and troposphere, it is not certain that this link exists exclusively through a large-scale hemispheric change to the flow. Examination of geopotential height anomaly maps at various times in the evolution of 'downward propagating events' shows a much more highly convoluted anomaly pattern than a simple hemisphere scale exchange of mass between the polar cap and sub-polar latitudes (Cash et al., 2003). This issue is discussed further in chapter 4.

2.5 Extending the Model to Other Levels

Fitting the model with 70hPa as one of the predictors suggested that a relationship between the stratosphere and troposphere may exist. An extension of this approach to other pressure levels is necessary to fully understand the nature of the relationship. This is done by fitting the model with the stratospheric predictor ($x_z(t)$) replaced by each of the other levels in the dataset. The fit parameters for different levels are shown in Fig. 2.7. The parameters for each model are plotted on the panels at the corresponding pressure. For example, a cut across Fig. 2.7 (a) at 70hPa would produce the dotted line in Fig. 2.4 (a) and a a cut across Fig. 2.7 (b) at 70hPa would produce the dashed line in Fig.2.4 (a).

Figure 2.7 (b) shows the large increase in the value of the indirect relationship ($\rho(y_{1000}(t), x_z(t))\ \beta_1(\tau)$) can be seen on 10 to 60 day time scales at the 70hPa level (B). There are similar effects on surrounding levels (50hPa-250hPa), but this increase is smaller at levels in the middle stratosphere (50hPa-10hPa) and the middle and lower troposphere (250hPa-925hPa).

The large increase in the indirect relationship is accompanied by a similar decrease in the direct relationship ($\beta_0(\tau)$) (Fig. 2.7 (a)). This reduction is largest in the same region between 50hPa

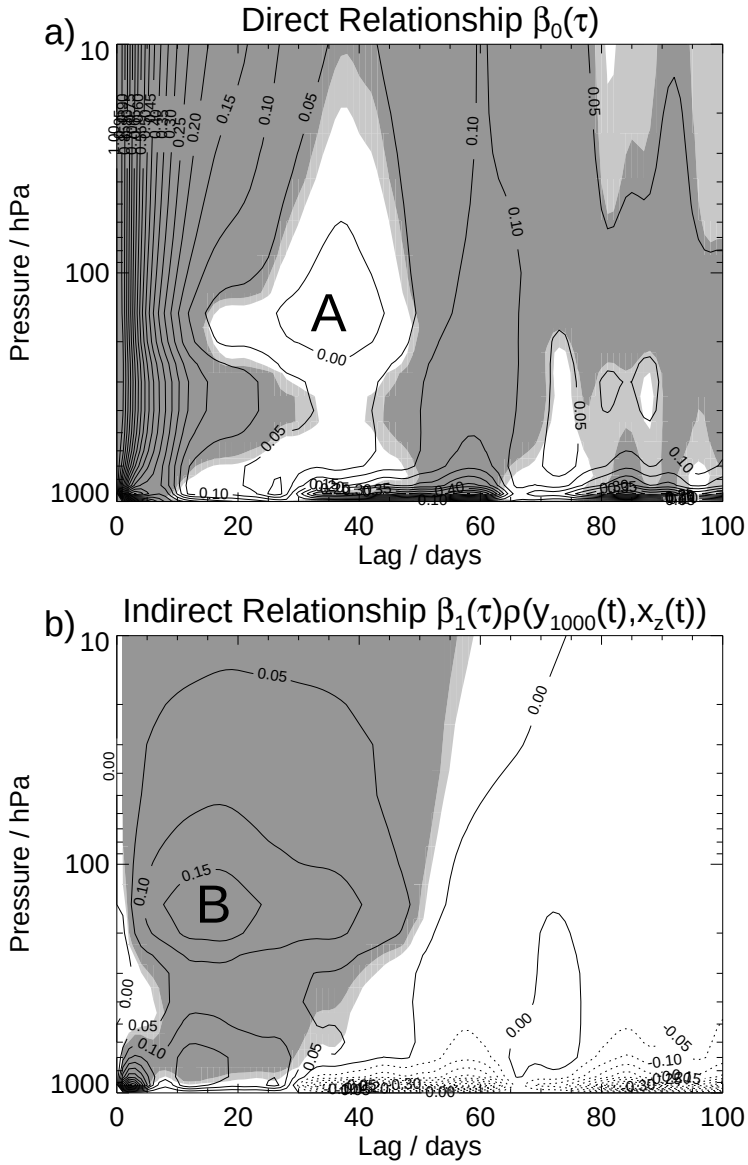

Figure 2.7: *Model parameters for various predictor levels. Panel a) shows $\beta_0(\tau)$ for fits with various levels, panel b) shows product of $\beta_1(\tau)$ and instantaneous correlation for various predictor levels. Regions where the parameters are significantly different from zero at the 5% level are shaded in dark grey, and at the 10% level are shaded in light grey. A and B mark salient features see text for details.*

and 250hPa (A), but there is a general reduction in the significance for levels into the middle stratosphere. The indirect relationship has largest magnitude on the 150hPa surface. 150hPa is in the troposphere at most latitudes. It is therefore suggested that while some predictability of the

1000hPa AO may be obtained from the UTLS region, the relationship with levels in the middle stratosphere is very weak.

It might be expected that the state of the AO near the tropopause has an impact on the surface AO; but the longer time scale (10-45 days) of this link is unexpected. The long time scale of this relationship requires further investigation in a dynamical context. The early part of this relationship (10-20 days) is investigated in chapter 4, the remainder (20-45 days) is not investigated.

2.6 Stability of Relationship

In order to assess the stability of the relationship between upper levels and the surface AO, it is necessary to investigate the relationship for different sub-periods within the data record. To do this the data was split into a series of ten year blocks and the model fitting procedure applied to each block. The model fit is made for the 1000hPa and 70hPa levels in the dataset as in section 2.4. The lag is fixed at 30 days as the largest indirect correlation is seen at this lag. Other lags were investigated and it was found that the results were robust within the region of increased indirect relationship ($\rho(y_z(t), x_z(t))\ \beta_1(\tau)$) (10-45 days).

Figure 2.8 shows the autocorrelation ($\rho(y_{1000}(t+\tau), y_{1000}(t))$), direct relationship ($\beta_0(\tau)$) and indirect relationship ($\rho(y_z(t), x_z(t))\ \beta_1(\tau)$) at 30 days lag for each decade of the data. The size of the indirect correlation is relatively constant between each decade and is of similar magnitude to the indirect relationship for the entire record. This suggests that the indirect relationship is stable throughout the data. It is also interesting that the relationship between 70hPa and 1000hPa is relatively similar between decades with significantly different variability in the stratosphere. In particular the 1990s had relatively few stratospheric sudden warmings but the relationship is still statistically significant.

The magnitude of the direct relationship ($\beta_0(\tau)$) (and therefore the autocorrelation, see Eq. 2) is extremely variable between different decades. In particular during the 1990s the direct correlation is very large at this lag. An examination at other lags (not shown) reveals that this is part of a large increase in the direct relationship between 20 and 60 days.

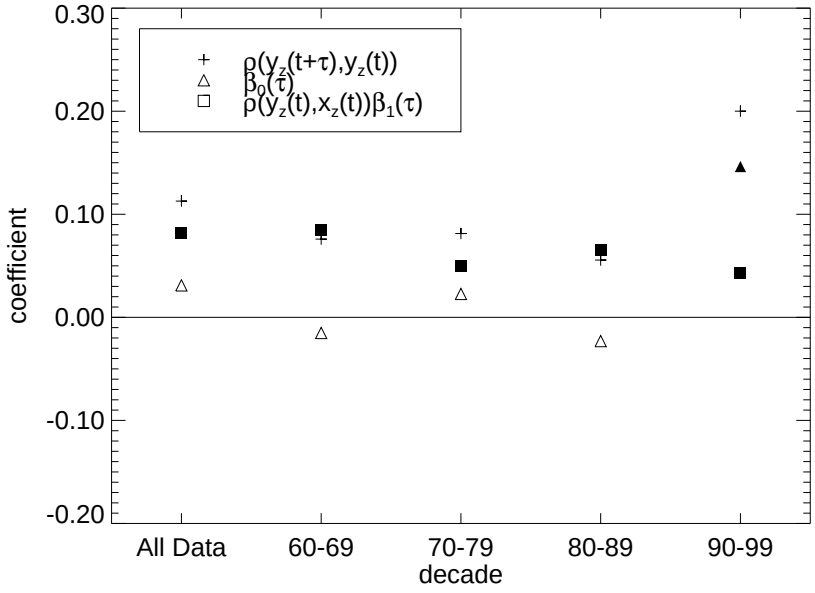

Figure 2.8: *Model parameters for various subsections of data at lag of 30 days. The autocorrelation of the dataset is plotted with crosses, $\beta_0(\tau)$ is plotted with triangles and $\rho(y_z(t), x_z(t))\ \beta_1(\tau)$ is plotted with squares. Symbols for model parameters are filled in black if the parameter is significantly different from zero at the 5 $\%$ level.*

2.7 Out of sample linear predictive skill

The ultimate application of the relationships suggested in the Baldwin and Dunkerton dataset is to improve forecasting of the tropospheric AO and hence surface parameters. A simple experiment was constructed to test the forecasting capability of this dataset. In order to test the fitted model it should be tested against an independent dataset. As no other dataset is available we divide the data in half and then fit the model for one half of the dataset and test it using the other half.

To assess the benefit of using stratospheric data to forecast the 1000hPa AO we fit two different models to the dataset. The first one is structured as in Eq. 2.1. The second control model is shown in Eq. 2.6.

$$y_z(t+\tau) = \gamma_0 y_z(t) + \epsilon(t) \tag{2.6}$$

This model has only one predictor, the state of the 1000hPa AO at a previous time. It is not expected to be a good model of the future state of the 1000hPa AO.

We measure the skill of each of the models by comparison with an AO climatology using the Skill Score (SS)

$$SS = 1 - \frac{MSE_{forecast}}{MSE_{climatology}} \tag{2.7}$$

where MSE represents the mean square error of the forecast. The difference in Skill Score between the two models gives a measure of the gain in skill obtained by including extra information in the model on each level.

Figures 2.9 (a) and (b) shows the difference in skill score between the 1000hPa only control regression model and the two predictor model as in Eq. 1. Positive values indicate including data at a particular pressure level and lag adds skill to forecasts of the 1000hPa AO (compared with a 1000hPa AO only model) and negative values indicate including data at a particular lag and pressure level reduces skill to forecasts of the 1000hPa AO (compared with a 1000hPa AO only model).

The skill is plotted for different lags and different pressure levels. The two columns show results when different halves of the data set are used to train the model.

Figures 2.9(a) and (b) show the SS of the two predictor model is greater than the 1000hPa only control model in the lower and middle stratosphere (250hPa - 10hPa) on time-scales between 10 and 60 days. This is the region highlighted in the model fit as the significant region for the indirect relationship ($\rho(y_z(t), x_z(t))\ \beta_1(\tau)$).The magnitude of the increase is small $\sim 5\%$.

In contrast for levels in the middle and lower troposphere the SS of the two predictor model and the 1000hPa only control model is approximately comparable. The addition of extra information from the middle and lower troposphere into a statistical model of the 1000hPa AO provides little extra forecast skill.

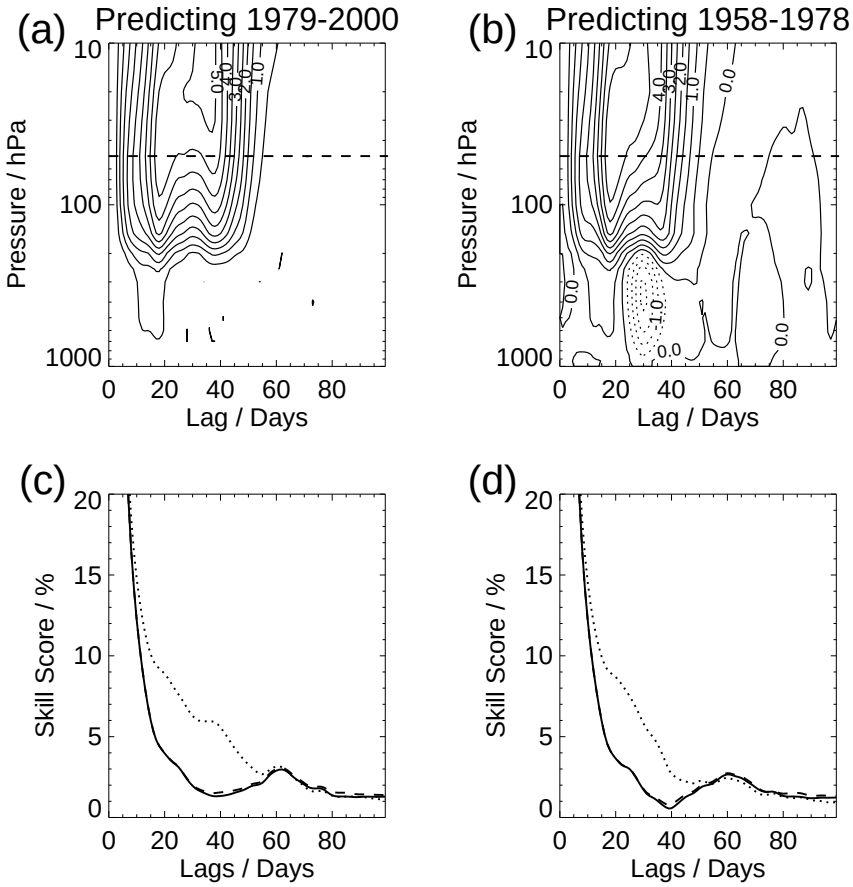

Figure 2.9: *Skill Score diagnostics (a) shows difference in Skill Score of multiple predictor model and 1000hPa predictor only model versus climatology in percentage gain in Skill (1958-1978 used as training period). Contour interval is* 0.5%*. Solid contours show the multiple predictor model has larger Skill Score than the 1000hPa predictor only model. Dotted contours show the multiple predictor model has smaller Skill Score than the 1000hPa predictor only model. See text for details of models. (b) shows difference in Skill when 1979-2000 is used as the training period. (c) shows actual percentage skill against lag for 1000hPa only model (solid line), model with 1000hPa and 70hPa as model predictors (dotted line) and model with 1000hPa and a time reversed 70hPa time series as model predictors (dashed line). Training period is 1958-1979. (d) shows as (c) but for training period 1979-2000.*

As was suggested in the introduction to this section, it was not expected that the troposphere only model would provide useful skill on longer time-scales. Figure 2.9(c) and (d) shows the actual skill for the model with only a 1000hPa predictor (solid line) and both a 1000hPa predictor and a

70hPa predictor (dotted line). The region of increased skill highlighted above can clearly be seen between 10 and 60 days for both training periods. On 10-60 day time-scales the 1000hPa only model has less than 5% skill. The inclusion of extra lower stratospheric information results in a large increase in this skill. For example at 20 days lag the forecast skill is increased from 5% to 10%. The inclusion of extra information in the two-level model does give a significant increase in the skill of 1000hPa forecasts. Nevertheless, the actual forecast skill derivable from such a model is still small.

It could be suggested that the increase in skill is simply due to the addition of an extra predictor in the two level model. This hypothesis can be tested by repeating the analysis with the 70hPa time series reversed in time. In this case the 1000hPa only control model will have identical skill and the additional predictor dataset will have identical statistical properties as in the normal fit. Any predictive relationship between the two datasets is destroyed. Therefore if the gain in skill in this test is comparable to the gain in skill in the normal case then this is likely to be due to the addition of an extra predictor.

The skill score of a model which has a 1000hPa AO predictor and a time-reversed 70hPa predictor is shown in Figure 2.9 (c) and (d) in the dashed line. It is hard to distinguish this line from the solid line which shows the skill of a 1000hPa AO only model. This indicates that including extra, unrelated information with the same statistical properties as the 70hPa time series results in a very small increase in skill. The gain in skill introduced by including extra lower stratospheric information in a statistical model of the 1000hPa AO represents a real increase in the forecasting skill of such a model.

The lack of increase in the skill for tropospheric levels is somewhat surprising. It might be expected that including information in the troposphere which could have a direct impact on the development of individual weather systems in the middle troposphere may lead to better forecasts of the AO. However it seems that in terms of the AO the lower and middle troposphere contains very little information not contained in the 1000hPa AO. Examination of AO time series such as Fig. 1.2 suggests that the middle and lower tropospheric AO often has very similar variability in time. The suitability of the AO diagnostic in a forecasting context is therefore somewhat limited, as we do not suggest that a tropospheric forecasting model should not include information in the lower and middle troposphere. The gain in forecast skill presented here is for a forecast of the

hemispheric scale AO structure. A standard tropospheric forecast would be dominated on daily time-scales by more localised variability.

2.8 Conclusions

In this chapter we have presented a quantitative examination of the relationship between the lower stratosphere and surface using a simple statistical model. The model relates the amplitude of the tropospheric AO at some time to the previous amplitude of the AO in the troposphere and the previous amplitude of the AO in the stratosphere.

The statistical model has been used to partially answer the first of the questions posed in the introduction, "Does the stratospheric state have an influence on the tropospheric flow ?"

A relationship between the amplitude of the AO in the lower stratosphere and 1000hPa has been identified. Typical correlations between the lower stratosphere and 1000hPa are small (~ 0.2), but significant (at the 5 $\%$ level) over extended range time scales (10-45 days).

The character of this relationship has been determined by further analysis, this gives information which together with the modelling studies of chapters 3 and 4 helps to answer the second part of question 1.

- The relationship is most prominent in the upper troposphere lower stratosphere region (50-250hPa). This region spans different parts of the atmosphere at different latitudes, but can broadly be thought of as the location of the tropopause.
- The relationship is strongest during the winter season, in particular during February and March. This is the time in which the polar vortex undergoes major dynamical changes in the final warming phase.
- The relationship is present in all periods of the data, and shows remarkable consistency throughout the time series. In contrast the relationship between the 1000hPa AO and itself over extended range time scales is extremely variable between different 10 year slices of the data (-0.02 $\leq \beta_0(\tau) \leq$ 0.15).

The statistical model can also be used in forecasting mode to answer the second question posed in the introduction, "Are medium, extended and long range forecasts of the tropospheric state improved by considering the stratospheric state ?"

Including stratospheric information in a simple statistical forecasting model of the 1000hPa AO provides an increase in Skill Score of $\sim 5\%$ over a statistical forecasting model which only includes 1000hPa AO information. This increase is not due to the inclusion of an extra predictor in the model.

The statistical model is a simple way of finding a relationship between the stratosphere and troposphere and examining some of its character. Further understanding of the relationship is obtained from the modelling studies outlined in chapters 3 and 4. Remaining issues which cannot be determined from the statistical model are:

- Is the relationship between the stratosphere and troposphere found in the statistical model the result of a causal link between the stratosphere and troposphere ? In other words does making a change to the stratospheric circulation have a direct impact on the troposphere.
- By what mechanism does the stratosphere have an impact on the troposphere ?

CHAPTER 3

Design of medium-range ensemble forecasting experiments

3.1 Introduction

Results presented in Chapter Two showed that the forecast skill of a simple statistical model of the AO in the troposphere could be improved by using stratospheric AO information on extended-range and long-range timescales. It is not possible to attribute the increase in forecast skill in the statistical model to a causal link between the stratosphere and troposphere. It is only possible to do this using a numerical model where the response of the troposphere to an explicit change to the stratospheric flow can be examined.

In this chapter the design of a set of experiments to determine if the stratosphere has a causal effect on the troposphere is presented. The results of these experiments are shown in chapter four.

An experiment to determine the relationship between the stratosphere and troposphere involves making a change to the stratosphere and examining the effect of this change on the tropospheric flow. As reviewed in the introduction the problem can be formulated in two ways.

- **Model Dynamics Problem** Make changes to the model dynamics of the stratosphere and examine the impact upon the troposphere.
- **Initial Value Problem** Make changes to the initial conditions in the stratosphere and examine the impact upon the troposphere.

In this study the problem is formulated as an initial value problem. Recent studies of this problem which adopted the model dynamics approach (Norton, 2003; Polvani and Kushner, 2002) demonstrated that the stratosphere could effect the troposphere when its circulation was vastly different to its current climatological state. By using the initial condition approach the impact

of the stratosphere on the troposphere when the stratospheric circulation is similar to its current climatological state can be investigated.

3.2 Experimental Design

To examine the effect of stratospheric initial conditions on the tropospheric flow a number of extended-range forecast case studies are run. The experiments examine the transient response of the troposphere to an initial change in the stratosphere.

Each experiment compares two extended-range ensemble forecasts:

- A **Nature** ensemble, to simulate conditions where 'downward propagation' was observed in the AO Index.
- A **Non-Nature** ensemble with identical tropospheric conditions and different stratospheric initial conditions. Stratospheric conditions in the non-nature run are chosen to have the opposite sign in the stratospheric AO. For example in cases where the nature run is a simulation of a stratospheric sudden warming (the polar vortex is weak and displaced from the pole) the non-nature stratospheric initial conditions would be taken from analyses when the polar vortex was strong and centred on the pole. A schematic of the construction of the non-nature initial conditions is shown in figure 3.1

In Numerical Weather Prediction ensemble experiments are used to assess the uncertainty in the forecast due to uncertainties in the initial conditions. In the experiments detailed in this chapter the ensembles are used to assess the relative magnitude of changes to the tropospheric flow due to changes in the stratospheric initial conditions and the spread of the ensemble forecasts due to initial condition uncertainty. Changes to the tropospheric flow due to changes to the stratospheric initial conditions which are significant compared to the ensemble spread are deemed to be important for tropospheric forecasting.

Notice that a spin-up period was not included in the non-nature experiment. It is important to initialise the model from identical tropospheric conditions, for corresponding ensemble members

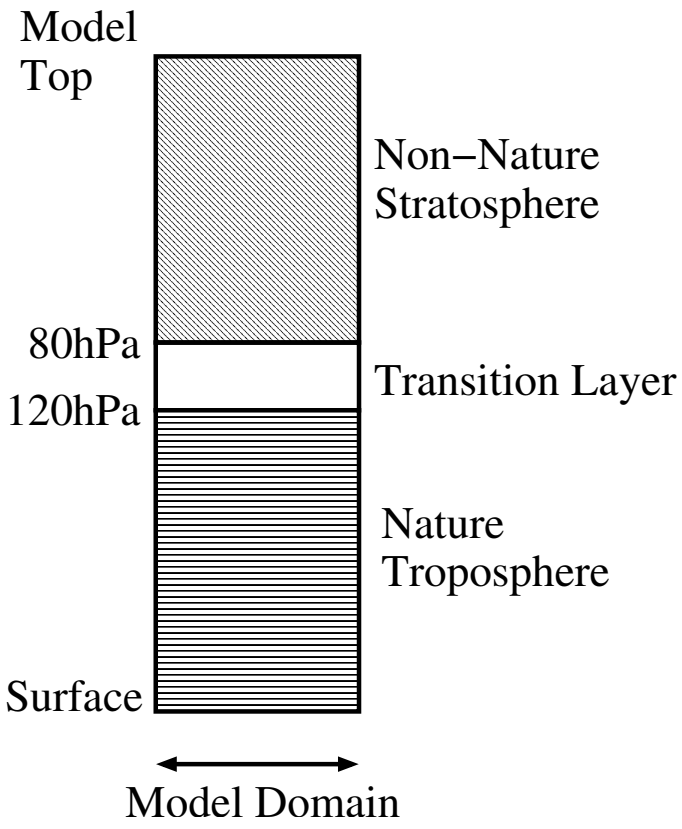

Figure 3.1: *Schematic showing construction of initial conditions for non-nature runs*

in the nature and non-nature runs, and impose an instantaneous change to the stratospheric initial conditions. The surface pressure at initial time in the nature and non-nature runs is chosen to be identical. Choosing the surface pressure field to be identical in the nature and non-nature runs ensures that the initial tropospheric flow is identical in the nature and non-nature runs, due to the hydrostatic formulation of the model.

It is also important to avoid imposing a shock to the model which would cause it to crash (Daley, 1991). The construction of initial conditions in the non-nature runs includes a transition layer between 80hPa and 120hPa. In the transition layer initial conditions are formed by linear interpolation between the initial conditions from the imposed, non nature stratosphere above and nature troposphere below.

The model's initial conditions in the non-nature run are not in balance. In particular there are two processes in the model which adjust the fields toward balance in response to the imposed initial condition in the stratosphere.

- The change to divergence fields in the stratosphere causes a change to the time-tendency of the surface pressure field. After one timestep of the model integration the surface pressure will recognise the different divergence field aloft. Changes to the surface pressure field can be communicated through the atmosphere because the model is hydrostatic.

- In the transition layer in the non-nature run flow and mass fields may be more out of balance than in the same region in the nature run. The model removes imbalances between the mass and flow fields through the emission of gravity waves.

Section 3.4 examines the quantitative size of these re-adjustment processes. If the quantitative size of re-adjustment processes are large then this may obscure any impacts of the stratospheric state on the tropospheric flow due to genuine dynamical relationships in the real atmosphere. The re-adjustment processes in the model are not present in the real atmosphere and constitute spurious impacts of the change made to the stratospheric initial conditions.

3.3 Choice of Model

At the start of the project the choice of General Circulation Model to be used for the experiments outlined in section 3.2 was not clear. Running the experiments with a climate model such as the UKMO Unified Model would require less computer time than with a numerical weather prediction model such as the ECMWF IFS model, which would allow a much larger number of case studies to be run. It was not clear, however, that a climate model would be appropriate for the experiments in section 3.2 owing to its lower horizontal resolution and lack of forecasting skill on short timescales.

A test experiment was devised to examine the performance of the UKMO Unified Model in simulating a stratospheric sudden warming which would be the basis of the first case study. Both ECMWF and UKMO produce operational troposphere-stratosphere analyses which could be used as the definition of 'truth'; because of the disagreements in these analyses, 'truth' in each test case was defined as the analysis produced by the corresponding model system. NCEP re-analysis data was used to compare the two runs.

The criteria on which the model's performance were judged are:

1. The model should have a good representation of the stratosphere. If we are attempting to evaluate the impact of the stratosphere on the troposphere then it is important that the model should well represent the stratosphere. *This was measured using the polar temperature and zonal mean zonal wind at 60N.*

2. The model should be able to simulate the break up of the stratospheric vortex. The dynamics involved in the breaking stage of the vortex are likely to be quite complicated and highly non-linear. The break up may have an important role in the case studies we investigate so the model must simulate these events well. *This was assessed with maps of geopotential height at 10hPa.*

3. The model should have an accurate simulation of tropospheric dynamics on medium-range timescales. The mechanism for the impact of the stratosphere on the troposphere may depend on the state of the troposphere. Hence if the troposphere is poorly simulated this may affect the model's simulation of this mechanism. *This was assessed with maps of geopotential height at 1000hPa.*

Both models are based on the primitive equations. These equations can be derived from the full equations of mass for a gas in a rotating frame by :

- Assuming the vertical momentum equation can be replaced by hydrostatic balance.
- Neglecting the Coriolis force associated with the horizontal component of the Earth's rotation vector.
- Assuming a shallow atmosphere. This means that the distance from any point in the atmosphere to the centre of the earth is approximated by the same constant distance a.

3.3.1 Met Office 64L HadAM3 Model

The Hadley Centre Atmosphere Only Model 64 Level version is a climate prediction model ((Austin, 2002), the version of the model used in this study does not include the coupled strato-

spheric chemistry component) . This model is an extended version of the Met Office unified model which is used for both forecasting and climate prediction (Cullen, 1993). The model has relatively low horizontal resolution (3.75° longitude x2.5° latitude). The horizontal discretization is via a gridpoint method on an Arakawa 'B' staggered grid.

The model has a similar number of vertical levels as the IFS model (see section 3.3.3) and a similarly well resolved stratosphere. The vertical coordinate used is a hybrid sigma-pressure coordinate (Simmons and Burridge, 1981).

The HadAM3 model does not have the capability to automatically generate ensemble members. For these test runs we used a similar technique to that used by Lahoz (2000). Separate sets of atmospheric initial conditions were generated by running a control model integration and selecting model dumps 6 hours apart.

- **Equation Set** Primitive Equations
- **Horizontal Representation** Gridpoint
- **Horizontal Resolution** 3.75 °longitude / 2.5 °latitude
- **Horizontal Grid** Arakawa 'B' (Arakawa and Lamb, 1977)
- **Vertical Representation** Gridpoint
- **Vertical Coordinate** Hybrid Sigma-Pressure (Simmons and Burridge, 1981)
- **Vertical Resolution** L64
- **Time Stepping** Split-Explicit two step procedure with adjustment and advection phases. Two step Heun scheme used in the advection phase.
- **Hydrostatic**
- **Levels above 100hPa** 38

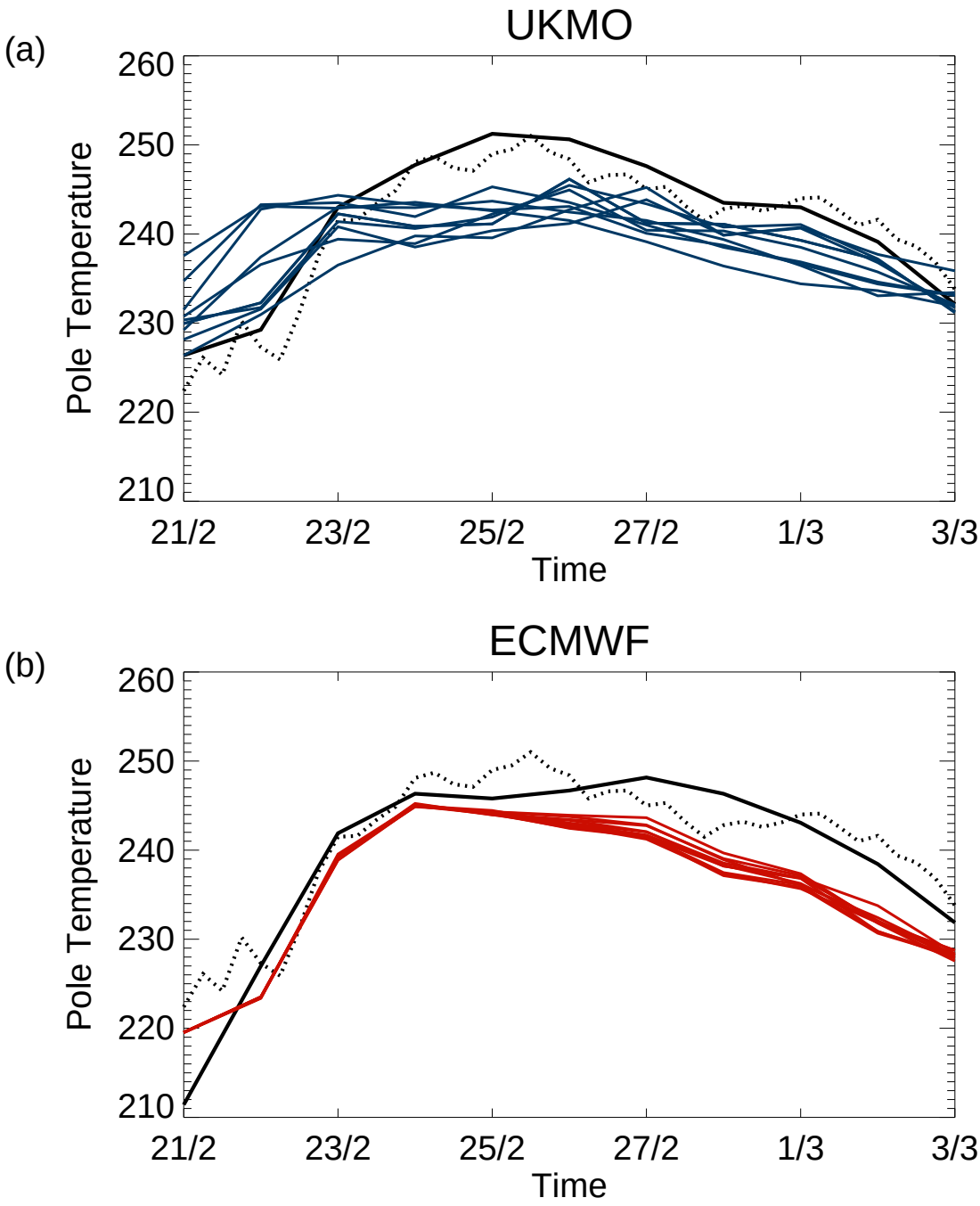

Figure 3.2: *Pole temperature at 10hPa for two control ensemble simulations. a) shows UKMO simulation, UKMO analysis plotted in solid black, NCEP Re-Analysis plotted in dotted line. Blue lines show individual ensemble members. b) shows ECMWF simulations, ECMWF analysis plotted in solid black, NCEP Re-Analysis plotted in dotted line. Red lines shows individual ensemble members.*

3.3.2 Results of test experiments with UKMO Hadam3 Model

1. The model does not adequately represent the evolution of the stratosphere in zonal mean diagnostics. The stratospheric sudden warming in the UKMO analysis is shown as an increase in polar temperature, reaching a maximum on 25/02 (Fig. 3.2 (a)) and a reduction of zonal mean zonal wind at 60N (Fig. 3.3 (a)) from westerly to easterly values. The UKMO ensemble captures the polar temperature warming and the reduction in zonal mean zonal wind speed, but fails to capture the maximum in polar temperature or minima in zonal mean zonal wind. This is particularly evident in the polar temperature; the ensemble members appear to be limited in the amount of polar warming which they can achieve.

2. The model is not able to simulate the split in the polar vortex. Figure 3.4(a) shows the UKMO analysis on 27/02. In the analysis the polar vortex is split into two parts, one to the north of the UK and one over Eastern Asia. The corresponding ensemble mean forecast (Fig. 3.4(b)) shows the development of two separate centres in the polar vortex, but these centres are still linked through the ring of moderately low geopotential height (for example shown by the 30.4 km contour).

3. The model has a limited representation of tropospheric dynamics which may be related to its low horizontal resolution (Buizza et al., 2003). Figure 3.5 (a) and (b) show the UKMO analysis on 27/02 and the ensemble mean forecast. The ensemble mean forecast does not simulate some of the features in the tropospheric flow such as the two intense low height centres in the Pacific basin (over western North America and Eastern Eurasia), combining these features into a single low height centre over the central Pacific.

The UKMO Hadam3 model does not suitably simulate the tropospheric or stratospheric evolution of the stratospheric sudden warming. As this test case would be the first of the three case studies investigated in chapter 4 this implies that the model would not be suitable for the experiments outlined in this chapter.

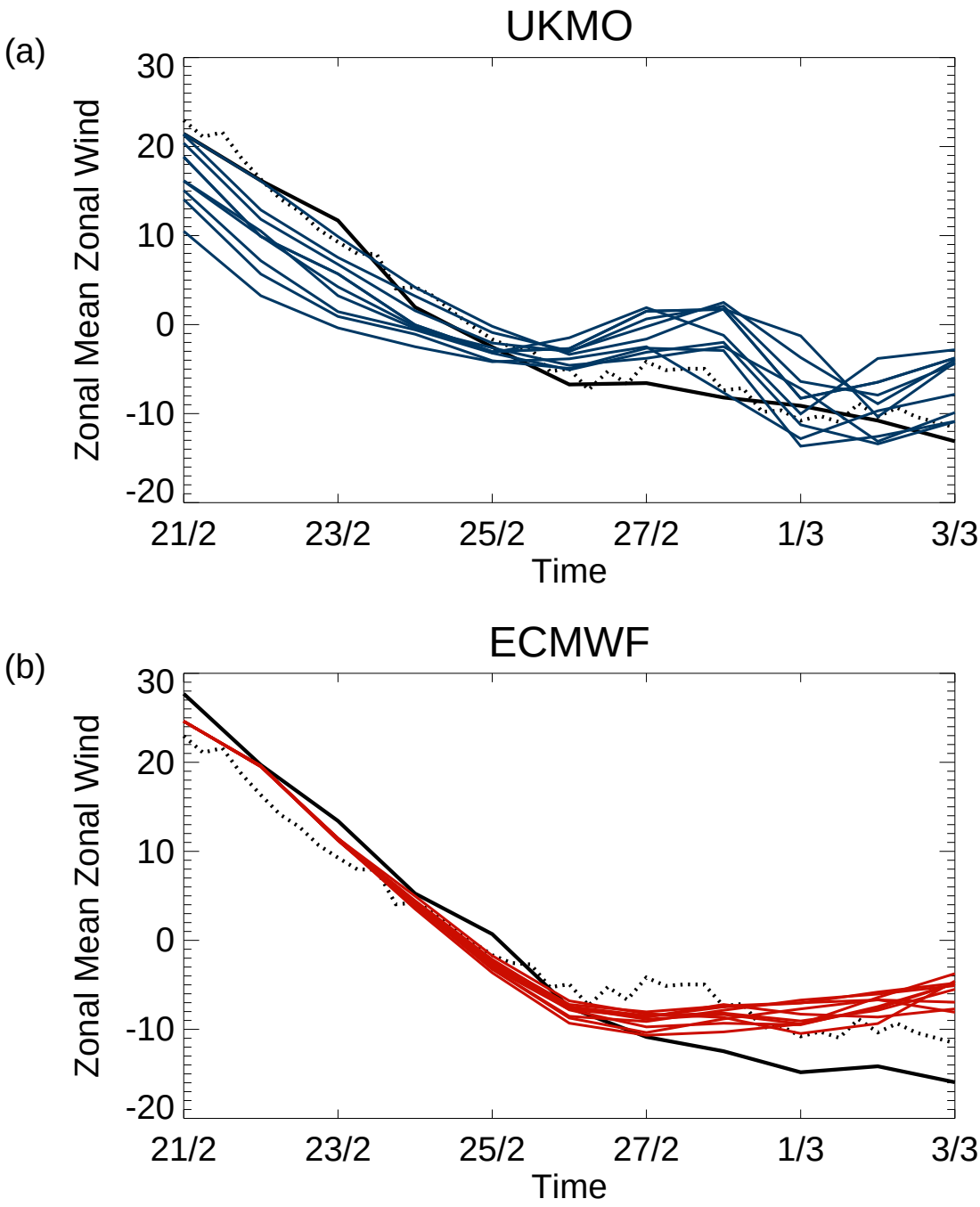

Figure 3.3: *Zonal Mean Zonal Wind at 60N and 10hPa for two control ensemble simulations. a) shows UKMO simulation, UKMO analysis plotted in solid black, NCEP Re-Analysis plotted in dotted line. Blue lines show individual ensemble members. b) shows ECMWF simulations, ECMWF analysis plotted in solid black, NCEP Re-Analysis plotted in dotted line. Red lines shows individual ensemble members.*

3.3.3 ECMWF IFS Model

The ECMWF IFS model is the standard model used by ECMWF to make medium-range weather forecasts. The version of the model used here has 60 levels in the vertical and includes 25 levels in the stratosphere. The model is a spectral formulation of the primitive equations. In this version of the model the truncation is T255, this results in an approximate horizontal resolution of 0.6° longitude x0.6° latitude.

The vertical coordinate is a hybrid sigma-pressure coordinate described by Simmons and Burridge (1981) and will be discussed in more detail later.

The modelling system has an operational capability to generate ensemble forecasts. Ensembles are generated by making small perturbations to the initial conditions of the model. Perturbations are defined by examining the singular vectors of the initial conditions. Singular vectors are selected which involved the largest growth over the initial evolution. This should result in an efficient sampling of the initial probability distribution function (pdf). A full integration of the model is completed for each of the sets of initial conditions. For more details see Molteni et al. (1996). This system has been used operationally at ECMWF for a number of years and as such is well tested.

The model is structured as follows.

- **Equation Set** Primitive Equations
- **Horizontal Representation** Spectral
- **Horizontal Resolution** T255 (approx. 0.6°x0.6° grid)
- **Horizontal Grid** Reduced Gaussian (Hortal and Simmons, 1991)
- **Vertical Representation** Gridpoint
- **Vertical Coordinate** Hybrid Sigma (Simmons and Burridge, 1981)
- **Vertical Resolution** L60
- **Time Stepping** Semi-Implicit Semi-Lagrangian

- **Hydrostatic**
- **Levels above 100hPa** 25

3.3.4 Results of test experiments with ECMWF IFS Model

The ECMWF forecasting model performs much better in the test case than the UKMO model

1. The models simulation of the stratospheric evolution is close to the ECMWF analysis in both polar temperature (Fig. 3.2(b)) and zonal mean zonal wind (Fig. 3.3 (b)). For the first five days of the model run the ensemble follows the analysis closely, toward the end of the run polar temperatures decrease more rapidly in the model ensemble than in the analysis and the zonal mean zonal wind starts to increase in the ensemble.
2. The model has a much better simulation of the polar vortex split than the UKMO model. Figure 3.4 (c) and (d) shows the ECMWF analysis and ensemble mean forecast on the 10hPa pressure surface. The model forecast has a split in the polar vortex and places the two halves of the split vortex in the correct geographical locations (to the north of the UK and over eastern Eurasia).
3. The tropospheric forecast of the model (Fig. 3.5(d)) closely resembles the ECMWF analysis (Fig. 3.5(c)). The location and number of tropospheric synoptic scale systems is correct although their central magnitude in the ensemble mean is smaller than in the analysis.

The ECMWF IFS modelling system is much more appropriate for the experiments outlined in this chapter. In each of the four diagnostic tests outlined in this section the ECMWF IFS model outperforms the UKMO Hadam3 Model. This is perhaps unsurprising as the ECMWF model is designed for numerical weather prediction on short timescales whereas the HadAM3 model is designed for long climate integrations. There have been several studies which have suggested that increasing horizontal resolution increases the skill of tropospheric forecasts (Simmons et al., 1989). Also the parameterisations and their tuned parameters in the UKMO model will have been designed to simulate a good model climate and may not necessarily be particularly appropriate for

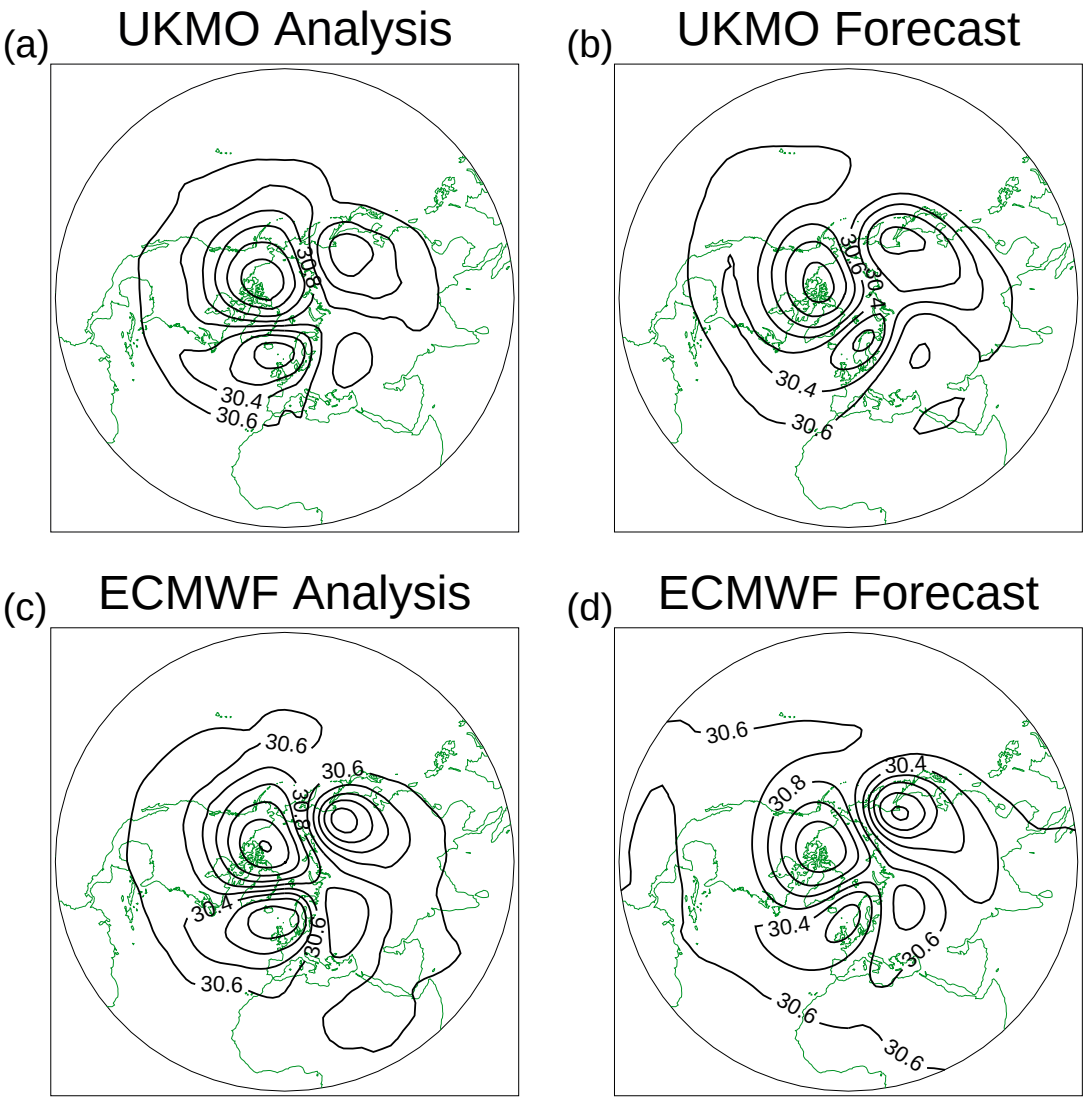

Figure 3.4: *Geopotential Height maps at 10hPa 6 days into forecast period (27/2/1999). Contour interval is 0.2km. a)Shows UKMO Analysis, b) shows ensemble mean UKMO Forecast, c) shows ECMWF Analysis and d) shows ensemble mean ECMWF Forecast.*

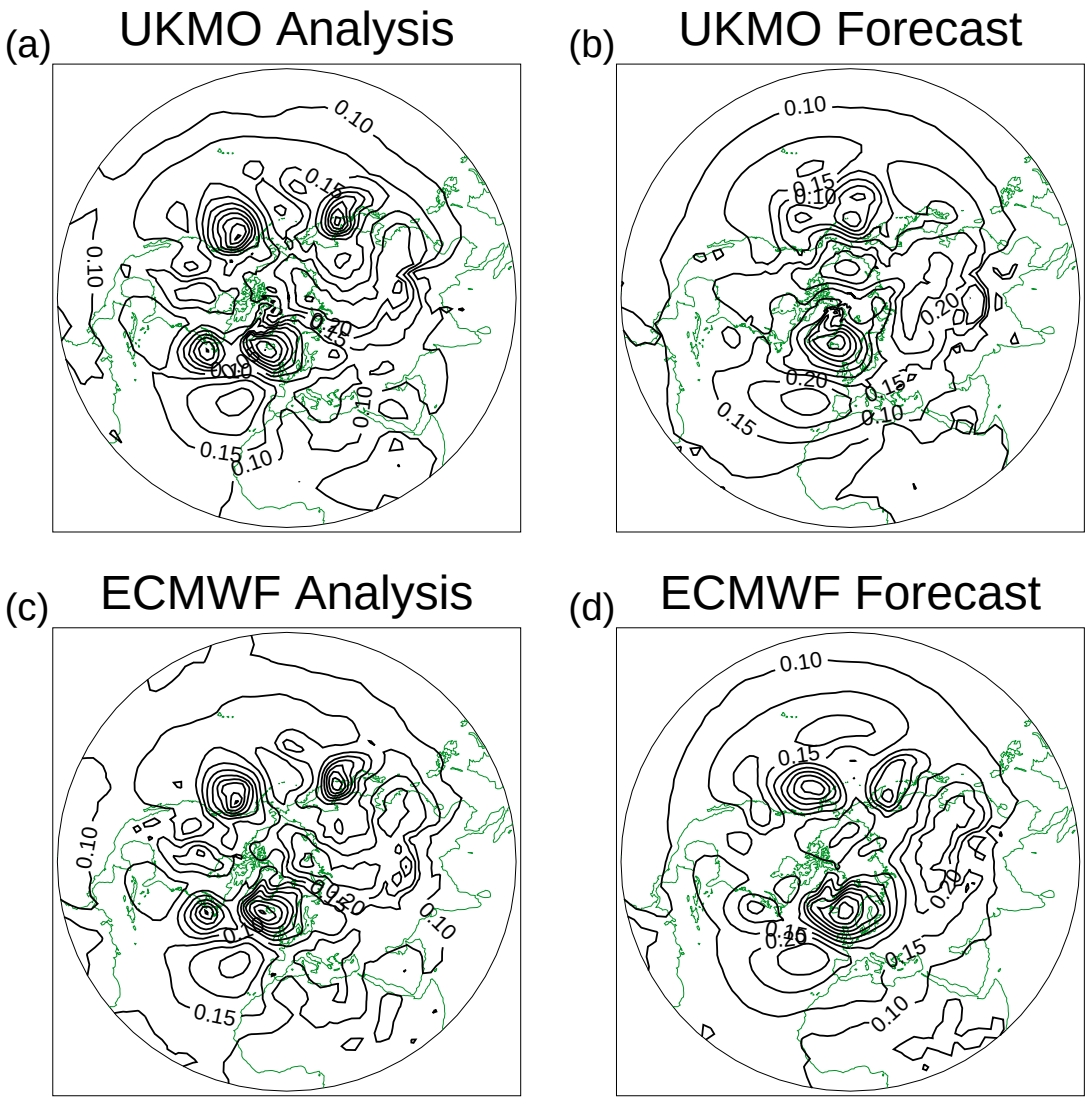

Figure 3.5: *Geopotential Height maps at 1000hPa 6 days into forecast period (27/2/1999). Contour interval is 0.1km. a)Shows UKMO Analysis, b) shows ensemble mean UKMO Forecast, c) shows ECMWF Analysis and d) shows ensemble mean ECMWF Forecast.*

medium and extended range forecasting. The ECMWF IFS model was chosen for the experiments in chapter 4.

3.4 Adjustment Processes

To the extent that the atmosphere exhibits balanced flow, making a change to the stratospheric PV distribution will immediately have an impact on the tropospheric flow due to the elliptic nature of the PV inversion operator. It has also been shown in a number of studies that the magnitude of this impact is not trivial (Hartley et al., 1998; Black, 2002). In these experiments the stratosphere will have an impact on the troposphere as soon as the model runs one timestep. However it is important to check that while the experimental design will capture this feature of the flow, there are no spurious impacts of the stratosphere on the troposphere due to the design of our experiments.

As mentioned in the introduction the initial conditions in the non-nature run are not in balance. The model will attempt to adjust the initial conditions toward a more balanced state in two ways:

- The divergence fields in the stratosphere are not the same in the nature and non-nature runs. This causes a large change to the time-tendency of the surface pressure field in the first timestep.
- In the transition layer in the non-nature run flow and mass fields are more out of balance than in the same region in the nature run.

This section examines the quantitative size of these effects and their impacts on the tropospheric flow.

3.4.1 Adjustment of surface pressure to stratospheric divergence field

In this section the adjustment of the model surface pressure field to the initial distribution of divergence in the stratosphere is examined.

The ECMWF IFS model is hydrostatic and uses a Simmons et al. (1989) vertical sigma coordinate. This vertical coordinate is a terrain following coordinate at the surface and a pure pressure coordinate in the stratosphere. Pressure on each model level is given by:

$$P_{k+\frac{1}{2}} = A_{k+\frac{1}{2}} + B_{k+\frac{1}{2}}\, P_s \tag{3.1}$$

where :

$P_{k+\frac{1}{2}}$ - is pressure on half levels

$A_{k+\frac{1}{2}}$ and $B_{k+\frac{1}{2}}$ - are constants which determine the structure of the model levels

P_s - is the surface pressure

The hydrostatic equation in the model is expressed as

$$\phi_{k+\frac{1}{2}} = \phi_s + \sum_{j=k+1}^{NLEV} R_{dry}\,(T_v) \ln \frac{P_{j+\frac{1}{2}}}{P_{j-\frac{1}{2}}} \tag{3.2}$$

where:

Model levels run from 0-60, ie j=0 is the model top and j=NLEV=60 is the lowest model level

ϕ_s - is the surface geopotential

$\phi_{k+\frac{1}{2}}$ - is the geopotential on model level k+$\frac{1}{2}$

T_v - is the virtual temperature. This is defined as

$$T_v = T\left[1 + \{R_{vap}/(R_{dry} - 1)\}\right]$$

where:

T - is the temperature

q - is the specific humidity

R_{vap} - is the gas constant for water vapour

R_{dry} - is the gas constant for dry air

The hydrostatic equation is calculated in the model starting at the surface and working to the model top, so the geopotential on model level 10 depends on the surface geopotential and the sum of the temperature structure multiplied by the log pressure below level 10.

The first term on the right hand side of Equation 3.2 is the surface geopotential which is fixed. The summation term is made up of the virtual temperature on all levels below the level on which height is to be calculated and the pressure on the two half levels adjacent to the virtual temperature.

The virtual temperature below the level in question is independent of the stratospheric state. However the log pressure term is influenced by the stratospheric state because of the way in which pressure levels are defined and the time tendency equation for surface pressure.

Pressure on each half level is defined from equation 3.1. At initial time the surface pressure in both the nature and non-nature runs is identical so the height distribution in the troposphere is also identical.

After one timestep the surface pressure changes according to the following equation.

$$\frac{\partial\,(\ln\ P_s)}{\partial\,t} = \sum_{k=1}^{NLEV}\ \left\{\frac{1}{P_s}\,D_k\,\Delta\,P_k + (\mathbf{v_k}\ \cdot\ \nabla\ \ln\ \mathrm{P_s})\,\Delta\,\mathrm{B_k}\right\} \tag{3.3}$$

where:

P_s - is surface pressure

P_k - is pressure on a model level

D_k - is divergence on a model level

v_k - is wind vector on a model level

$\Delta\ B_k$ is the difference in the amount of weighting given to the surface pressure at the adjacent

model half levels in the sigma coordinate (equation 3.1). $\Delta\ B_k$ is zero above model level 24. Changes to initial conditions are made at level 24 and there is interpolation between level 24 and 27. This means that for a large part of the stratospheric changes the second term on the right hand side is zero.

The divergence fields in the stratosphere in the nature and non-nature runs are very different. This means that the first term on the right hand side of equation 3.3 will be different at the first timestep in the nature and non-nature runs. Therefore there will be an immediate impact on the surface pressure as soon as the model is run through one timestep which will be communicated throughout the depth of the model by equation 3.2. Experiments run to test the impact of these changes on the surface pressure and geopotential distribution are described below. To find the difference in surface pressure tendency at the first timestep between the nature and non-nature runs we can use equation 3.3. This difference can be calculated for each set of model initial conditions. Figure 3.6 (a) shows the difference in surface pressure between the nature and non-nature cases after 1 hour. This difference is calculated off-line, assuming that the only contribution to the tendency is due to the difference in the initial divergence field (the change of surface pressure over time from the initial conditions is calculated from equation 3.3, the derivative can then be integrated forward to give the change to the surface pressure after an hour of the model run). The changes to the surface pressure associated with this difference are very small ($< 5Pa$) and have little coherent spatial structure. In contrast the differences between the nature and non-nature runs after one hour taken from model output (Figure 3.6 (b), note different contour interval from Fig. 3.6 (a)) are much larger. This suggests that the divergence adjustment process outlined above is a relatively minor change compared to changes to the surface pressure caused by changes to the evolution of the stratosphere and troposphere in each case.

Figure 3.6 (c) shows the typical percentage difference in geopotential height on each model level if changes are made to the surface pressure. A reference temperature profile,taken from the model is used in these calculations (we assume that virtual temperature can be replaced by temperature). The maximum change to the surface pressure in the off-line divergence calculation is 5 Pa. The solid line shows that a change to the surface pressure of 5 Pa results in a very small change in geopotential height in the troposphere. Even if this change is multiplied by a factor of 10 (dashed line) there is a very small change in geopotential height ($< 0.05\%$).

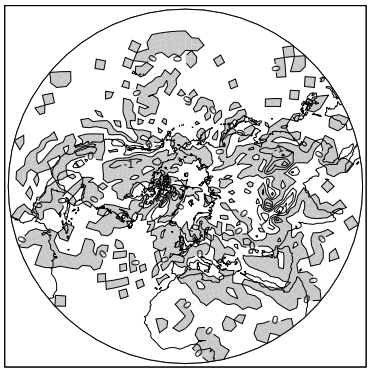

(a) Difference in Surface Pressure between Nature and Non-Nature runs calculated off-line using surface pressure tendency equation. Units are Pa, shading shows negative difference.

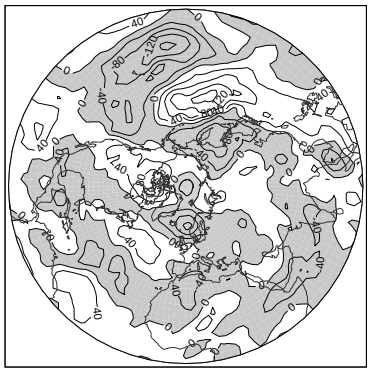

(b) Difference in Surface Pressure between Nature and Non-Nature runs calculated by numerical model. Units are Pa (note contours are 40 times those in figure (a)), shading shows negative difference

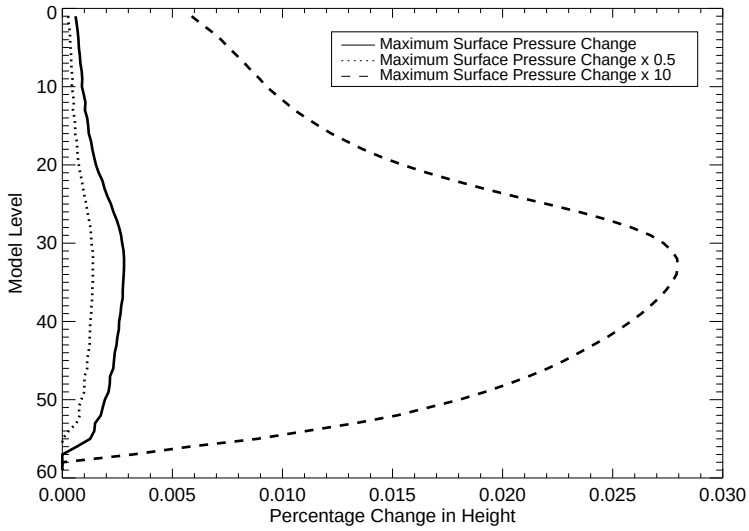

(c) Percentage difference in height on each model level when surface pressure is changed by 5Pa (solid line, maximum from tendency calculation), 2.5Pa (dotted line) and 50Pa (dashed line).

Figure 3.6: *Surface Pressure adjustment diagnostics*

The impact of the change to the stratospheric divergence field on the surface pressure field is very small. The divergence field in the non-nature run has only a small impact on the geopotential field in the troposphere. It is not unreasonable to imagine that the stratospheric divergence may have an impact on the tropospheric flow in the real atmosphere, to the extent that the atmosphere

is hydrostatic.

3.4.2 Changes to gravity wave propagation

In the transition layer in the non-nature run flow and mass fields are more out of balance than in the same region in the nature run. Above and below the transition layer initial conditions are taken from the nature run in the troposphere (below 120hPa) and from a zonal mean of a cold stratospheric state in the stratosphere (above 80hPa). These fields are approximately balanced as they both come from analysis produced by the model. In the region between these two states initial fields are created by linearly interpolating between the two states. This process introduces imbalances into the initial condition. These imbalances will be removed by propagation of internal gravity waves. If there is a large extra flux of gravity wave activity from the stratosphere into the troposphere then they may affect the evolution of the troposphere.

3.4.2.1 Initialisation Procedures

There are a number of methods which can be used to initialise a numerical weather forecast to remove initial imbalances. In particular, ECMWF has developed a Normal Modes Initialisation (NMI) procedure (Temperton, 1988). When this procedure was applied to the non-nature initial conditions it made large changes to initial fields throughout the stratosphere and troposphere. Applying the NMI procedure to the nature initial conditions introduced changes to the troposphere which were not identical to the changes to the troposphere in the non-nature initial conditions.

Our experimental design requires that the troposphere should be identical in corresponding ensemble members in the nature and non-nature runs. The NMI procedure cannot be configured to make changes to the stratosphere and troposphere alone. The NMI procedure cannot be used in these experiments to remove additional imbalances in the the initial conditions of the non-nature run. This means that there will be additional gravity wave activity in the non-nature run introduced by the construction of the artificial set of initial conditions. If this additional gravity wave activity propagated mainly into the troposphere then it may change the tropospheric flow. The vertical propagation of gravity wave activity in the model was investigated in a test run of the

control member of the first case study. Output from the tests runs was obtained at high frequency (1 hour) so that the vertical propagation of gravity wave activity could be diagnosed.

3.4.2.2 Momentum Flux Diagnostics

To diagnose gravity wave propagation in the model there are a number of techniques which could be used. An obvious choice is the Eliassen-Palm Flux.

$$F^{(\phi)} \equiv \rho_0 a \cos\phi(\overline{u}_z \overline{v'\theta'}/\overline{\theta}_z - \overline{v'u'}) \tag{3.4}$$

$$F^{(z)} \equiv \rho_0 a \cos\phi \left(\left[f - (a\cos\phi)^{-1} (\overline{u}\cos\phi)_\phi \right] \overline{v'\theta'}/\overline{\theta}_z - \overline{w'u'} \right) \tag{3.5}$$

$$\nabla \cdot \mathbf{F} \equiv (a\cos\phi)^{-1} \frac{\partial}{\partial\phi}(F^{(\phi)} cos\phi) + \frac{\partial F^{(z)}}{\partial z} \tag{3.6}$$

where:

u - is zonal wind

v - is meridional wind

θ - is potential temperature

ρ_0 - is basic state density

a - is the radius of the Earth

f - is the coriolis parameter

z - is the log-pressure height

ϕ - is the latitude

Eliassen-Palm Flux is derived from the Transformed Eulerian Mean (TEM) formulation of the primitive equations. The formulation divides atmospheric motions into zonal mean and eddy parts. The divergence of the Eliassen-Palm flux gives an indication of the forcing of eddy motions on the mean flow (Andrews et al., 1987).

However diagnosis of the direction of propagation of the group velocity of the waves is somewhat complicated when using EP Flux. In the WKB (Salby, 1996) approximation (that the wave period

and wavelength of the background flow is much larger than that of the incident wave, a reasonable approximation here)

$$\mathbf{F} = \mathbf{c_g A} \tag{3.7}$$

where:

A - is the wave-activity density

c_g - is the group velocity, which is in the same direction as the propagation of energy.

$$A = -k\left(\frac{E}{\omega - k\overline{u}}\right) \tag{3.8}$$

where:

E - is the wave energy density $\frac{1}{2}\rho_0(\overline{u'^2} + \overline{v'^2} + \overline{\Phi'^2_z}/N^2)$

ω - is the frequency of the wave and k is the zonal wavenumber

Wave-activity density can take either positive or negative sign so the direction of propagation of the group velocity is not always in the same sense as the Eliassen-Palm flux. Also wave-activity density is defined for individual waves with a particular frequency and wavenumber. It is not clear how this could be generalised for model output which has oscillations on a number of frequencies and wavenumbers.

An alternative to using the full EP Flux is to use the vertical momentum flux.

$$-\overline{u'\omega'} \tag{3.9}$$

where

u' - is the deviation of the zonal wind from its zonal mean

ω' - is the deviation of the pressure vertical velocity from its zonal mean

Miyahara et al. (1986) states that using this diagnostic allows for better discrimination between planetary wave and gravity wave fluxes. Planetary waves have a large heat flux term which would dominate calculations of EP Flux (see equation 3.5).

The vertical momentum flux alone cannot diagnose the direction of propagation of gravity waves in the vertical. For example a downward and westward propagating gravity wave transports westerly momentum downward and an upward and eastward propagating gravity wave transports easterly momentum upward. Both of these momentum fluxes involve anti-correlation of zonal and vertical velocity.

Regions in which the magnitude of the vertical momentum flux is increased indicate an increase in the gravity wave activity. It is assumed that the only region in which the initial conditions in the non-nature run are further from balance than in the nature run is the transition layer. It is reasonable to assume that any increase in the gravity wave activity in the first three days of the run originated in the transition layer. Therefore if there are large increases in the downward propagation of gravity waves then it is assumed that this will be observed as a large increase in the magnitude of the tropospheric vertical momentum flux.

The mean vertical momentum flux over the first three days of the run is shown in Fig. 3.7. The mean vertical momentum flux is very similar in the nature and non-nature runs. The largest differences in vertical momentum flux occur in the middle stratosphere. This suggests that most of the increased gravity wave activity in the transition layer propagates upward into the stratosphere. Although there are differences in the vertical momentum flux in the troposphere, these are much smaller than those in the stratosphere and represent only a small percentage change to the total vertical momentum flux in the troposphere.

Further information about the changes to vertical momentum flux (and hence gravity wave activity) can be obtained by considering the total absolute vertical momentum flux (TA). This is calculated as follows:

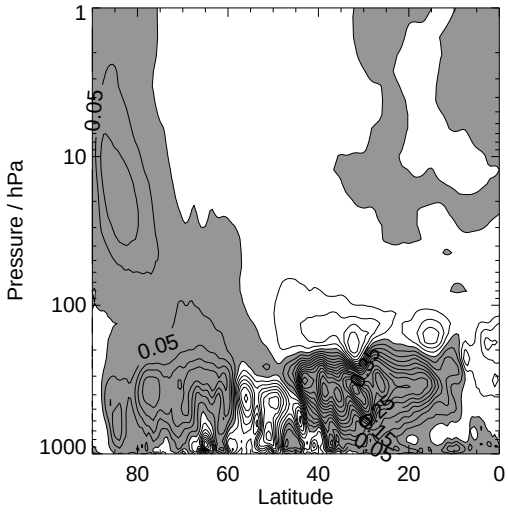

(a) Mean Vertical Momentum Flux ($m^2 s^{-4}$) for first three days of Nature Run. Shading shows positive flux. Contour interval is 0.05 $m^2 s^{-4}$.

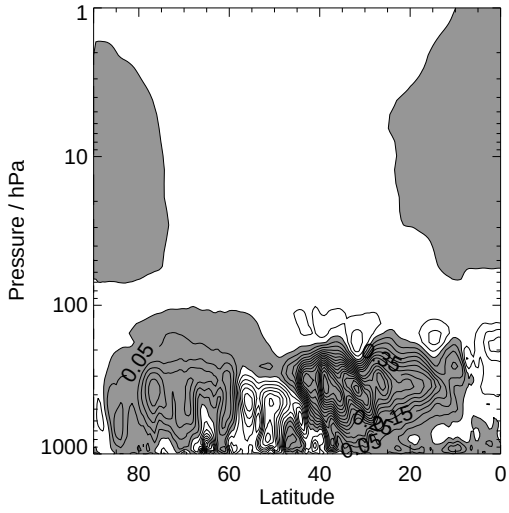

(b) Mean Vertical Momentum Flux ($m^2 s^{-4}$) for first three days of Non-Nature Run. Shading shows positive flux. Contour interval is 0.05 $m^2 s^{-4}$.

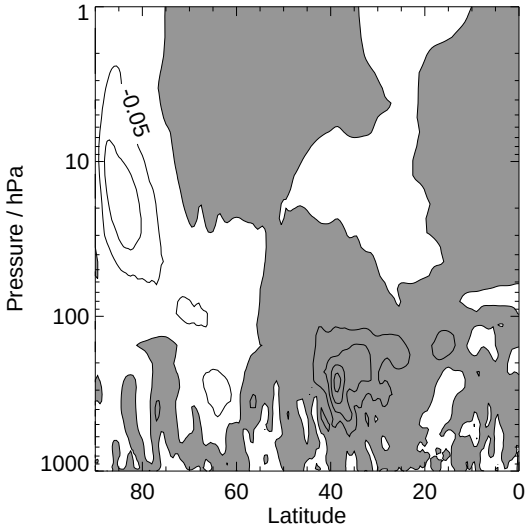

(c) Difference in Mean Vertical Momentum Flux ($m^2 s^{-4}$) for first three days Runs. Shading shows positive difference. Contour interval is 0.05 $m^2 s^{-4}$.

Figure 3.7: *Vertical Momentum Fluxes*

$$TA(l,t) = \sum_{\phi=0}^{90} |\overline{u'\omega'}(\phi, l, t)| \tag{3.10}$$

where :

TA - is a function of model level (l) and time (t)

u - is zonal velocity

ω - is pressure vertical velocity

ϕ - is latitude.

Total absolute vertical momentum flux indicates the amount of gravity wave activity on a given model level at a particular time.

Figure 3.8 shows the evolution of the total absolute vertical momentum flux for the first three days of the run over a number of model levels. Figure 3.8 (a) shows the total absolute vertical momentum flux on a level in the buffer zone. On this level the amount of gravity wave activity in the non-nature run (dotted line) is much larger than in the nature run over the first day of the integration. After this the total absolute vertical momentum flux is very similar. The increase in gravity wave activity in the transition layer indicated by the increase in total absolute vertical momentum flux is only present in the first day of the non-nature integration.

Figure 3.8 (b) and (c) show the total absolute momentum flux just below and just above the buffer zone. Above the buffer zone (Figure 3.8) there is a similar increase in total absolute momentum flux in the first day of the run which is sustained for the first 10-20 hours. Below the buffer zone (Figure 3.8) there is an increase in the total absolute momentum flux after the first hour of the run but this is rapidly reduced and after 5 hours of the run the total absolute momentum flux is very similar in the nature and non-nature runs. This suggests that the majority of extra gravity wave activity in the non-nature run propagates upwards from the buffer zone into the stratosphere. While a small amount may propagate downwards into the upper troposphere the total absolute momentum flux in the upper troposphere of the non-nature run rapidly returns to a level comparable with the nature run.

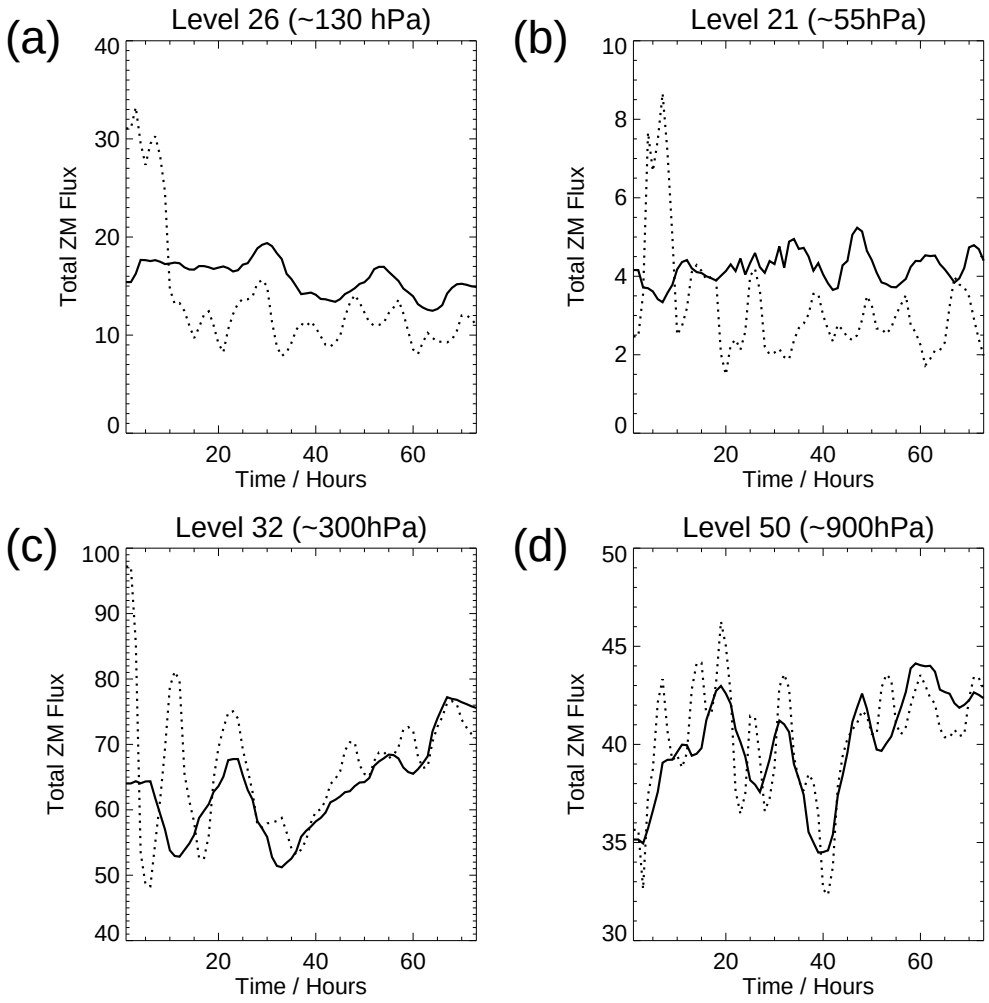

Figure 3.8: *Total absolute vertical momentum flux ($m^2 s^{-4}$) for the first three days of the nature run (solid line) and the non-nature run (dotted line) on model level (a) 26, near 130hPa, in the buffer zone, (b)21, near 55hPa, above the buffer zone, (c) 32, near 300hPa, below the buffer zone and (d) 50, near 900hPa, in the lower troposphere.*

In the lower troposphere (Figure 3.8 (d)) there is no evidence of a similar change in the magnitude of the total absolute momentum flux, although there is enhanced variability of this flux in the non-nature run.

Vertical momentum flux diagnostics can give an indication of the amount of gravity wave activity in a particular location and at a particular time in test runs of the nature and non-nature initial conditions. The results in this section suggest that the amount of vertical momentum flux, which is related to gravity wave activity, is very similar on tropospheric model levels in the nature and non-nature test runs. This suggests that much of the extra gravity wave activity introduced into the transition layer in the non-nature run propagates upward into the stratosphere and does not adversely affect the tropospheric flow.

3.4.2.3 Hayashi Analysis

Another method for analysing the propagation of gravity waves in the model is to run a Hayashi Analysis (Hayashi, 1982) on vertical velocity output from the model. Hayashi analysis computes the power of the vertical velocity timeseries as a function of zonal wavenumber and frequency of eastward propagating, westward propagating and stationary waves. Estimates of the power associated with short timescale oscillations in the vertical velocity can be made by analysing the output of the Hayashi analysis. As in the previous section it is assumed that any increase in the power of short timescale oscillation over the first three days of the model run is due to the increased gravity wave activity in the transition layer. An increase to the power of short timescale oscillations in the troposphere of the non-nature run compared to the nature run would be related to increased downward propagation of gravity waves in the non-nature run.

An example of the output of the Hayashi analysis is shown in figure 3.9. Figure 3.9 (a) shows the power of the 100hPa vertical velocity timeseries from the nature run. This shows that a large part of the power of this timeseries comes from low frequency and small wavenumber oscillations.

Figure 3.9(b) shows the power of the 100hPa vertical velocity timeseries from the non-nature run. There is much greater power on the 100hPa pressure surface in the non-nature run then in the nature run. This is expected as the 100hPa level lies in the transition layer in the non-nature run, where we expect a large increase in gravity wave activity at the start of the integration. Figure

3.9(b) also shows that there is an increase in power at higher frequencies. Oscillations with periods smaller than 1 day are likely to be gravity waves.

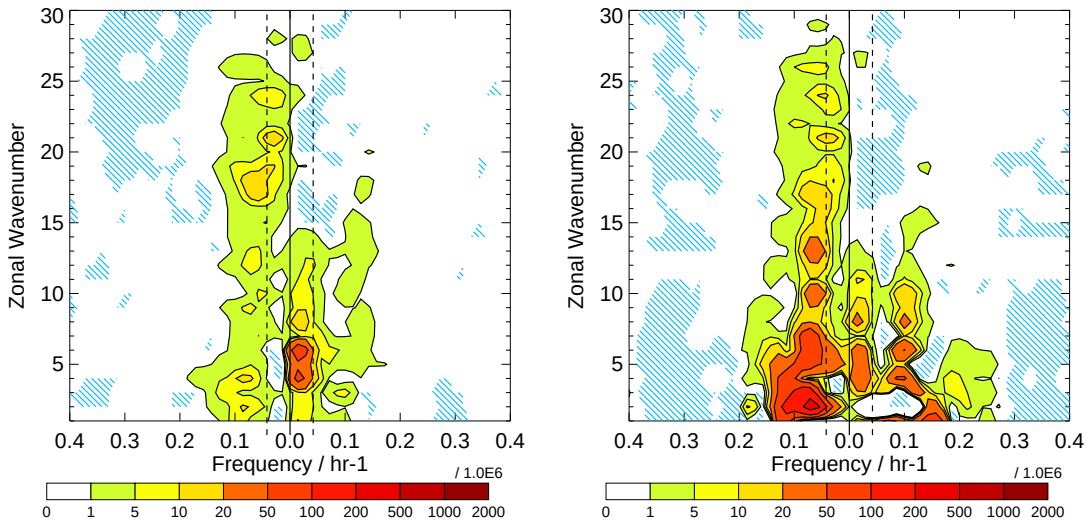

(a) Hayashi Analysis of Vertical Velocity at 60N on 100hPa surface from Nature Run

(b) Hayashi Analysis of Vertical Velocity at 60N on 100hPa surface from Non-Nature Run

Figure 3.9: *Power of 100hPa vertical velocity timeseries for different frequencies and wavenumbers. Negative frequencies indicate westward travelling components, positive frequencies indicate eastward travelling components. Blue shading shows regions which have negative power. In these regions the Hayashi analysis fails because the assumption that oscillations can be partioned into standing and travelling parts which are incoherent with each other is not true (Hayashi (1982),p.161). Dotted lines indicate frequency of oscillations equal to a period of 1 day.*

By performing a Hayashi analysis on the vertical velocity at a number of different pressure surfaces we can attempt to isolate the gravity wave activity throughout the model in the nature and non-nature runs. An estimate of the power associated with gravity waves on each level is made by summing the power for all wavenumbers with period less than one day.

Figure 3.10 shows the percentage change in the power associated with oscillations with period less than one day between the nature and non-nature runs. A positive change indicates an increase in the non-nature run. This figure shows a small percentage increase in the power at high frequencies in the stratosphere. In the troposphere there is very little change in the power at high frequencies. There is a small increase in westward propagating gravity wave activity at 60N. This can also be

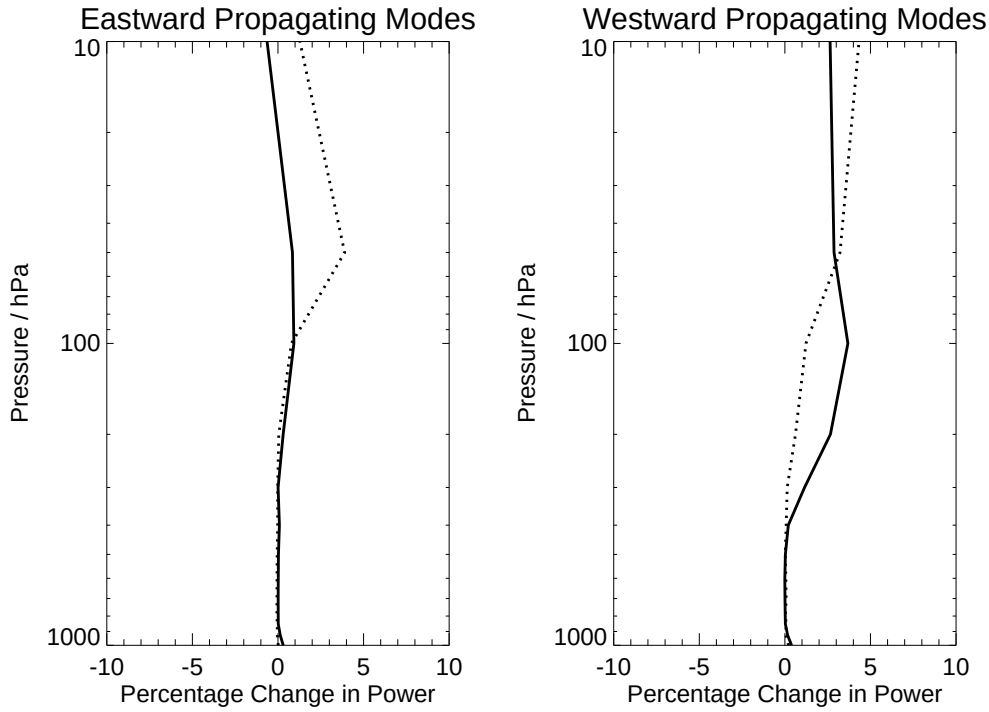

Figure 3.10: *Percentage change in power of oscillations with period less than one day between nature and non-nature runs. Solid lines show change at 60N, dotted lines show change at 40N.*

seen in the positive increase in vertical momentum flux in figure 3.7 (c).

This suggests that the increase in gravity wave activity in the transition layer in the non-nature run propagates upward into the stratosphere and very little of this wave activity propagates into the troposphere.

The wave diagnostics shown in the previous two sections suggest that although there is an increase in gravity wave activity in the non-nature run caused by imbalance in the buffer zone, most of this wave activity propagates upward into the stratosphere. Gravity wave activity in the troposphere in the non-nature run is similar to that in the nature run. The extra gravity wave activity introduced into the transition layer in the non-nature run does not adversely effect the tropospheric evolution because we hypothesis that most of the extra activity propagates upward into the stratosphere.

3.5 Summary of Experimental Design

This chapter outlines the design of medium-range ensemble forecasting experiments which examine the impact of the stratosphere on the troposphere during three 'downward propagation' events in the AO index.

Each experiment consists of two medium-range forecast ensembles. The experiments are run with the ECMWF IFS forecasting model which produces a good medium-range simulation of the stratospheric and tropospheric flow during stratospheric sudden warming events.

Experiments are run for 20 days with 30 ensemble members. Ensemble members are generated using the standard ECMWF ensemble generation technique based on singular vector analysis of the initial tropospheric state.

The two ensembles are referred to as the nature and non-nature ensembles. The ensembles are identical in all aspects apart from their initial conditions. The initial conditions in the nature run are taken from analysis. Initial conditions in the non-nature run are identical in the troposphere but have initial conditions in the stratosphere replaced by initial conditions from a separate analysis. The stratospheric initial conditions in the non-nature ensemble are chosen to have the opposite polarity in the AO index as the stratospheric initial conditions in the nature run.

CHAPTER 4

Results of medium-range ensemble forecasting experiments

4.1 Introduction

Chapter 2 found and characterised a relationship between the stratosphere and troposphere in a long AO amplitude dataset. This chapter shows the results from the experiments described in chapter 3. These experiments seek to further answer the questions posed in the introduction and to determine if the predictive relationship between the stratospheric and tropospheric AO timeseries in chapter 2 is related to a causal impact of the stratospheric state on the tropospheric flow.

4.2 Choice of Case Studies

Case studies are chosen to replicate 'downward propagation' events in the AO index. Three winters are selected for study. The time evolution of the AO index is shown in Fig. 4.1. In this and similar figures, negative (red) values indicate a weak stratospheric polar vortex displaced from the pole, positive (blue) values indicate a strong stratospheric polar vortex placed more symmetrically about the pole. Thick black lines indicate the dates chosen for the three case studies examined in this chapter.

The first case study is for a mid-winter stratospheric sudden warming event during winter 1998/1999 (Fig. 4.1(a)). This is an example of a "wave-two" sudden warming of the kind described by O'Neill (2003). The stratospheric sudden warming is shown by the large negative AO index values in the stratosphere in late-February. Following this event, the tropospheric AO index is biased toward negative values up to 60 days after the event.

The second case study is for a hybrid "wave-one/wave-two" type of mid-winter stratospheric sudden warming during winter 2001/2002 (Fig. 4.1(b)). The vortex was displaced from the pole

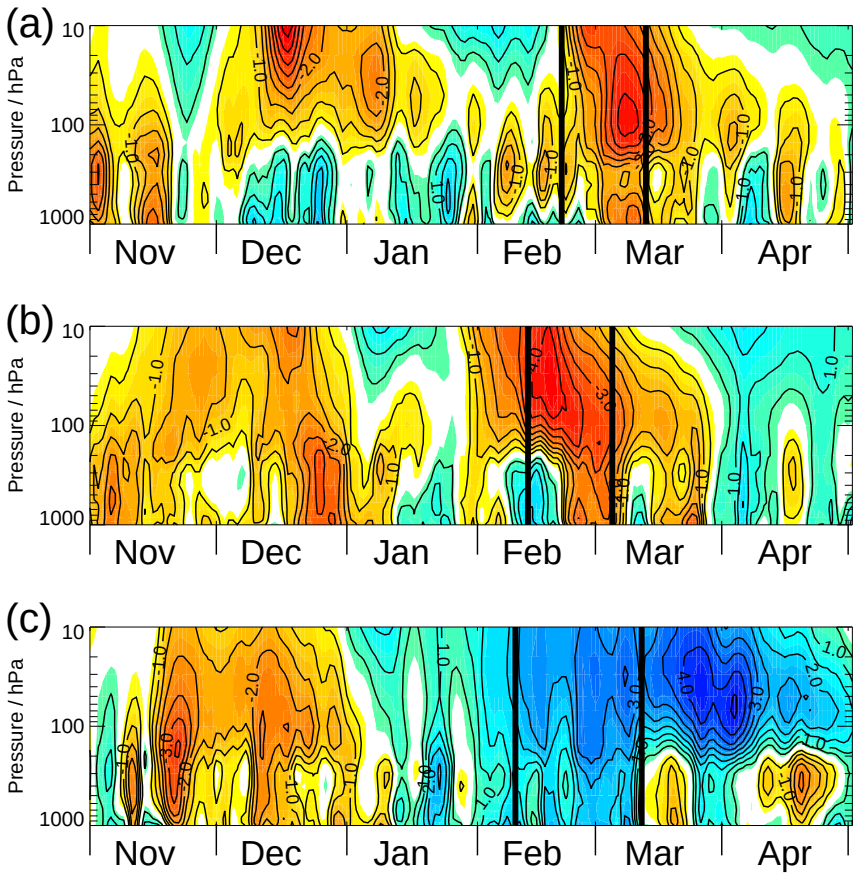

Figure 4.1: *AO Index for NH winter (a) 1998/1999, (b) 2000/2001 and (c) 1996/1997. Red and yellow colours show negative index or warm disturbed conditions. Blue and Green colours show positive index or cold disturbed conditions. Index between -0.5 and 0.5 is not shaded. Thick vertical lines show start and end of integration for each case study.*

and split into one large vortex and one small vortex. A second case study is included as a check on the robustness of results emerging from the first case study.

The third case study is for the opposite situation in which the stratospheric polar vortex was much stronger than normal during winter 1996/1997 (Fig. 4.1 (c)) Although there is no similar downward tilt in AO index values here as in case studies one and two, the AO index in the troposphere during February is biased toward positive values.

The case studies chosen for these experiments represent large departures of the AO index, and hence the stratospheric variability, from its climatological winter state. We chose to examine very

large amplitude stratospheric events to maximise the signal-to-noise ratio of our experiments. Data analysis suggests that the relationship between the stratosphere and troposphere is small and occurs on timescales greater than 10 days (chapter 2). On these timescales initial condition uncertainty is expected to be large. Typical root mean square spread of a 32 member ensemble forecast, using the ECMWF IFS system at T106 resolution, is 60m in the 1000hPa geopotential height field at 10 day lead time (Buizza et al., 1998). To determine a statistically significant impact of the stratosphere on the troposphere the largest amplitude stratospheric events should be examined.

4.3 Large scale changes in the Stratosphere-Troposphere system.

This section examines the large scale differences in the troposphere between the nature and non-nature runs. We use the AO Index diagnostic to characterise the large scale variability in the stratosphere and troposphere. A number of contentious issues surround the interpretation of the AO (see section 1.3.1.1). We use the AO index as a practical tool for examining the hemispheric scale flow in the stratosphere and troposphere.

AO index can be determined from the model integration by comparing geopotential height anomalies in the model against the AO patterns derived from analysed data. This is done by a least squares minimisation given by the formula:

$$min|Z(p,t) - AOI(p,t)\ Z(p)_{AO}|^2, \tag{4.1}$$

where Z(p,t) indicates geopotential height anomaly at a given pressure and time, AOI(p,t) indicates the AO Index at the same pressure and time and $Z(p)_{AO}$ indicates the signature of the AO at the same pressure.

To test whether the mean of the two distributions from the nature and non-nature ensembles are significantly different we use the student t-test (Wilks, 1995).

4.3.1 Case Study 1:Mid-winter stratospheric sudden warming 1998/99

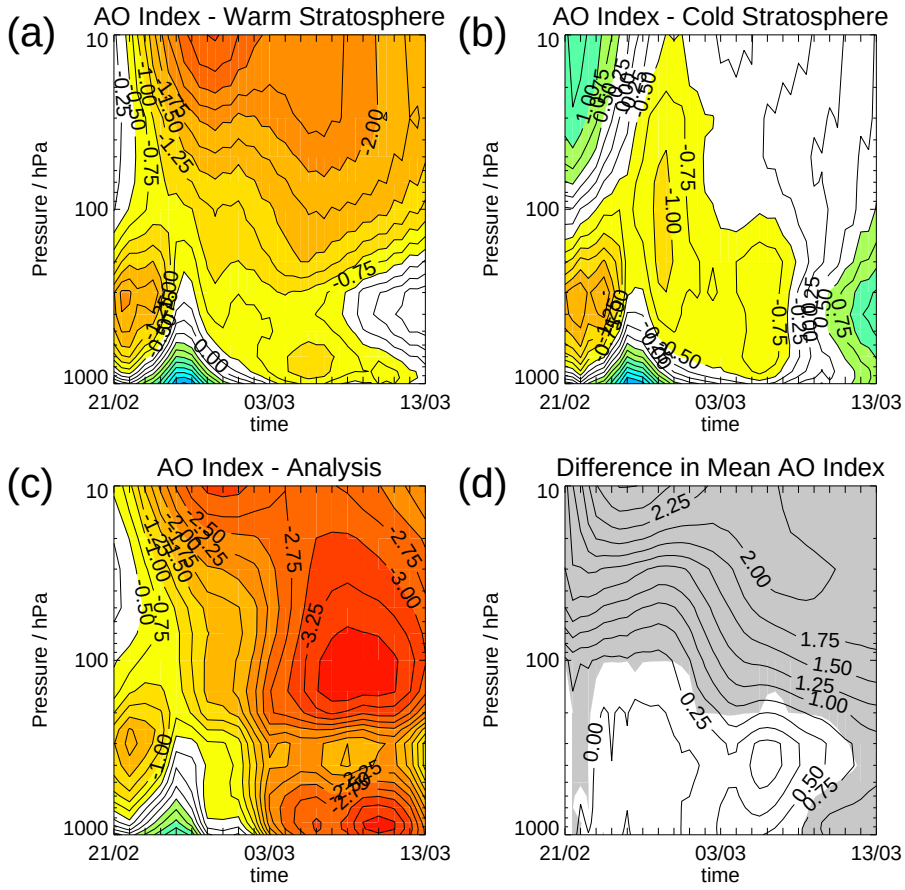

Figure 4.2: *AO Index versus pressure and time for Case Study 1. (a)Ensemble mean of nature ensemble (warm stratospheric initial condition), (b)Ensemble mean of non-nature ensemble (cold stratospheric initial conditions, (c)Derived from NCEP reanalysis (Baldwin and Dunkerton, 1999) (d)Difference between ensemble mean of nature run and ensemble mean of non-nature run (shading shows significant difference at 95 % confidence.)*

Figure 4.2(a) shows the ensemble mean AO Index of the nature ensemble. This shows the qualitative structure evident in the analysis (Figure 4.2(c)). However, the magnitude of the ensemble mean AO index in the lower troposphere in the later part of the run (08/03 - 13/03) is much less than in the analysis. This discrepancy is related to the increasing spread of the ensemble at this time. An ensemble mean in this case tends to smooth out large magnitude features present in individual members. The AO index in individual ensemble members (not shown) achieves similarly large values as shown in Figure 4.2 (c).

Figure 4.2(b) shows the ensemble mean AO index in the non-nature stratosphere case. The initial strong vortex conditions in the stratosphere present in this run are shown as blue colours in the stratosphere at initial time. The blue colours are rapidly replaced by white/yellow colours indicating a disturbance to the vortex. The vortex is being disturbed by the growth of an anticyclonic feature throughout the stratosphere which develops as planetary scale eddies penetrate upward from the troposphere. The stratosphere has some memory of its initial cold vortex state; its dynamical state is not exclusively determined by tropospheric disturbances. Therefore the evolution of the stratosphere is significantly different in the nature and non-nature runs at all times during the integration.

Figure 4.2(b) also shows a small difference in the ensemble mean AO index in the troposphere in the first three days of the run. Figure 4.2(d) shows that this difference is small but statistically significant. This difference is due to the adjustment of the surface pressure in the non-nature ensemble to the initial stratospheric divergence field in the non-nature ensemble (see section 3.4.1). The magnitude of the change caused by this adjustment process is very small. It seems reasonable to hypothesise that this process is not responsible for the large change to the AO amplitude seen toward the end of the run and the re-emergence of statistical significance in the difference fields.

The key result displayed in Fig. 4.2(b) shows that the tropospheric evolution is different in the nature and non-nature ensembles. The non-nature ensemble has a much stronger return to undisturbed conditions at the end of its evolution (15-20 days) than is shown in the warm ensemble.

The nature of this change over the ensemble can be examined by plotting histograms of the AO amplitude on the 1000hPa surface for different time periods throughout the run (Fig. 4.3). For the first 10 days of the run (Fig. 4.3 (a) and (b)) the distribution of the AO on the 1000hPa pressure surface is very similar in the nature and non-nature ensembles. As the run progresses the AO distribution in the nature ensemble moves toward negative values and increases its spread and the AO distribution of the non-nature ensemble remains close to zero and increases its spread (Fig. 4.3 (c) and (d)). By the end of the run the PDF of the tropospheric AO is shifted toward the mean AO in the stratosphere.

The difference between the runs is highlighted in Fig. 4.2(d). There is a difference in the ensemble mean AO index of 1.0 (non-dimensional units) over 15-20 days which is statistically significant.

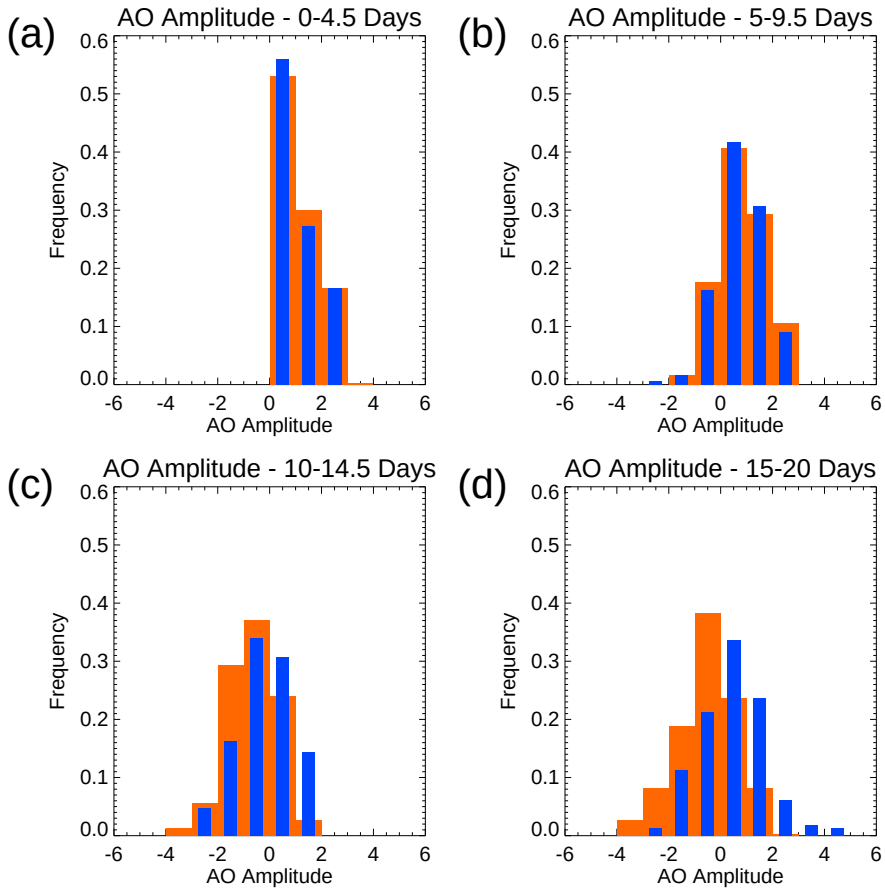

Figure 4.3: *Normalised histograms for AO index on 1000hPa surface for nature ensemble (red bars) and non-nature ensemble (blue bars) for four periods of the run (a) 0-4.5 days, (b) 5-9.5 days, (c) 10-14.5 days and (d) 15-20 days. Blue bars are plotted at half the appropriate width for comparison with red bars eg blue bar between 0.25 and 0.75 represents frequency of AO amplitudes between 0 and 1.0.*

The relationship between this difference and standard meteorological variables is noted in the section 4.4. The isopleths in Fig. 4.2(d) also show evidence of an apparent downward progression through the stratosphere toward the troposphere. In the troposphere differences in the AO index appear to occur almost simultaneously in common with the analysis.

We conclude that, in this case study, stratospheric initial conditions have a small but significant impact on the mean evolution of the troposphere. This change is statistically significant after approximately 15 days of the model integration. Broadly speaking the effect is in the sense that a stronger, colder stratospheric vortex induces a stronger zonal flow in the troposphere, though there are important regional effects which we discuss later.

4.3.2 Sensitivity tests

The sensitivity of tropospheric differences to the region over which changes to the initial conditions are made in the non-nature ensemble is investigated by running two further 30 member ensemble forecasts of Case Study 1. In the new ensemble forecasts changes to the stratospheric initial conditions are made above 40hPa (transition layer 40-80hPa) and above 10hPa (transition layer 10-40hPa). The difference between the ensemble mean AO index of these new runs and the nature ensemble is shown in Fig. 4.4. This figure should be compared to the differences between the nature and non-nature ensembles shown in Fig. 4.2 (d).

Making changes to the stratospheric initial conditions above 40hPa (Fig 4.4(a)) has a similar response in the troposphere to making changes to the stratospheric initial conditions above 80hPa (Fig. 4.2(d)). There are significant differences to the tropospheric flow after 15 days into the run which have typical sizes of 1.0 non-dimensional AO index.

In contrast making changes to the stratospheric initial conditions above 10hPa (Fig. 4.4(b)) does not have a similar response in the troposphere to making changes to the stratospheric initial conditions above 80hPa. Although there are similar downward tilting structures in the AO index difference through the stratosphere, the change to the tropospheric AO index is much smaller than when changes are made to the stratospheric initial conditions at 80hPa (0.25 non-dimensional AO index in the 10hPa case compared to 1.0 non-dimensional AO index).

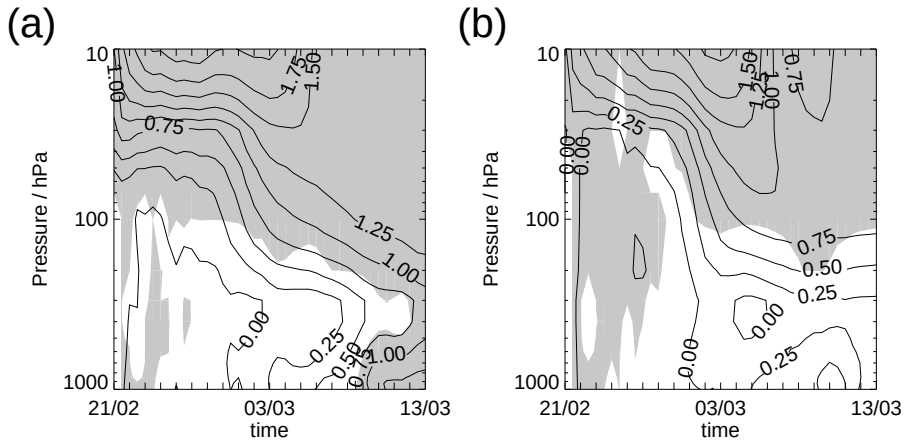

Figure 4.4: *Difference in AO Index versus pressure and time for sensitivity tests. (a) Changes to the stratospheric initial conditions made above 40hPa (transition layer 40-80hPa). (b) Changes to the stratospheric initial conditions made above 10hPa (transition layer 10-40hPa). Shading shows significant differences at 95 % confidence.*

This suggests that making changes to the lower stratospheric PV distribution has the most impact on the tropospheric evolution (as was suggested by the data analysis in chapter 2). The impact on the troposphere is relatively insensitive to the exact level at which changes are made to the stratospheric initial conditions, the impact on the troposphere, in AO terms, is very similar if changes to the stratospheric initial conditions are made above 80hPa or above 40hPa. For the remainder of experiments described in this chapter changes to the stratospheric initial conditions are made above 80hPa.

4.3.3 Case Study 2: Mid-winter stratospheric sudden warming 2001/02

As in case study 1 the evolution of the nature ensemble (Figure 4.5(a)) is qualitatively similar to the evolution of the AO in the analysis (Figure 4.5(c)). However the middle troposphere in particular has very low intensity toward the end of the run. Examination of individual members suggests that this is due to large variability in the middle troposphere between ensemble members.

Figure 4.5 (b) shows the ensemble mean of the non-nature ensemble. There is evidence here, as in case study 1, of a rapid disturbance of the vortex, which is evidence of strong impact of the tropospheric circulation on the stratosphere at this time.

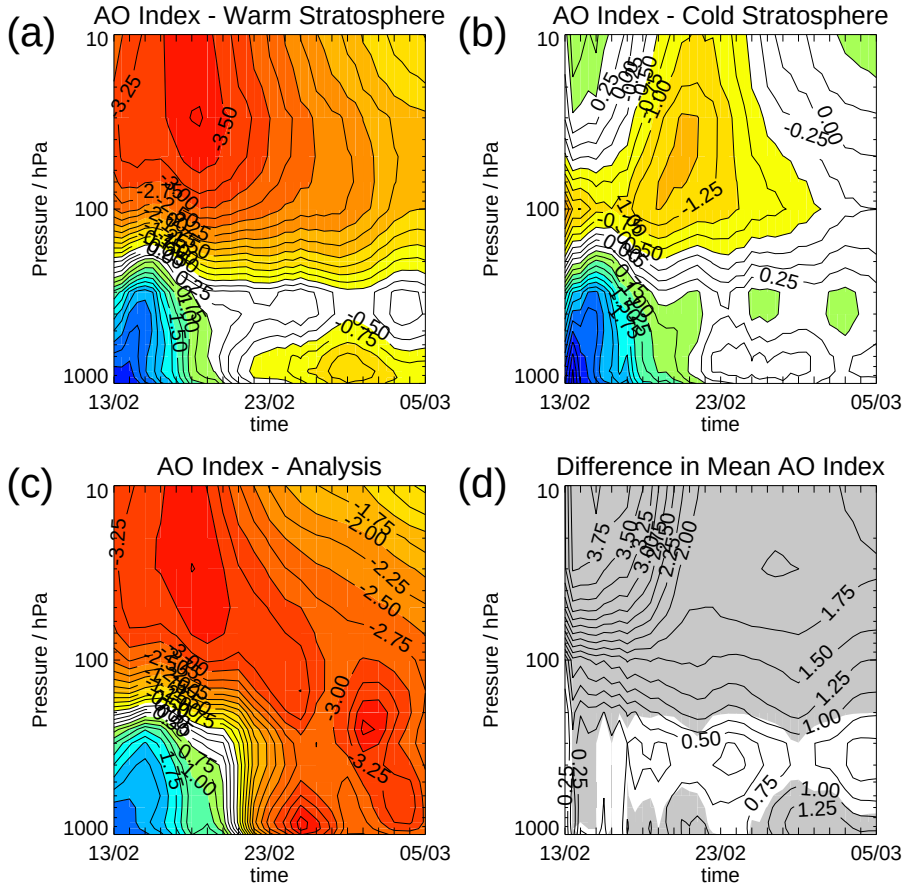

Figure 4.5: *AO Index versus pressure and time for Case Study 2. (a)Ensemble mean of nature ensemble (warm stratospheric initial condition), (b)Ensemble mean of non-nature ensemble (cold stratospheric initial conditions, (c)Derived from NCEP reanalysis (Baldwin and Dunkerton, 1999) (d)Difference between ensemble mean of nature run and ensemble mean of non-nature run (shading shows significant difference at 95 % confidence).*

As in the first case study there is a small but significant difference at the start of the run due to the hydrostatic adjustment. As before this difference is only significant over the first two days of the run. Sporadic patches of statistically significant difference between the runs occur between 3-20 days of the integration. The largest differences to the tropospheric flow occur between 15-20 days of the run as in the first case study (Figure 4.5(d)). This difference also has a similar magnitude to the difference in case study 1 (approx 1.25 non-dimensional AO Index). The apparent disconnect in the significance in the middle troposphere is related to the large variability in the timing of the differences in individual ensemble members (not shown).

4.3.4 Case Study 3: Strong polar vortex 1996/97

Conversely to the first two case studies in this case the initial conditions in the stratosphere in the nature run consist of a strong quasi zonally symmetric polar vortex and in the non-nature run consist of a weak, disturbed polar vortex.

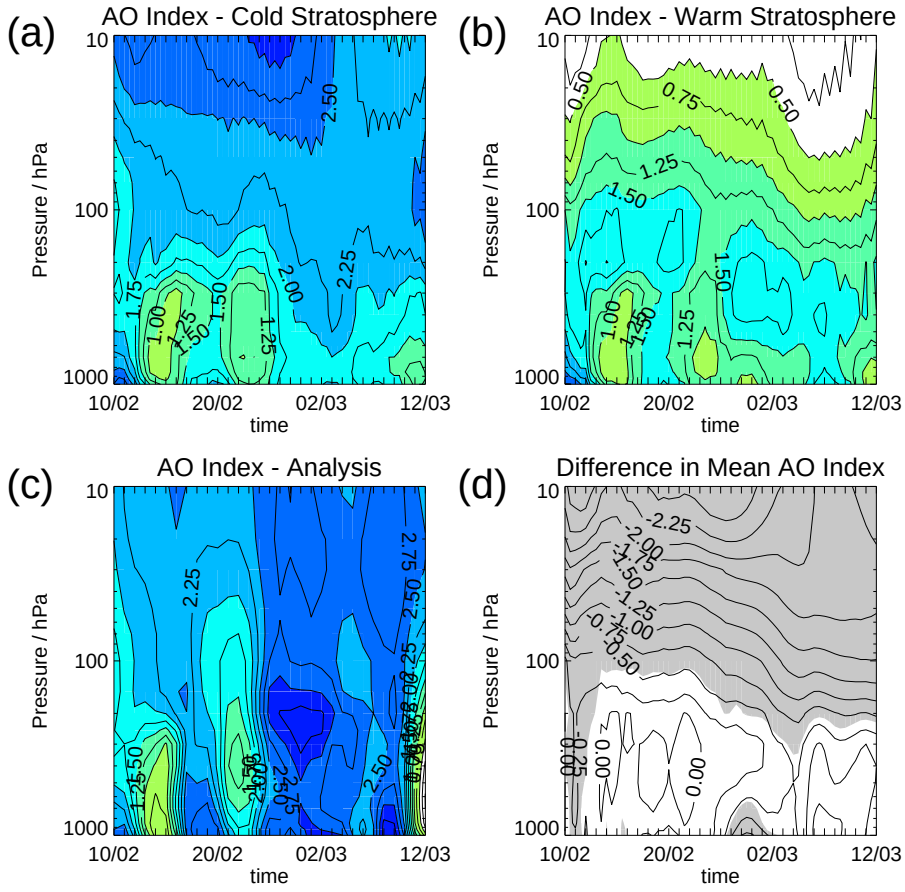

Figure 4.6: *AO Index versus pressure and time for Case Study 3. (a)Ensemble mean of nature ensemble (cold stratospheric initial condition), (b)Ensemble mean of non-nature ensemble (warm stratospheric initial conditions, (c)Derived from NCEP reanalysis (Baldwin and Dunkerton, 1999) (d)Difference between ensemble mean of nature run and ensemble mean of non-nature run (shading shows significant difference at 95 % confidence).*

Figure 4.6 (c) shows the AO index from analyses. The whole figure is dominated by blue colours indicating that the zonal flow is strong throughout the stratosphere and troposphere. There is no apparent 'downward propagating' anomaly from the stratosphere to the troposphere as in case

studies 1 and 2. As in the previous case studies the ensemble mean of the nature run (Fig. 4.6) has a similar evolution to the analysis.

Figure 4.6 (b) shows the ensemble mean AO index from the non-nature run. White colours in the stratosphere indicate that the polar vortex is more disturbed in the non-nature run than in the nature run. This difference is shown in Fig. 4.6 (d) and is statistically significant throughout the run.

The time evolution of the differences in the AO index in case study 3 is similar to the time evolution of the differences in case studies one and two, though of the opposite sign. In particular after 10-15 days the differences in the troposphere are of the same sign as the initial difference in the stratosphere; when a weaker zonal flow is imposed as an initial condition in the stratosphere there is weaker zonal flow 10-15 days later in the troposphere. A note of caution with this case is that the differences are not statistically significant at the 95% confidence level for the sample size of 30 ensemble members. The changes to the AO index in the lower troposphere become statistically significant at and below the 90% confidence level.

4.3.5 Results common to all case studies

- Stratospheric initial conditions in the model have an impact on the later evolution of the hemisphere-scale flow in the troposphere as measured by the AO index. The downward propagation of AO index signals from the stratosphere to the troposphere is not simply an apparent phenomenon resulting solely from different rates of evolution of dynamical processes in the two regions.

- In the AO index this link is represented as a change in the tropospheric AO towards the sign of the initial index of the stratospheric AO. In all three case studies such a change is evident after about 15 days. The change is statistically significant in all three case studies at at least the 90% confidence level.

- The gain in predictive skill of statistical models of the tropospheric AO which include stratospheric AO information (chapter 2) is not a statistical artifact but in part reflects a real impact of the stratospheric state on the tropospheric flow.

4.4 Dynamical Structure of tropospheric changes.

To further investigate the mechanism by which the stratospheric initial conditions have an impact on the troposphere we now examine changes to the tropospheric flow in more detail.

4.4.1 Changes in Geopotential Height

It is natural to start with geopotential height fields since such fields are used in constructing the AO index. We begin with an examination of the geopotential height difference in the troposphere between individual ensemble members. Each ensemble member in the nature and non-nature runs is generated using the same initial tropospheric perturbation. Any change to the evolution of the tropospheric flow is related to the changes to stratospheric initial conditions.

Although the difference between the stratospheric circulations in the two runs are on a large scale, as characterised for example by potential vorticity, differences in the troposphere occur on the synoptic scale. Figure 4.7 shows a single time slice 10 days into the run from ensemble member 3 of case study 1 in the nature and non-nature runs. Figure 4.7(b) shows the difference between the nature and non-nature runs. The horizontal scale of differences at one time slice and for one member is comparable to the typical size of synoptic scale, baroclinic instabilities. The differences in figure 4.7(b) can be directly traced to changes to the position or intensity of individual synoptic structures in figure 4.7 (c) and (d).

The question arises : “Are there statistically significant differences between synoptic systems in the two ensembles and where do these differences occur ?”

To isolate the synoptic systems we apply a 0-6 day high pass filter to the geopotential height at 300hPa. We then calculate the gridpoint by gridpoint standard deviation for each ensemble member and then calculate the ensemble mean. The standard deviation highlights the main storm track regions of the northern hemisphere.

Figure 4.8 (a), (c) and (e) shows the ensemble mean standard deviation of geopotential height at 300hPa in the nature run for the three case studies. In all three panels the storm track regions over the Atlantic and Pacific ocean basins are highlighted as regions of large standard deviation.

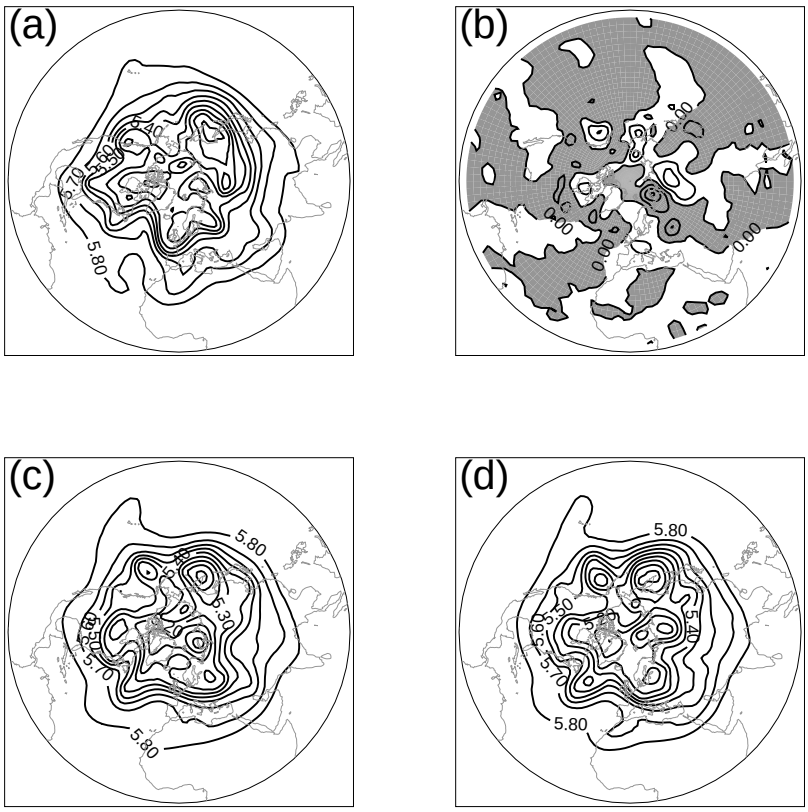

Figure 4.7: *Geopotential Height at 500hPa for ensemble member 3 of case study 1. (a) shows ECMWF analysis, (b) shows difference between nature and non-nature runs, shading indicates negative differences, contour interval is 100m (c) shows nature run and (d) shows non-nature run. All figures are for a single time slice 10 days into the run.*

Figures 4.8 (b), (d) and (f) show the difference in the ensemble mean standard deviation between the nature and non-nature runs in the three case studies. The statistical significance of the difference in standard deviation between two datasets can be determined with an f-test (Wilks,1995). Regions in which the standard deviation of the two runs is not significantly different at 95% confidence are not shaded.

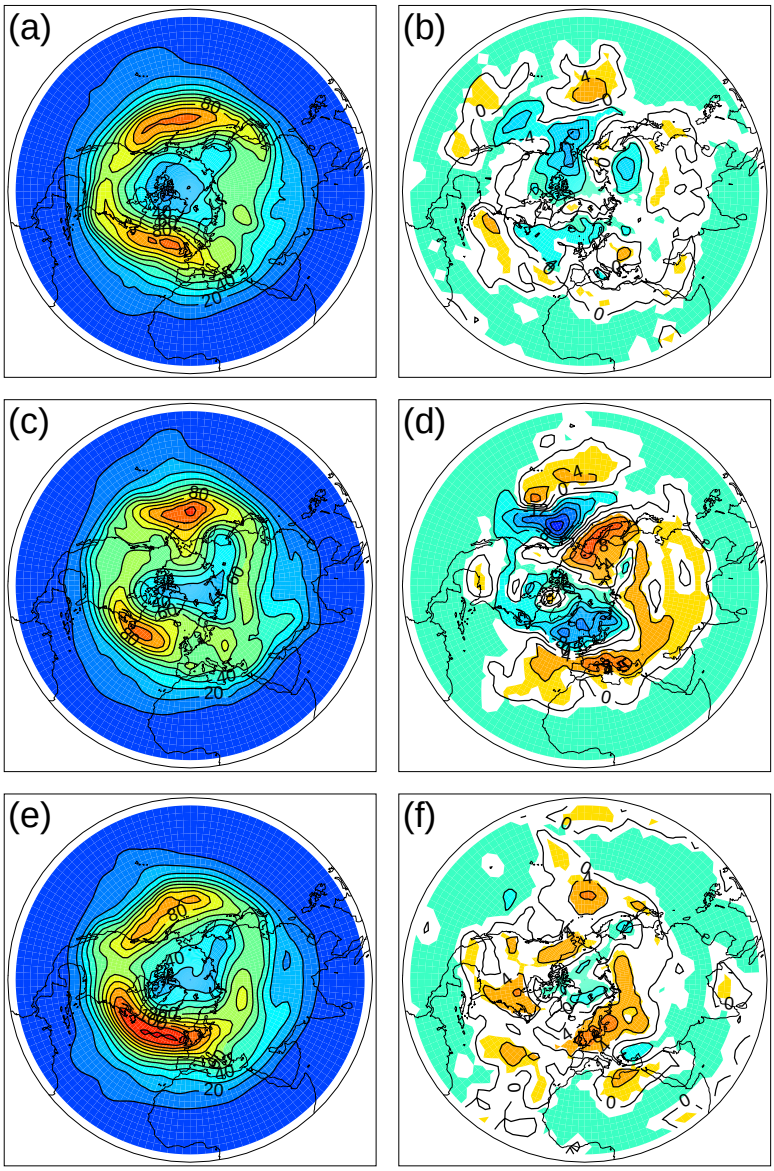

Figure 4.8: *Standard Deviation of high pass filtered 300hPa geopotential height field.(a) shows ensemble mean for nature run, case study one. (b) shows the difference between the nature and non-nature runs in case study one. Shading shows regions of standard deviation which are significant at 95 % confidence. Blue colours indicate standard deviation is larger in non-nature ensemble. Yellow and Red colours indicate standard deviation is larger in nature ensemble.(c) as (a) but for case study two, (d) as (b) but for case study two, (e) as (a) but for case study three, (f) as (b) but for case study one.*

4.4.1.1 Case Studies 1 and 2 (Stratospheric Vortex strengthened in non-nature run)

In case studies 1 and 2 the nature run has reduced synoptic timescale variability over the UK and Scandinavia and increased synoptic timescale variability over Southern Europe compared to the non-nature run. This corresponds to a southward shift of the storm track in the nature run as compared to the non-nature run. Both case studies show the same, statistically significant, southward shift of the storm track, but the differences are larger and show statistical significance over a wider area in case study 2. Such a shift corresponds to a change to the negative index of the so called North Atlantic Oscillation (NAO).

Although the differences between the nature and non-nature runs in the Pacific sector are of similar magnitude to those over the Atlantic sector the structure of these difference fields is not the same for both case studies.

4.4.1.2 Case Study 3 (Stratospheric vortex weakened in non-nature run)

In marked contrast to the previous two cases, in case study 3 the nature run has increased synoptic timescale variability over the UK and Scandinavia and reduced synoptic timescale variability over Southern Europe compared to the non-nature run. This corresponds to a, statistically significant, northward shift of the storm track in the nature run as compared to the non-nature run.

Over the Pacific the spatial pattern of the statistically significant differences to synoptic timescale variability in the nature and non-nature runs does not have an obvious interpretation in terms of the properties of the storm track.

4.4.2 Aggregate differences between nature and non-nature runs

In order to discern the aggregated impact of changes to synoptic scale systems on the tropospheric flow we average geopotential height differences both over the ensemble and over 5 day periods of the integration.

Figure 4.9 shows the difference in the ensemble mean between the nature and non-nature ensem-

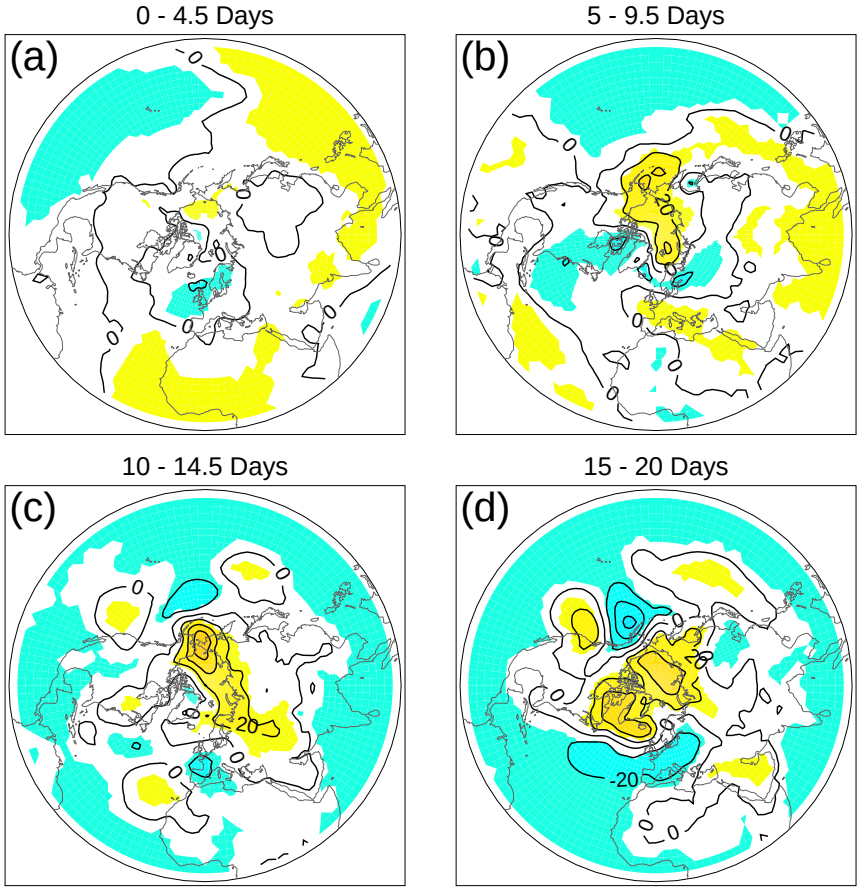

Figure 4.9: *Difference in Ensemble Mean Geopotential Height (nature-non-nature run) for case study 1. (a)Average between 0 and 4.5 days into run,(a)Average between 5 and 9.5 days into run,(a)Average between 10 and 14.5 days into run,(a)Average between 15 and 20 days into run. Yellow and Red colours indicate larger height in nature run. Blue colours indicate smaller height in nature run. Shaded regions shows difference at 95% is significant.*

bles in case study 1. Each panel shows a subsequent five day mean of the differences.

There are statistically significant differences to the mean geopotential height distribution between the nature and non-nature runs. The magnitude of the mean differences is around 20-40m. Compared to the nature run, geopotential heights in the non-nature run are smaller over the polar cap and larger over the Atlantic and Pacific ocean basins. In other words, strengthening the stratospheric polar vortex leads to lower geopotential heights over the polar cap on the 1000hPa pressure surface. Differences in the geopotential height are largest toward the end of the 20 day run.

The differences to the geopotential height map strongly onto the AO pattern and therefore are reflected by the change in the AO index in Fig. 4.2. There is no indication, however, that the differences depicted in Fig. 4.9 are part of an anomaly pattern of hemispheric extent, as is the AO pattern itself (cf Fig. 1.1) The anomaly structure between 15 and 20 days into the run is concentrated in the Atlantic and Pacific oceanic storm track regions. This is particularly true in the Atlantic sector where the difference would produce a strong signal in the North Atlantic Oscillation index.

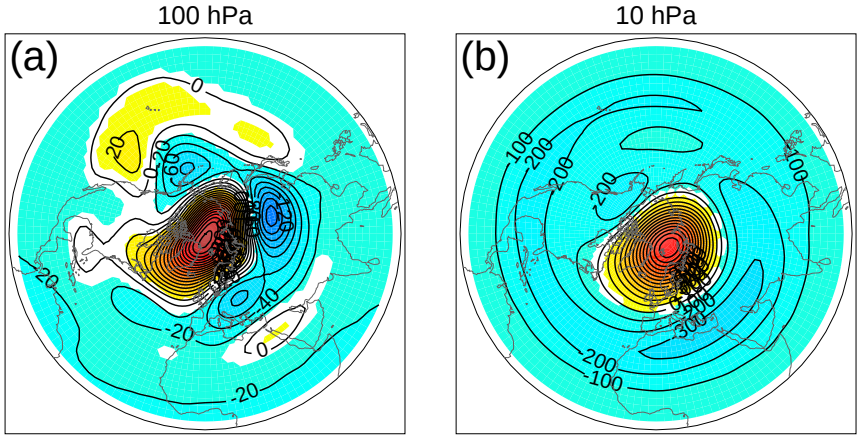

Figure 4.10: *Geopotential Height difference between nature and non-nature runs averaged between 15 to 20 days for case study 1 (a) on 100hPa surface and (b) on 10hPa surface. Yellow and Red colours indicate larger height in nature run. Blue colours indicate smaller height in nature run. Shaded regions shows difference at 95% is significant.*

In the stratosphere the aggregated differences between the nature and non-nature runs are of much larger, hemispheric scale, as shown for 100hPa and 10hPa in Fig. 4.10. We conclude, for case study 1, that the large scale differences between the nature and non-nature runs in the stratosphere do not lead to changes to the flow in the troposphere on the same large spatial scales. Rather they lead to more localised anomaly patterns which project onto the hemispheric AO. Similar conclusions can be drawn for the other two case studies.

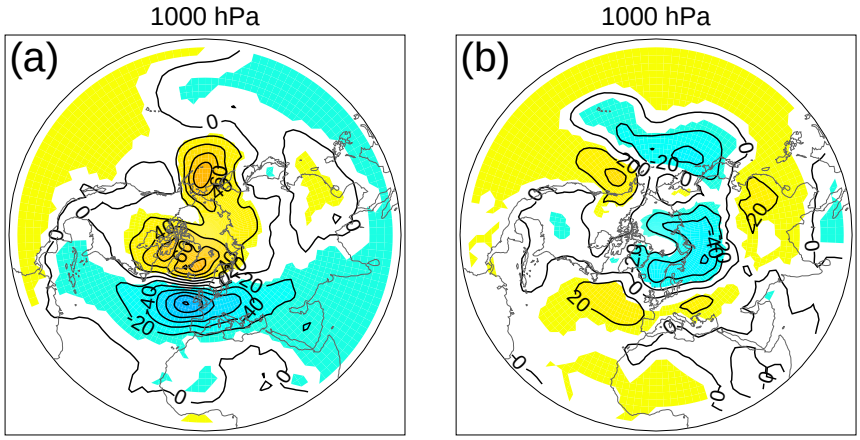

Figure 4.11: *Geopotential Height difference between nature and non-nature runs. Differences averaged between 15 and 20 days into run. (a) 1000hPa pressure surface Case Study 2, (b) as (a) for Case Study 3. Yellow and Red colours indicate larger height in nature run. Blue colours indicate smaller height in nature run. Shaded regions show difference is significant at 95% confidence.*

4.4.3 Comparison with other Cases

In case study 2, (qualitatively similar to case study 1 in that the polar vortex in the non-nature run is strengthened relative to the nature run) the near surface geopotential height difference fields (Fig. 4.11(a)) are very similar to the near surface geopotential height difference fields, in the Atlantic sector, in case study 1 (Fig. 4.9 (d)). In case study 3, (qualitatively opposite to case studies 1 and 2 in that the polar vortex in the non-nature run is weakened relative to the nature run) the near surface geopotential height fields have similar structure and magnitude to the geopotential height differences in the Atlantic sector, in case studies 1 and 2 but are of opposite sign.

In the Pacific sector, although there are statistically significant differences to the geopotential height field in all three case studies, there is not such a clear cut relationship between the three cases as there is for the Atlantic sector.

4.4.4 Lower Stratospheric Potential Vorticity Distribution

Differences to the stratospheric flow cause changes to individual synoptic systems in the troposphere. The aggregate effect of these differences has a strong signature in the North-Atlantic and a less obvious structure in the North-Pacific. We hypothesise that the changes to the tropospheric synoptic systems are related to the Potential Vorticity (PV) structure in the lower stratosphere.

Figure 4.12 shows an example of the difference in Potential Vorticity between the nature and non-nature ensembles in the first case study on the 500K isentropic surface. In the lower stratosphere the signature of a stratospheric sudden warming (nature run) in the PV distribution is a reduction in PV over the polar cap (north of 60N) and a corresponding (though not zonally symmetric) increase in PV in mid-latitudes

We define Atlantic and Pacific storm track regions as shown by the solid and dotted lines in Fig. 4.12. Averaging the difference in PV over these two regions gives an indication of the development of PV anomalies in the lower stratosphere over time. The difference to PV in the lower stratosphere in the three case studies is shown in Fig. 4.13

In case studies 1 and 2 (vortex strengthened in non-nature run) the largest differences to the PV distribution in the lower stratosphere are associated with the polar vortex. In case studies 1 and 2 this results in a reduction in the PV over the polar cap associated with the weakening of the polar vortex.In the Atlantic sector (Fig. 4.13 (a) and (c)) significant differences to the lower stratospheric PV extend down to 50°-60° N, in the Pacific sector the negative PV differences are confined further north (particularly in case study 2).

An indication of the location of synoptic variability in the troposphere during the evolution can be obtained by finding the mean latitude of maximum in the high pass standard deviation of geopotential height at 300hPa (cf Fig. 4.8). The solid and dotted lines show the mean position of the storm track in the Atlantic and Pacific sectors in each panel of Fig. 4.13. The storm track in the Atlantic sector is generally much further north than the storm track in the Pacific. Analysis of storm tracks (Hoskins and Hodges, 2002) in long reanalysis datasets shows that the Atlantic storm track extends much further to the north as it passes through the Norwegian Sea between Iceland and Scandinavia.

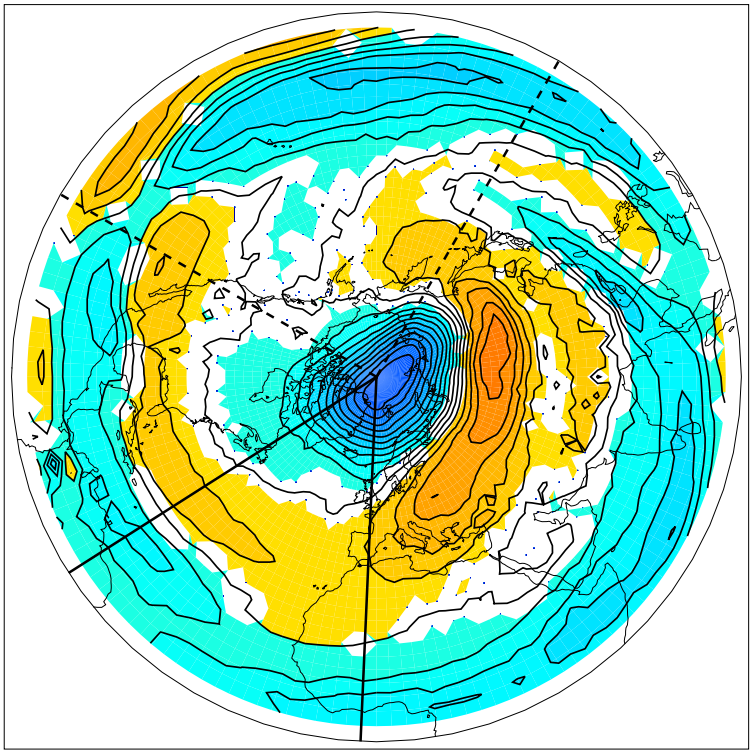

Figure 4.12: *Ensemble Mean difference (nature - non-nature runs) in Potential Vorticity on 500K isentropic surface average over 15-20 days of the integration. Difference is not significant at* 95% *confidence in regions which are not shaded. Blue colours indicate negative differences (smaller potential vorticity in nature ensemble), Yellow and Red colours indicate positive differences (larger potential vorticity in nature ensemble). Solid lines indicate region defined as Atlantic sector, dotted lines indicate region defined as Pacific sector.*

In case study 3 (Fig 4.13 (e) and (f)) the largest differences to the PV distribution in the lower stratosphere are positive and associated with the strengthened polar vortex in the nature run. As in case studies 1 and 2 the differences to the PV associated with the polar vortex extend further south in the Atlantic sector.

The influence of the stratosphere on tropospheric flow is stronger in the Atlantic sector due to close proximity of the tropospheric storm track and the lower-stratospheric polar vortex in the Atlantic sector.

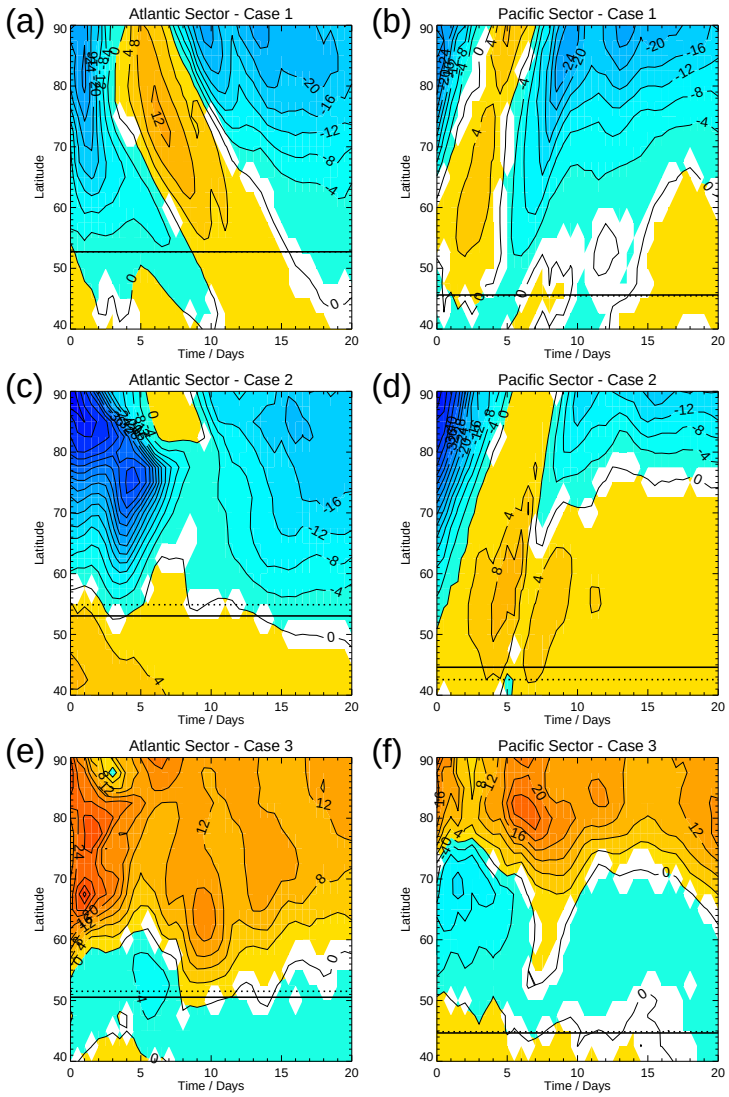

Figure 4.13: *Ensemble Mean difference (nature - non-nature runs) in Potential Vorticity on 500K isentropic surface averaged over Atlantic and Pacific sectors. Difference is not significant at* 95% *confidence in regions which are not shaded. Blue colours indicate negative differences (smaller potential vorticity in nature ensemble), Yellow and Red colours indicate positive differences (larger potential vorticity in nature ensemble). Solid line shows mean position of storm track in nature ensemble, dotted line shows mean position of storm track in non-nature ensemble. (a) shows mean over Atlantic sector case study 1, (b) shows mean over Pacific sector case study 1, (c) as (a) but case study 2, (d) as (b) but case study 2, (e) as (a) but case study 3, (f) as (b) but case study 3.*

4.5 Impact on Forecast Skill

Sections 4.2 and 4.3 demonstrated that there is a statistically significant difference in the tropospheric evolution when changes are made to the stratospheric initial conditions. In this section some simple forecast skill diagnostics are calculated with the three case studies to determine the impact on forecast skill of the stratospheric initial conditions.

We assess the skill of the forecast fields against the actual outcome using the Anomaly Correlation Coefficient (ACC, Jolliffe and Stephenson (2003)) defined as:

$$ACC = \Sigma_{i=1}^{n} \frac{(\hat{x}_i' - \overline{\hat{x}}')(x_i' - \overline{x}')}{n s_{\hat{x}'} s_{x'}} \tag{4.2}$$

where:
$\hat{x}_i'$ - is the forecast anomaly (i.e. difference between forecast and climatology) at each gridpoint i
$\overline{\hat{x}}'$ - is the mean of the forecast anomalies
s - is the standard deviation of either the forecast or analysed field
n - is the number of gridpoints

The Anomaly Correlation Coefficient is frequently used as a measure of a model's forecast skill. Typically a model is regarded as having no useful skill when its anomaly correlation coefficient is below 0.6. The anomaly correlation for a number of forecast lead times is calculated for each of the ensemble members in the three case studies. The mean of the ACC for the ensemble members with correct initial conditions (nature runs) and for those with incorrect initial conditions (non-nature runs) is taken.

Figure 4.14 shows the ACC for 500hPa and 1000hPa. Dots indicate that there is a significant difference in the ACC when incorrect stratospheric initial conditions are used. On timescales greater than 7 or 8 days, the ensemble members with the correct stratospheric initial conditions have a much increased ACC compared to those with incorrect stratospheric initial conditions. For most of the integration the difference in ACC throughout the lower troposphere is statistically

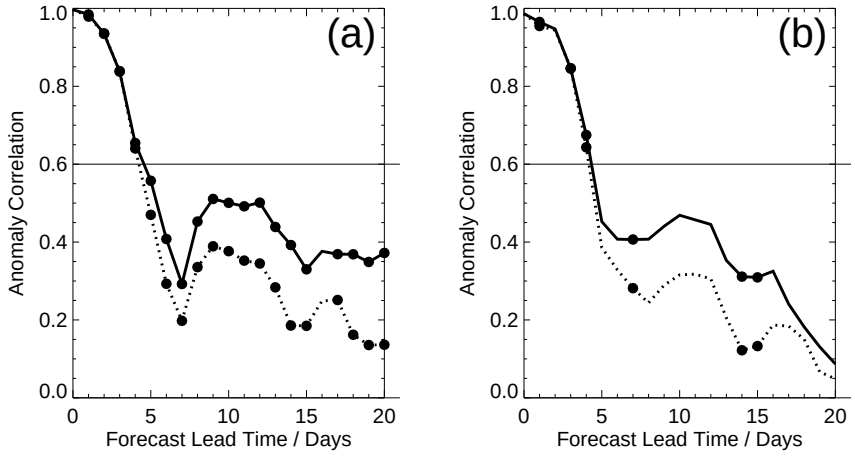

Figure 4.14: *Pooled anomaly correlation for all case studies. Solid line shows anomaly correlation for runs with correct stratospheric initial condition, dotted line shows anomaly correlation for runs with wrong stratospheric initial condition. Circles show forecast times where there is a significant difference in the anomaly correlation between the two sets of runs. (a) shows 1000hPa, (b) shows 500hPa.*

significant. In particular after about 12 days there is a 50 % improvement in ACC when the correct stratospheric initial conditions are used.

4.6 Conclusions

In chapter 2 a relationship between the stratosphere and troposphere in a long AO amplitude dataset was determined. The character of this relationship were:

- Timescale 10-45 days.
- Largest during the winter season (particularly February and March)
- Largest between the lower stratosphere / upper troposphere and the surface (50-250hPa)
- Present in all periods of the data

Data analysis, however cannot show a causal link exists between the stratosphere and troposphere (ie if a change to the stratospheric circulation would have an impact on the troposphere). This chapter further investigated the character of this relationship and its mechanism.

Experiments were performed with the ECMWF IFS numerical weather prediction model. This model has high horizontal and vertical resolution in the stratosphere and troposphere. It also has an operational system for generating large ensemble forecast by varying tropospheric initial conditions. This enables us to estimate the statistical significance of changes to the tropospheric circulation in response to variations in the stratospheric initial conditions.

The primary conclusions of this chapter are,

- A change in the initial state of the stratosphere results in a statistically significant change in the troposphere on time-scales relevant to medium-range weather forecasting (greater than about 10 days).
- The changes in the Arctic Oscillation (AO) index in the troposphere are positively correlated with the preceding changes in the AO index in the stratosphere. Thus, an increase in the stratospheric AO index (strengthening the stratospheric polar vortex) leads to an increase in the AO index near the surface.
- Changes to the tropospheric flow occur on typical synoptic scales and represent changes to the propagation or intensity of individual synoptic systems. The typical size of these differences is 100-200m in the 1000hPa geopotential height.
- Averaging these differences over ensemble members and over a number of timesteps reveals the aggregated impact of changes to tropospheric, synoptic-scale systems. The averaging reveals a coherent spatial structure which is closely tied to the tropospheric storm-tracks, particularly in the Atlantic sector. The typical size of aggregated differences is 20-40m.
- Comparison of the skill score of tropospheric forecasts with correct and incorrect stratospheric initial conditions shows that the stratospheric initial conditions have a statistically significant effect on the skill of tropospheric forecasts. On extended-range timescales (greater than 10 days) the ensemble mean anomaly correlation coefficient of tropospheric forecasts can be increased by as much as 50%, from 0.2 to 0.4, by the inclusion of correct

stratospheric initial conditions. Although it is unlikely that a modern numerical weather prediction system would have errors in the stratospheric initial state as large as the changes we have made in our experiment, nevertheless stratospheric forecasts can have large errors, for example when the polar vortex fails to split in a wave-two type warming. Our results show that such an error in the stratospheric forecast could impact the troposphere in such a statistically significant way.

The conclusions of this chapter are broadly consistent with the conclusions of chapter 2. That is to say that a relationship between the lower stratosphere and the troposphere on timescales greater than 10 days is revealed. The choice of case studies in this chapter were guided by the results of chapter 2 in that all three of the cases examined here involved large departures of the stratospheric state from its climatological norm which took place during February and March. Further case studies might examine the relationship for smaller departures of the stratospheric state from its climatology and at other times during the winter season.

Combining the conclusions of this chapter with those of chapter 2 it is possible to answer three of the four questions posed in the introduction. The lower stratospheric state has an impact on the tropospheric flow. This chapter demonstrated that this is a causal link, ie making a change to the stratospheric initial conditions has an impact on the future tropospheric evolution. This chapter has shown that the quantitative impact on the tropospheric flow is relatively small. Typical changes to the tropospheric geopotential height field are around 100-200m (see Fig. 4.7) when changes of the order 500-750m (see Fig. 4.10) are made to the stratospheric initial conditions. In both chapter 2 and in this chapter using correct stratospheric information in tropospheric forecasts improved the skill of those forecasts.

The remaining question posed in the introduction which remains unanswered concerns the mechanism by which the stratosphere impacts the troposphere. The results in this chapter have shown that the impact of the stratosphere on the troposphere in individual ensemble members is dominated by synoptic scales. When averages are taken over the ensemble and over a number of days of the model integration differences aggregate into large scale anomalies which map onto the AO structure, particularly in the Atlantic sector.

What is not clear from the results in this chapter is exactly what role the synoptic systems play in this link. The results in this chapter could be interpreted in two ways.

- The troposphere adjusts geostrophically and hydrostatically, on large spatial scales, to the large-scale features in stratospheric PV distribution. Synoptic scales in the difference fields of the model integrations are noise on this large-scale difference.
- Individual tropospheric synoptic systems respond non-linearly to the stratospheric PV distribution. This small-scale adjustment is an important intermediate step in the interaction between the large-scale lower stratospheric PV anomalies and the eventual time and ensemble averaged change to the tropospheric flow.

In the next chapter PV inversion techniques are used to try and differentiate between these possibilities.

CHAPTER 5

Investigating the mechanism

5.1 Introduction

Chapter 4 described numerical modelling experiments in which changes to the stratospheric circulation were shown to impact upon the tropospheric circulation. In this chapter experiments are conducted to attempt to better understand the mechanism for this impact. In particular the importance of small-scale synoptic features in this process is investigated using a hemispheric PV inverter. By careful design of PV inversion experiments the instantaneous geostrophic and hydrostatic adjustment of the troposphere to the lower stratospheric PV distribution (relative to a defined reference stratospheric PV distribution) can be calculated. There are a number of studies in the literature which have determined that there is a significant tropospheric adjustment to the lower stratospheric PV distribution (Hartley et al., 1998; Black, 2002).

If the spatial pattern of the tropospheric adjustment in the nature model run is similar to the aggregated differences to the tropospheric flow between the nature and non-nature ensembles this would suggest that the differences to the troposphere can be understood as a large-scale geostrophic and hydrostatic adjustment processes. If the spatial pattern of the tropospheric adjustment in the nature model run is different to the aggregated differences to the tropospheric flow between the nature and non-nature ensembles this would suggest that the mechanism for the influence of the stratosphere on the troposphere involves a more complicated, possibly non-linear interaction between the lower stratospheric PV distribution and tropospheric synoptic systems.

If the impact of the stratosphere on the troposphere can be understood in terms of a large scale tropospheric adjustment to the stratospheric PV distribution all three of the mechanisms proposed in the introduction could be responsible for this adjustment, wave reflection, critical line descent and the more general hydrostatic and geostrophic adjustment mechanism proposed by Ambaum and Hoskins (2002) are all inherently large-scale processes and would be captured by PV inversion.

If, however small-scale synoptic systems in the troposphere are important then none of the proposed mechanisms are fully capable of explaining the influence of stratospheric initial conditions on the troposphere and an entirely different mechanism is required.

In common with this approach a number of questions can be asked about the adjustment of the tropospheric flow to the stratospheric PV distribution.

- **Can differences to the tropospheric flow be explained entirely in terms of a balanced geostrophic and hydrostatic adjustment to the stratospheric PV distribution ?** Are the differences to individual synoptic systems seen in the model run important for understanding the impact of the stratosphere on the troposphere ?

- **How important is the middle stratosphere in understanding the adjustment of the troposphere ?** Black (2002) states that PV anomalies in the lower stratosphere (below 30hPa) contribute most to the adjustment of the troposphere in an inversion of a mean AO composite PV distribution, is this also the case at a particular time from the model integration ?

- **Do particular parts of the tropospheric flow adjust preferentially to the stratospheric PV distribution ?** Many of the previous studies in the literature have shown that the impact of the stratosphere on the troposphere has a structure similar to the AO. Is this because the troposphere adjusts preferentially to the stratospheric PV distribution over the centres of action of the AO?

- **Is there a particular time during the model integration at which the adjustment of the troposphere to the stratospheric PV distribution is larger than at other times ?** AO index diagnostics of the ensemble experiments showed that significant changes to the tropospheric flow occur after 15 days of the run (Fig. 4.2). If the mechanism for the impact of the stratosphere on the troposphere is through large scale adjustment of the troposphere to the stratospheric PV distribution, then this adjustment should be considerably different 15 days into the integration compared to the beginning of the run.

5.2 Experimental Design

All the experiments described in this chapter follow the same basic experimental design. The adjustment of the troposphere to a particular stratospheric PV distribution is determined by comparing the inverted tropospheric flow from two separate PV distributions.

- The PV distribution which we are investigating. This PV distribution is referred to as the **Nature State**. Inversion of this PV distribution is referred to as the **Nature Inversion** .
- A PV distribution which has the same tropospheric fields as the nature state but a different reference PV distribution in the stratosphere. The PV distribution is referred to as the **Reference State** . Inversion of this PV distribution is referred to as the **Reference Inversion** .

Inversion of the two PV distributions produces two separate tropospheric flow fields. The inverted fields in the nature inversion will be different to the tropospheric fields in the model because they represent the hydrostatically and geostrophically balanced part of the tropospheric flow in the model. Differences in the tropospheric flow fields can be attributed to the adjustment of the tropospheric flow to the stratospheric PV distribution in the first inversion (relative to the chosen stratospheric reference state) because only the stratospheric PV is different in the two PV distributions.

We assume a division can be made between the stratosphere and the troposphere on the 400K isentropic surface. This is consistent with a definition of the stratosphere consisting entirely of the "overworld" (Hoskins, 1991) and a definition of the troposphere which incorporates the "middleworld" and "underworld". Making changes to the PV distribution only in the "overworld" ensures that no changes are made to the tropospheric PV distribution at any latitude.

In the context of this setup it is important to understand the way in which PV inversion techniques are used in this chapter. Figure 5.1 shows schematically how the model integration can be understood in terms of the PV inversion experiments.

At each timestep of the model integration the model state (expressed by the PV distribution) in the nature run (the red and yellow boxes) can be compared to a reference PV distribution using

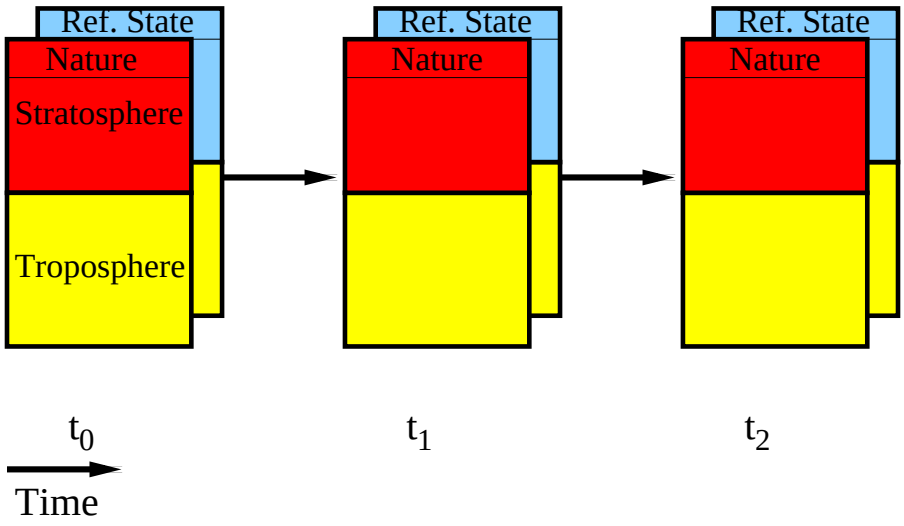

Figure 5.1: *Schematic showing how PV inversion is used in this chapter. Coloured boxes represent the state of the model in the stratosphere and troposphere at a particular point in the model integration. Red and Blue boxes represent the PV distribution in the stratosphere, yellow boxes represent the PV distribution in the troposphere. Each set of boxes represent a timestep of the model. At each timestep the front, red-yellow box represents the state of the nature run, the back blue-yellow box represents a reference PV distribution. The reference PV distribution has an identical PV distribution in the troposphere to the nature run and a different reference PV distribution in the stratosphere. Arrows indicate a timestep of the model, which represents solving the model equations. PV inversion techniques can be used to compare the adjustment of the troposphere to anomalies in the nature stratospheric PV distribution relative to the chosen reference state. It cannot be used to understand the evolution from one set of boxes to another (here the model equations are required).*

the PV inverter. By comparing the difference in flow fields in the troposphere, the instantaneous, balanced impact of the stratospheric flow in the nature run, compared to the specified reference state can be computed. The choice of the reference state is somewhat arbitrary, but it is natural to choose a zonally symmetric, undisturbed state. PV inversion techniques alone are not able to determine the evolution of the differences to the tropospheric flow in the model. This can only be computed from the model equations.

The results presented here also make use of a new, almost hemispheric inverter of the full Rossby-Ertel PV. The studies of Hartley et al. (1998) and Black (2002) used a much simpler quasi-geostrophic PV inverter. The inverter was written by Paul Berrisford (CGAM, Dept. of Meteorology, Univ. of Reading) and has been shown to be accurate in determining the hemispheric scale flow (Berrisford,*Pers. Comm.*)

5.3 Description of Inverter

The methodology used to construct the inverter is similar to Bleck (1973) but uses an extended hemispheric domain. The PV inversion problem is formulated in isentropic coordinates.

PV is defined as

$$P = (f + \zeta_\theta)\left(\rho\frac{\partial z}{\partial \theta}\right)^{-1} \tag{5.1}$$

where:

P - is PV

θ - is potential temperature

ζ_θ - is relative vorticity on an isentropic surface

ρ - is air density

z - is geopotential height

The other variable used in the formulation is the Montgomery Streamfunction.

$$M = gz + C_p T \tag{5.2}$$

where:

M - is the Montgomery streamfunction

T - is temperature

The hydrostatic relation can be expressed in terms of Montgomery Streamfunction as.

$$\frac{\partial M}{\partial \theta} = c_p \left(\frac{p}{p_0} \right)^{\kappa} = \frac{c_p T}{\theta} \tag{5.3}$$

Therefore

$$M = gz + \theta \frac{\partial M}{\partial \theta} \tag{5.4}$$

It follows that Montgomery Streamfunction is related to $\partial z / \partial \theta$ by

$$\frac{\partial z}{\partial \theta} = -\frac{\theta}{g} \frac{\partial^2 M}{\partial \theta^2} \tag{5.5}$$

and to ρ by

$$\rho\theta = \frac{p_0}{R}\left(\frac{\partial M/\partial\theta}{C_p}\right)^{C_v/R} \tag{5.6}$$

where:

p_0 - is a reference pressure surface

Inserting 5.5 and 5.6 into equation 5.1 gives

$$P\frac{p_0}{2\Omega\sin\phi Rg}\left(\frac{\partial M/\partial\theta}{C_p}\right)^{C_v/R}\frac{\partial^2 M}{\partial\theta^2} + \frac{\zeta_\theta}{f} = -1 \tag{5.7}$$

The isentropic relative vorticity on the sphere is given by

$$\zeta_\theta = \frac{1}{a\cos\phi}\left(\frac{\partial v}{\partial\lambda} - \frac{\partial(u\cos\phi)}{\partial\phi}\right) \tag{5.8}$$

where:

u - is zonal velocity

v - is meridional velocity

a - is the radius of the earth

ϕ - is latitude

λ - is longitude

The balance condition used in the inverter is geostrophic balance, this can be expressed as

$$fu = -\frac{1}{a}\frac{\partial M}{\partial\phi}; fv = \frac{1}{a\cos\phi}\frac{\partial M}{\partial\lambda} \tag{5.9}$$

By substituting 5.8 and 5.9 into 5.7 we arrive at the PV inversion equation for three dimensional

geostrophic flow.

$$P\,\frac{p_0}{2\Omega\sin\phi Rg}\left(\frac{\partial M/\partial\theta}{C_p}\right)^{(C_v/R)}\frac{\partial^2 M}{\partial\theta^2} + \frac{1}{\Omega^2 a^2}\left(\frac{1}{\sin^2 2\phi}\frac{\partial^2 M}{\partial\lambda^2} + \frac{1}{2\sin 2\phi}\frac{\partial}{\partial\phi}\left(\frac{cos\phi}{\sin\phi}\frac{\partial M}{\partial\phi}\right)\right) = -1 + R_d \tag{5.10}$$

where:
R_d is a residual from the iteration procedure

Equation 5.10 is the equation used in the inverter. If P is known then M is the only other unknown in the equation and so M can be determined by an iterative inversion procedure provided suitable boundary conditions are specified. The iteration procedure is as follows.

1. Input initial P and an initial guess of M to the inverter
2. Calculate non-linear term ($\frac{\partial M}{\partial\theta}$) on l.h.s. of Eq. 5.10. This leaves a linear problem where the coefficients of M on the l.h.s. are known.
3. Solve the resulting system of simultaneous linear algebraic equations using the Strongly Implicit Procedure in the NAG library
4. Update the non-linear term and repeat from step 3 until the solution converges. The convergence criteria used here is that the residual in Eq. 5.10 (R_d) is less than 10^{-10}.

5.3.1 Boundary Conditions

To solve equation 5.10 horizontal and vertical boundary conditions are required.

In the horizontal the equation is solved on a periodic grid. This is shown in Fig. 5.2. The inverter uses this grid because an appropriate hemispheric solver for the inversion equation (Eq. 5.10) was not available. The grid has a resolution of 5.625 °in the longitude and latitude directions. This grid has three horizontal boundaries.

1. At the pole. This boundary is simple as cos ϕ is zero at the pole.

2. On a latitude circle close to but not on the equator, in this case 5.625 °N. Montgomery streamfunction is specified on this latitude circle.

3. At the edge of the periodic grid. M is specified on the periodic boundary. It would not be physical to fix M on the periodic boundary and this may affect the inversion solution. Therefore it is necessary to implement a further procedure in the iteration which changes the position of the periodic boundary at the end of each iterative step. This method has been shown to produce physically realistic solutions (Berrisford, *Pers. Comm.*)

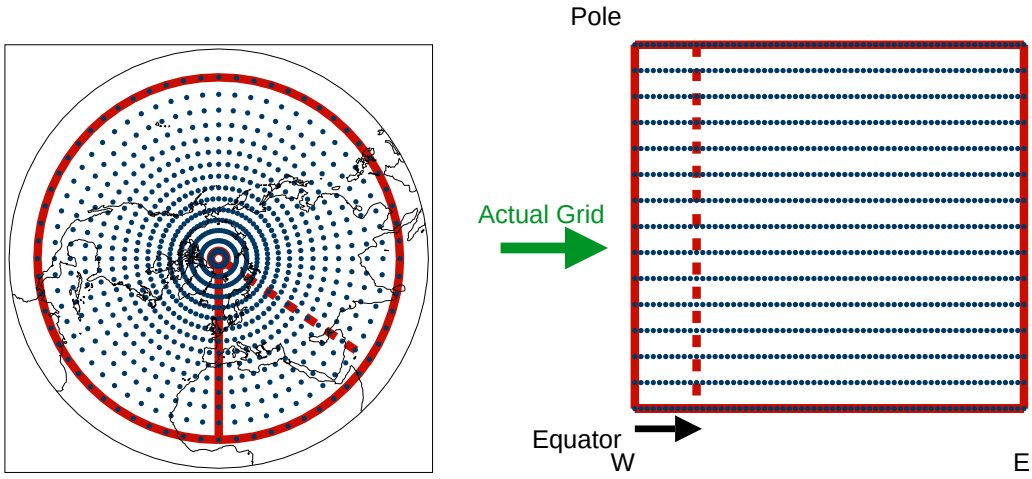

Figure 5.2: *Schematic showing construction of grid on each isentropic surface for inverter. Blue dots show position of grid points on hemisphere. Solid red lines show boundaries of grid used in inverter. The grid in the inverter is similar to the grid shown in the right figure. Boundary conditions on each surface are required along the solid red lines. At the position of the join in the plane in the longitudinal direction the boundary conditions are periodic. Because the inverter works on the grid and not on a hemisphere the solution at the longitudinal boundary may be affected. Therefore the position of the boundary is moved after each iteration. A new boundary position is shown in the red dotted line.*

In the vertical boundary conditions are required at the top and bottom of the domain. The boundary condition at the top of the domain is isentropic and is given by specifying pressure on an isentropic surface. This can be related to $\frac{\partial M}{\partial \theta}$ using the hydrostatic relation (Eq. 5.3).

The bottom boundary is more complicated owing to the intersection of isentropic surfaces with the ground. This means that the lower boundary occurs at different values of potential temperature at different horizontal locations. At the boundary a parabola is fitted to the lowest two theta levels above the ground to give a mixed boundary condition in M and $\frac{\partial M}{\partial \theta}$ (from Eq. 5.4), given the requirement that $z = z_s(\phi, \lambda)$ and $\theta = \theta_s(\phi, \lambda)$.

A further complication can arise when an isentropic surface intersect the ground close to mountain ranges. In this circumstance a further lateral boundary arises. This is shown schematically in figure 5.3. Boundary conditions here are provided by extrapolating Montgomery beneath the mountain from above, providing an extra boundary condition. This boundary condition is described as 'floating' as the condition changes after each iteration of the equation.

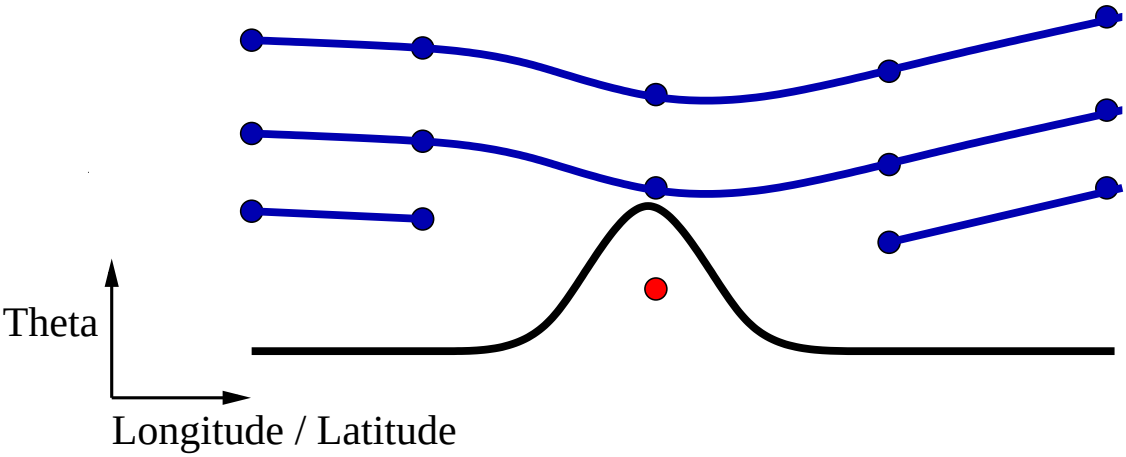

Figure 5.3: *Schematic of extra lateral boundary condition where isentropic surfaces intersect the ground. Blue lines show position of isentropic surfaces, black line shows ground. Blue points indicate grid points where PV is specified. Red point indicates an additional lateral boundary. Montgomery here is determined by interpolation of the Montgomery distribution from points above the ground.*

5.4 Idealised Experiments

Before performing experiments with the inverter on model conditions the response of an idealised atmosphere to stratospheric perturbations of wave one structure is examined. Calculating the adjustment of a very simple troposphere to a very simple stratosphere provides a way of un-

derstanding the adjustment of the troposphere to the stratospheric PV distribution when the more complicated model PV distribution is used.

5.4.1 Reference State Zonal Mean Input Conditions

A reference state zonal mean PV distribution is defined for the idealised experiments described in this section. It is also assumed that the ground has the same height at every grid-point (1500m). By stopping the inversion above the boundary layer we avoid complications to the vertical and lateral boundary conditions near the ground associated with boundary layer processes.

The distribution of PV in the stratosphere (900K) and troposphere (300K) in the idealised atmosphere is shown in figure 5.4 (a) and (b). In both the troposphere and stratosphere the initial PV distribution is a monotonic, zonally symmetric function increasing toward the pole. In the stratosphere there is a region of small PV gradients in the mid-latitudes which represents the stratospheric 'surf-zone' (McIntyre and Palmer, 1984). In the troposphere the zonal gradient of PV is much more uniform.

Figure 5.4 (c) and (d) show the geopotential height on pressure surfaces in the stratosphere (10hPa) and the troposphere (500hPa). At both levels there is a large scale cyclonic vortex centred on the pole.

Figure 5.5 shows the inverted zonal velocity profile when the idealised initial conditions are used. This shows the characteristic features of the zonal mean stratosphere and troposphere, northern hemisphere circulation. The zonal jet in the stratosphere is relatively strong and centred around 60N. In the troposphere the jet is further equatorward, centred around 30N. The structure of the PV=2 surface is shown in the thick dotted line. This surface approximates the tropopause in the high and middle latitudes (Highwood et al., 2000). It has the characteristic structure of small θ at high latitudes rising to much larger θ in low latitudes. There is also a large slope in the position of the tropopause around the region of the sub-tropical, tropospheric jet.

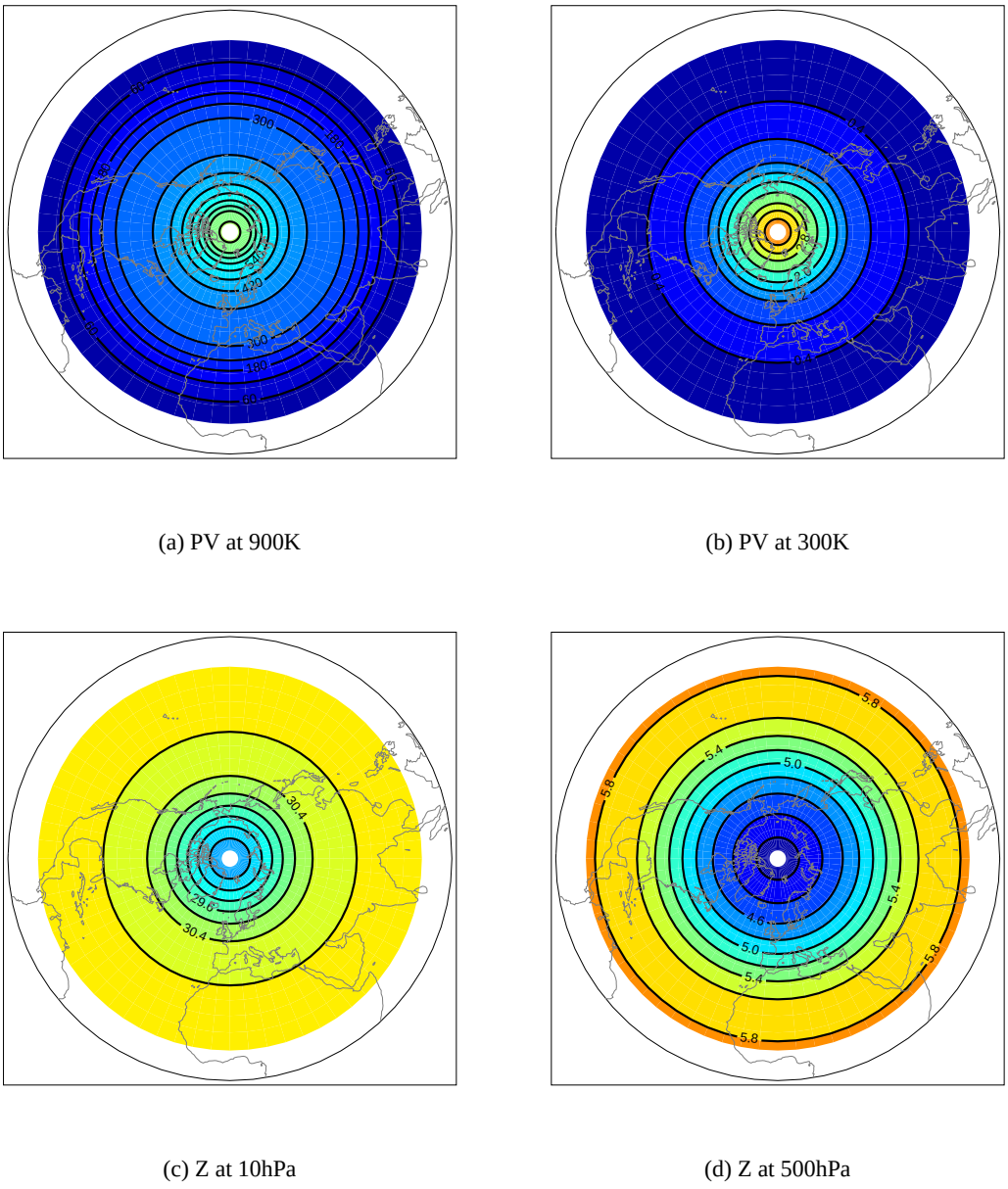

(a) PV at 900K

(b) PV at 300K

(c) Z at 10hPa

(d) Z at 500hPa

Figure 5.4: *PV distribution on theta surfaces from idealised initial conditions and height fields on pressure surfaces from inversion of idealised initial conditions.*

5.4.2 Adding Perturbations to idealised conditions

The influence of stratospheric PV anomalies on the troposphere can be investigated by comparing an inversion of the idealised zonal mean reference PV distribution described above with a new PV distribution in which anomalies are added to the idealised reference PV distribution in the

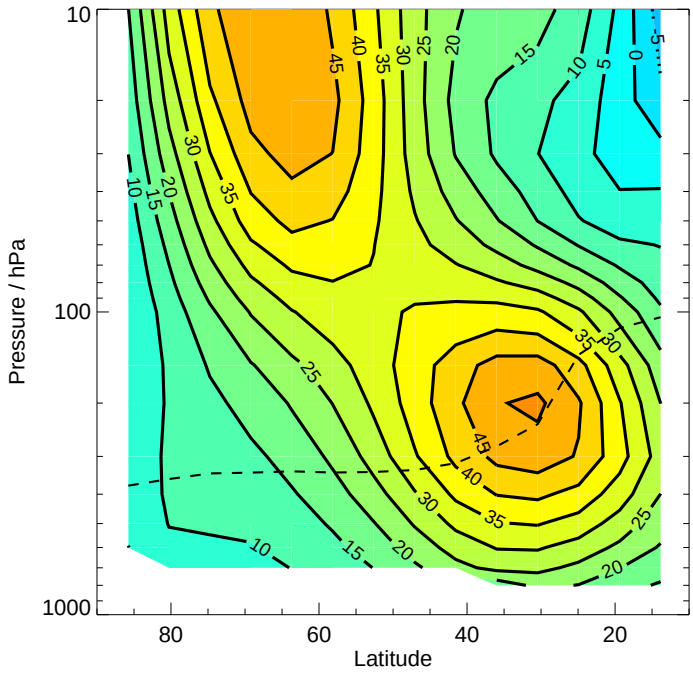

Figure 5.5: *Zonal Velocity profile for idealised initial conditions. Dashed line shows position of PV=2 unit surface.*

stratosphere. When changing the PV distribution in the stratosphere it is desirable to preserve some properties of the original PV distribution. PV is parcel wise conserved following adiabatic and frictionless flow. Therefore a sensible rearrangement of the stratospheric PV distribution would preserve the area integral of PV (PVA) on each isentropic surface.

$$PVA = \int \int_S PdA \tag{5.11}$$

where:

PVA - is the area weighted integral of P

S - is an isentropic surface

P - is Potential Vorticity, which is a function of latitude and longitude

dA - is an area element

In practice the area weighted PV on the grid is calculated by the sum.

$$PVA = \sum_{\lambda=0}^{N} \sum_{\phi=0}^{M} P \Delta x \Delta y \tag{5.12}$$

where:

Δx - is the longitudinal grid spacing

Δy - is the latitudinal grid spacing

N - is the number of latitudinal grid points

M - is the number of longitudinal grid points

The longitudinal and latitudinal grid spacing on each latitude circle is constant, this means that the area weighted PV can be calculated by,

$$\begin{aligned} PVA &= \sum_{\lambda=0}^{N} \Delta x \Delta y \sum_{\phi=0}^{M} P \\ &= \sum_{\lambda=0}^{N} PVAL \end{aligned} \tag{5.13}$$

where:

PVAL - is the area weighted sum of PV around each latitude circle

If the sum of PV around each latitude circle (PVAL) is preserved then this will preserve the area integral of PV around each latitude circle and hence over the hemisphere. A simple way of changing the PV distribution on each latitude circle is to add a sine wave perturbation.

$$PVAL = \Delta x \Delta y \sum_{\phi=0}^{M} (P + (H(\lambda)V(\theta))sin(A\lambda)) \tag{5.14}$$

where:

$H(\lambda)$ - is the amplitude in the horizontal and is a function of latitude

$V(\theta)$ - is the amplitude in the vertical and is a function of potential temperature

A - is the horizontal wavenumber

Adding a sine wave with an integer wavenumber (A) to the PV on each latitude circle preserves the total PV around the latitude circle. The horizontal and vertical amplitudes are used to control the structure of the PV anomaly added to the reference distribution in the horizontal and vertical.

The amplitude profile of stratospheric perturbations in the horizontal is chosen to maximise the amplitude of perturbations in mid-latitudes and have little impact on the PV distribution in the tropics. The amplitude profile used in these experiments is shown in Fig. 5.6.

The amplitude profile in the vertical is chosen to maximise the size of PV anomalies in the middle stratosphere and is shown in Fig. 5.7. The amplitude varies as a approximate Gaussian function with a maximum at 650K. The amplitude of the perturbation is zero at the top boundary (1400K) and below 400K. Adopting this profile in the vertical means that the anomaly is well separated from the troposphere, and also that we can assume the top boundary condition is unchanged when the perturbation is added to the stratosphere.

5.4.3 Adding a wave one perturbation

Figure 5.8 shows the difference between inversion of the idealised initial conditions and the same idealised initial conditions plus a wavenumber one type perturbation to the PV in the stratosphere above 400K. The structure and magnitude of the difference in the two PV distributions is shown in Figure 5.8 (a). The PV anomaly has a wavenumber one structure with an increase in PV over the Eurasian continent and a reduction in PV over North America in the perturbed PV distribution.

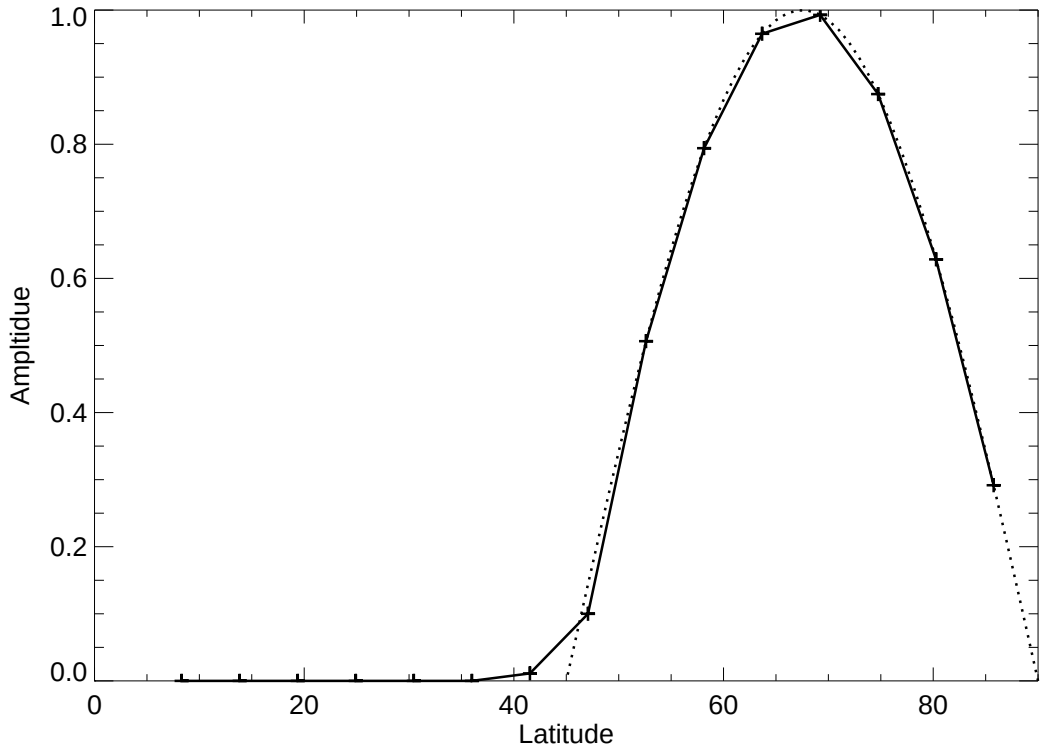

Figure 5.6: *Relative amplitude of perturbation applied to the stratospheric PV distribution (solid line, data points marked with crosses). Dotted line shows profile of sin((4x latitude)-π) which is used to define the perturbation north of 45N.*

The structure of the difference is designed to resemble the structure of a wave one type warming in the stratosphere with the growth of a large anticyclone in the stratosphere over the western side of North America and movement of the polar vortex toward Eurasia.

The impact of this change to the PV distribution on the inverted height field in the troposphere (500hPa) is shown in figure 5.8 (b). The resulting change to the tropospheric height field is also of similar wavenumber one structure. The change to the stratospheric PV distribution causes an increase in the height over western North America and a reduction in height over Eurasia.

Similar changes to the surface pressure distribution and the distribution of pressure on the PV=2 surface also occur (Figures 5.8 (c) and (d)). The change to the stratospheric PV distribution causes a similarly structured wavenumber one change to the surface pressure and to the pressure on the PV=2 surface. The mass increases over western North America and is reduced over Eurasia. The

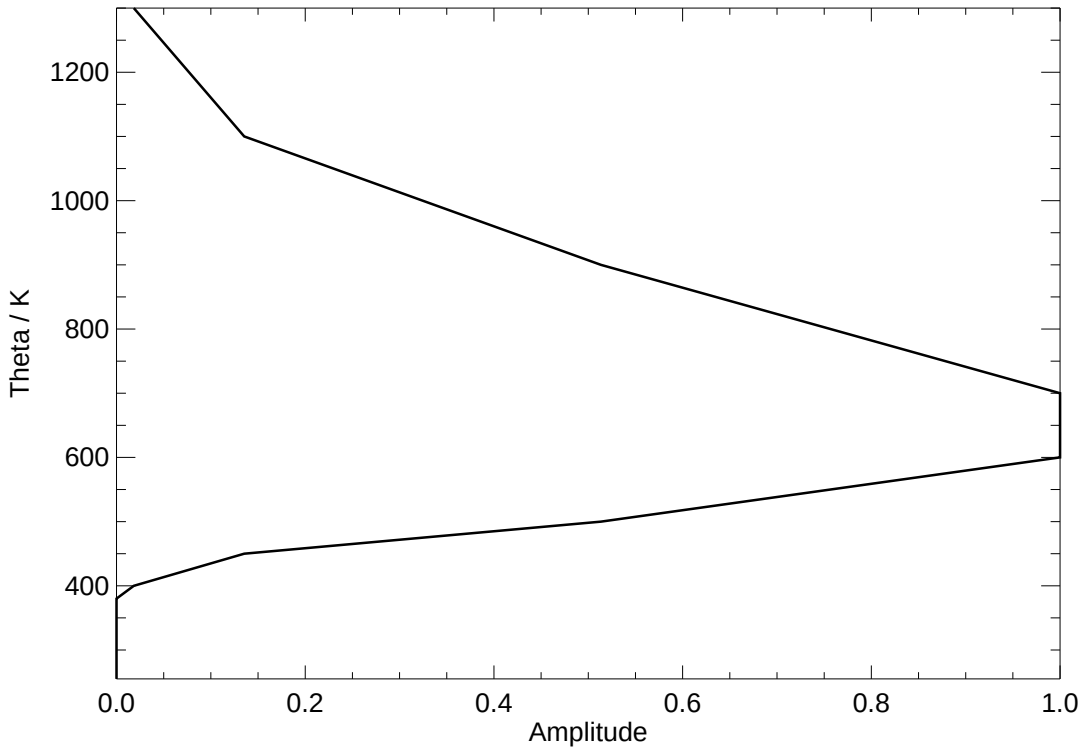

Figure 5.7: *Relative amplitude of perturbation applied to the stratospheric PV distribution in the vertical.*

size of the change is 20hPa in the pressure on the PV=2 surface which is roughly a change in height on the PV=2 surface of around 500m. The magnitude of the change in the height of the tropopause is similar to that given by Hartley et al. (1998) and Ambaum and Hoskins (2002).

Note that the change to the tropospheric mass field is not of equal size for equally sized but oppositely signed stratospheric PV anomalies. The change to the surface pressure beneath the negative stratospheric PV anomaly is $\sim 2hPa$ greater than the change beneath the positive stratospheric PV anomaly. This indicates a change to the total mass over the hemisphere.

There is no explicit constraint on the total mass in our PV inverter. The surface pressure is determined by the Montgomery Streamfunction which is free to achieve any solution consistent with the PV distribution and boundary conditions. Appendix A discusses these issues further.

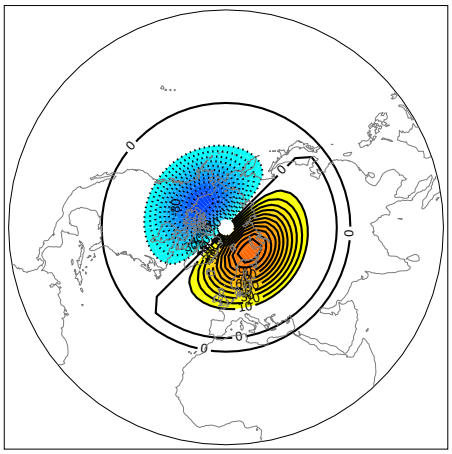

(a) PV difference at 700K. Units are PV Units $1PVU = 10^{-6}m^2s^{-1}Kkg^{-1}$.

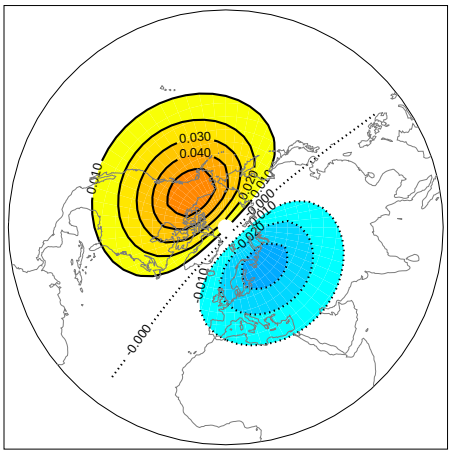

(b) Height difference at 500hPa. Units are km.

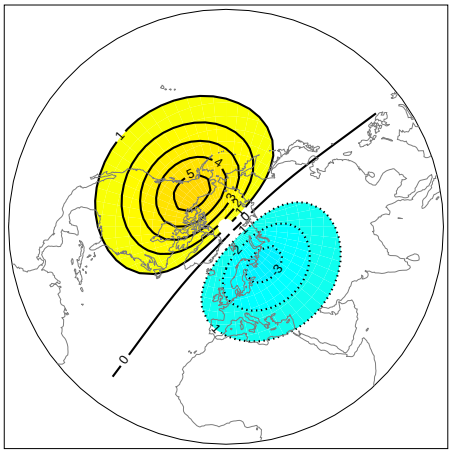

(c) Surface Pressure difference. Units are hPa.

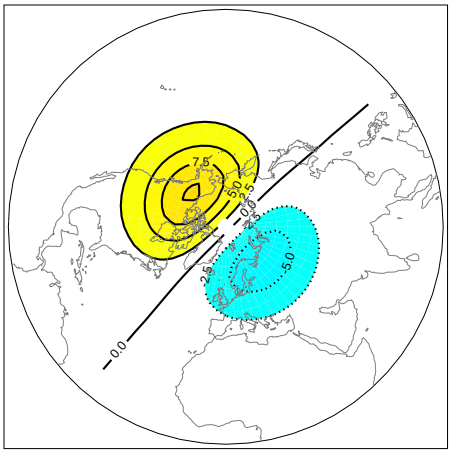

(d) Difference in pressure on PV=2 surface. Units are hPa.

Figure 5.8: *Differences between inversion of idealised reference PV distribution and inversion of idealised reference PV distribution plus a wave one perturbation in the extra-tropical stratosphere (above 400K).*

5.4.4 Sensitivity to a tilted stratospheric anomaly

In the real atmosphere it is unlikely that anomalies in the PV distribution throughout the stratosphere will be coherent in the vertical as is the case in the above inversion. Typically an anticy-

clonic feature is tilted 90 °over the range 1300K to 400K. This tilt may have a strong impact on the changes to the troposphere induced by stratospheric PV anomalies. To simulate this a further inversion is performed in which the PV anomaly is tilted by 90 °in the horizontal over the range 1300K to 400K.

Differences to the PV distribution in the stratosphere between the idealised reference state and the idealised reference state plus the tilted stratospheric anomaly are shown in figure 5.9 (a) and (b). The difference to the PV distribution is identical to the difference in the wavenumber one case but is tilted progressively toward the east as θ decreases.

The response of the troposphere to this tilted anomaly is shown in figure 5.9 (c) and (d). These figures should be compared with figures 5.8 (c) and (b). The anomaly in the troposphere due to the tilted anomaly is remarkably similar to the anomaly in the troposphere when the stratospheric PV anomaly is not tilted (Figure 5.8). There is a similar wavenumber one structure and the magnitude of changes to the surface pressure and the geopotential height on the 500hPa pressure surface are very similar.

The orientation of the anomalies in the troposphere is very close to the orientation of PV anomalies in the lower stratosphere. The orientation of the tropospheric differences have no tilt in the vertical with the PV differences on the 500K isentropic surface. This suggests that the troposphere is adjusting most in response to changes to the lower stratosphere and that there is little impact of the middle stratospheric PV distribution on the troposphere (as stated by Black (2002)). It is also interesting that the response of the troposphere has little tilt in θ. This suggests that the entire troposphere responds in the same way to the changes to the stratospheric PV distribution. It might be hypothesised that the upper troposphere would respond differently to the tilted stratospheric PV anomaly as it could effectively “see” the middle stratosphere. However this does not appear to be the case.

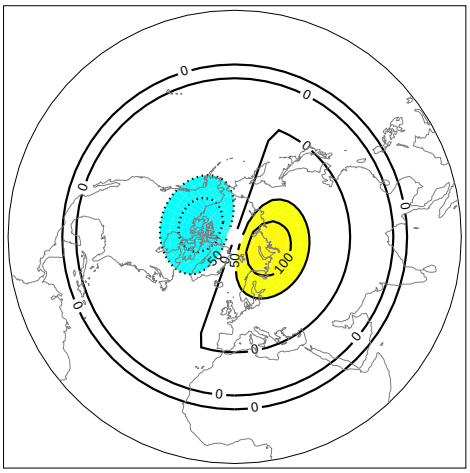

(a) PV difference between idealised initial conditions and idealised initial conditions plus titled wave one anomaly on 900K surface

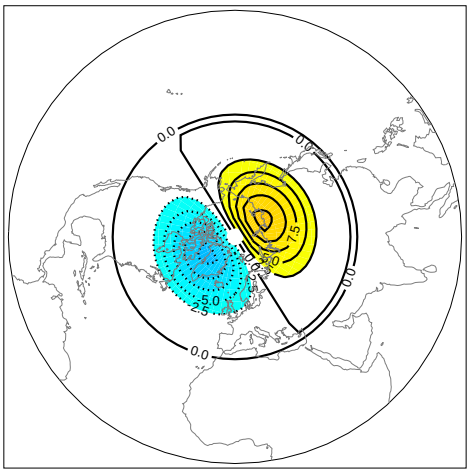

(b) PV difference between idealised initial conditions and idealised initial conditions plus titled wave one anomaly on 450K surface

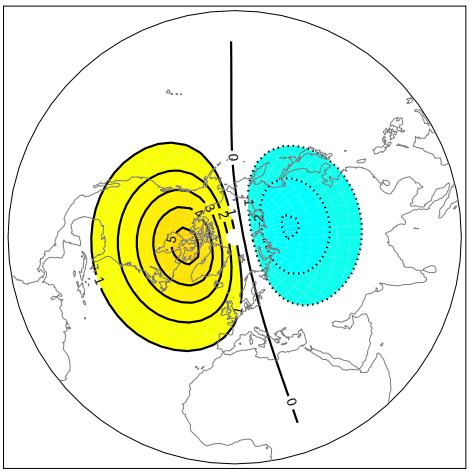

(c) Surface Pressure Difference between inversion of idealised initial conditions and idealised initial conditions plus a tilted wave one anomaly above 400K

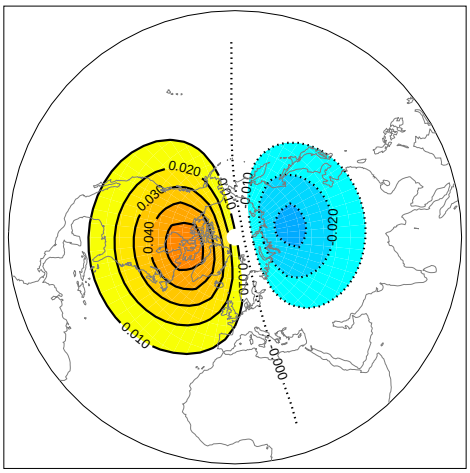

(d) Difference in Geopotential Height on 500hPa pressure surface between inversion of idealised initial conditions and idealised initial conditions plus a tilted wave one anomaly above 400K

Figure 5.9: *Differences between inversion of idealised conditions and idealised conditions plus a tilted wavenumber one perturbation*

5.5 Comparison of Nature and Non-Nature Runs

5.5.1 Introduction

Section 5.4 showed that making idealised changes to the PV distribution in the stratosphere has a small impact on the troposphere. Changes to the tropospheric flow which can be related to changes in the stratospheric PV distribution are typically on large spatial scales. This section attempts to investigate the adjustment of the troposphere to the stratospheric PV distribution in a single ensemble member of the nature run in case study one of chapter 4. It is assumed that the adjustment of the troposphere to the stratospheric PV distribution in this ensemble member is representative of the dynamics of all the members in the ensemble and of all three case studies.

The aim of this section is to understand the questions about the mechanism of the influence of the stratosphere on the troposphere posed in section 5.1. It is anticipated that the changes to the tropospheric flow will be similar to those in section 5.4 because the stratospheric PV distribution in the model has a similar wavenumber one structure.

5.5.2 Experimental design and initial results

This section describes an example PV inversion experiment which investigates the adjustment of the troposphere to the stratospheric flow at the initialisation time in the first case study described in chapter 4. In this experiment we examine the PV distribution from the initial conditions of the first ensemble member of the nature experiment. This inversion is referred to as the **Nature Inversion** . In this experiment the reference stratospheric PV distribution is taken from the first ensemble member of the non-nature experiment.

Figure 5.10 shows the nature and reference PV distributions in the stratosphere. Figure 5.10 (a) and (b) show PV on the 900K isentropic surface ($\sim$ 10hPa). 900K is in the middle stratosphere and can be assumed to be a level which is representative of large scale changes to the structure of the stratospheric polar vortex which occur throughout the middle stratosphere. The stratospheric PV distribution in the nature inversion (Figure 5.10 (a)) is characteristic of the early part of a zonal wavenumber two stratospheric sudden warming. The vortex, which is characterised by large

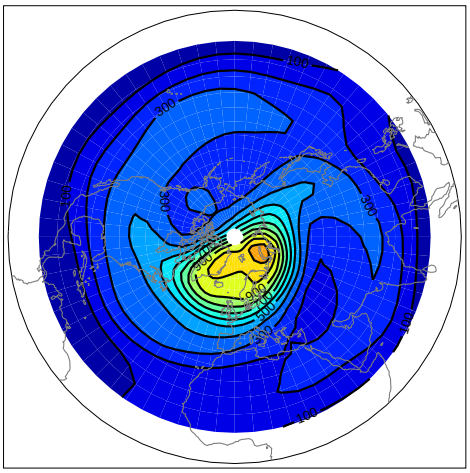

(a) Nature PV distribution on 900K isentropic surface. Units are PV Units $1PVU = 10^{-6}m^2s^{-1}Kkg^{-1}$.

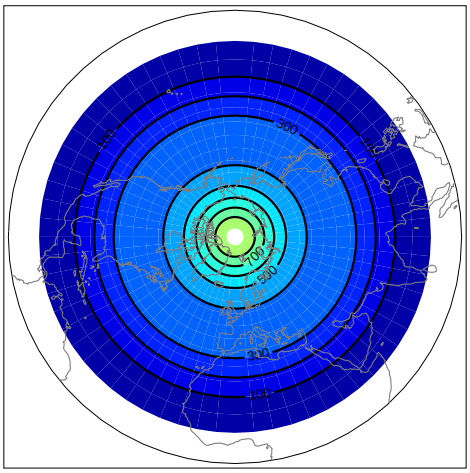

(b) Reference PV distribution on 900K isentropic surface. Units are PV Units.

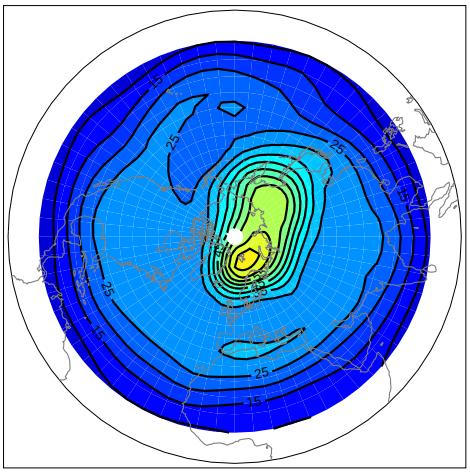

(c) Nature PV distribution on 500K isentropic surface. Units are PV Units.

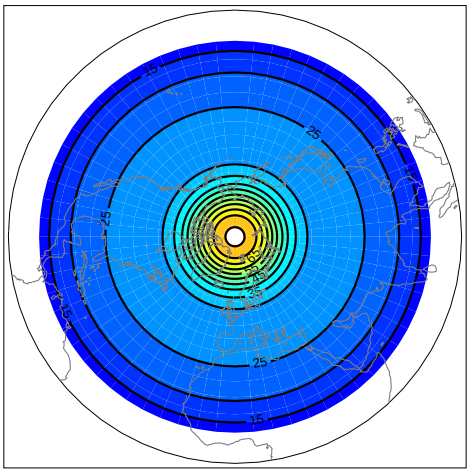

(d) Reference PV distribution on 500K isentropic surface. Units are PV Units.

Figure 5.10: *Nature and Reference PV distributions in the middle and lower stratosphere.*

values of PV with a large gradient at its edge, is displaced toward Eurasia and has an elliptical shape. Two anticyclonic features, characterised by low values of PV, can be seen over the west coast of North America and over central Eurasia. In contrast the reference state PV distribution

(Figure 5.10 (b)) is characteristic of a strong polar vortex with little disturbance.

Figure 5.10 (c) and (d) show PV on the 500K isentropic surface. 500K is in the lower stratosphere, flow on this isentropic surface is dominated by a larger polar vortex. Figure 5.10 (c) shows the nature PV distribution. During a stratospheric sudden warming it is unusual for the vortex to completely break down in the lower stratosphere. In figure 5.10 the vortex is displaced toward the East Pacific. There is also a signature of an anticyclone over Central North America. At this level the reference PV distribution (Figure 5.10 (d)) has a similar zonal mean structure as on the 900K isentropic surface.

Note that the spatial structure of anomalies in the nature PV distribution (relative to the zonal mean reference state) is very different in the middle and lower stratosphere in the nature run. The largest positive PV difference in the middle stratosphere is over the Arctic Basin; in the lower stratosphere the largest positive PV difference is over the East Pacific. In the idealised experiments differences to the tropospheric flow between an inversion with a zonally asymmetric PV distribution and a zonally symmetric PV distribution were coherent in the vertical with differences to the PV distribution in the middle stratosphere ($\sim$ 500K). Differences to the tropospheric flow between the nature and non-nature inversions are therefore expected to be higher surface pressure over North America and lower surface pressure over Eurasia.

The difference to the tropospheric flow between the nature inversion and the reference inversion is shown in Figure 5.11. Figure 5.11 (a) shows the difference to the surface pressure field. The largest difference is to the wavenumber one component with a large increase in surface pressure over North America associated with the larger of the two stratospheric anticyclone and a corresponding decrease in surface pressure over Eastern Eurasia associated with the polar vortex.

The largest reduction in the surface pressure is located over the East Pacific. There are large (20 x $10^{-6}m^2s^{-1}KKg^{-1}$, 30 $\%$ of the maximum PV at this level) PV anomalies over East Asia in the lower stratosphere but not in the middle stratosphere. This suggests that the lower stratospheric PV distribution has a much larger influence on the troposphere than the middle stratosphere. Similar conclusions were reached by Black (2002). Typical magnitudes of differences in the surface pressure are around $5hPa$. Figure 5.11 shows differences to the pressure on PV=2 surface. This shows a similar structure to the surface pressure change. Typical magnitudes of the change

in tropopause height which can be estimated from this field are similar to the differences from the idealised experiments ($\sim$ 250m).

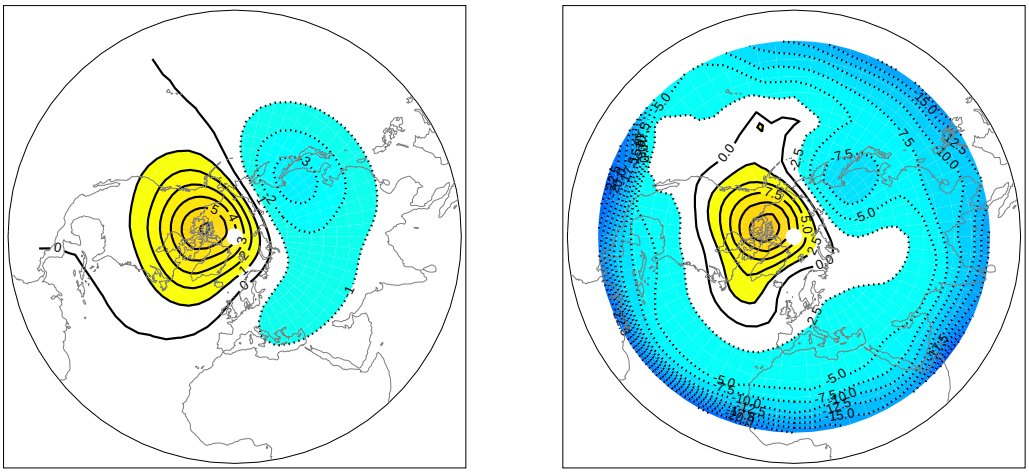

(a) Surface Pressure

(b) Pressure on PV=2 surface

Figure 5.11: *Difference in tropospheric fields after inversion. Nature - Reference Inversion. In this and similar plots positive differences indicate that the quantity in the nature inversion is larger than that in the reference inversion. Negative differences indicate that the quantity in the nature inversion is smaller than that in the reference inversion.*

The largest adjustment of the tropospheric flow to the nature PV distribution occurs over the land-masses of North-America and Eurasia. This pattern does not map strongly onto the AO structure (see Fig. 1.1). This is consistent with the relatively small change to the tropospheric AO structure over the first timesteps of the model integration (Fig. 4.2 (d)).

A vertical slice of geopotential height differences between the nature inversion and the reference inversion is shown in Fig. 5.12 (a). Geopotential height differences in isentropic space have opposite signs to differences to geopotential height in pressure space. The large negative anomaly in Fig. 5.12 (a) corresponds to the Aleutian Anticyclone in the nature inversion.

Both the negative anomaly (corresponding to the Aleutian anticyclone) and the positive anomaly (corresponding to the displaced polar vortex) in geopotential height tilt toward the west with θ. Below 400K (bottom panel of each figure), the PV distribution in the nature inversion and the reference state are identical. Differences to the geopotential height below 400K are coherent in

the vertical with differences to the geopotential height and PV (Fig. 5.12 (b)) at 400K. Typical sizes of the adjustment of the geopotential height field in the troposphere to the stratospheric PV distribution are $\sim$100m

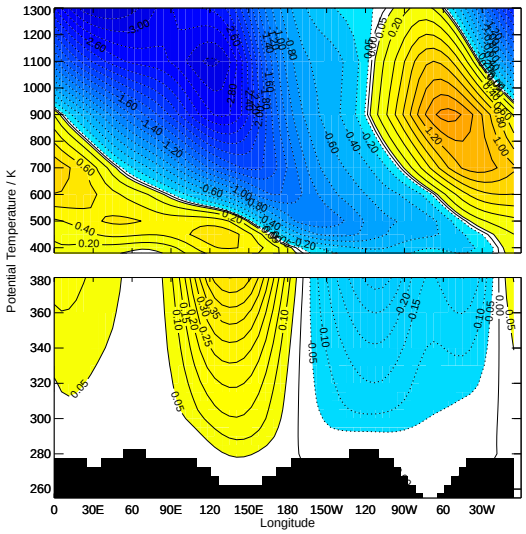

(a) Difference in Geopotential Height on isentropic surfaces between Nature Inversion and reference inversion. In top panel contour spacing is 0.2km (apart from contours at -0.05 and 0.05 km). Bottom panel has different vertical spacing and contour interval of 0.05km

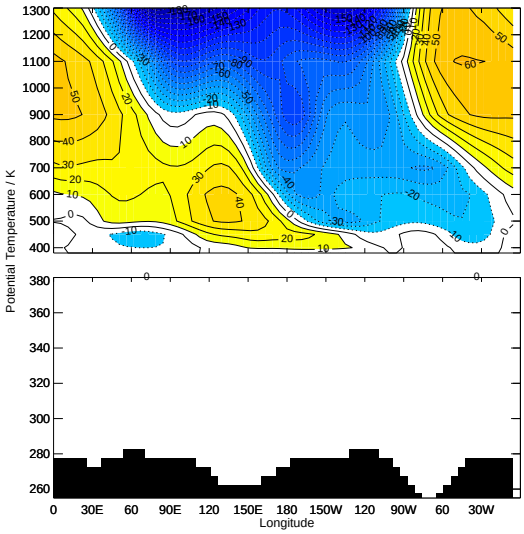

(b) Difference in Potential Vorticity on isentropic surfaces between Nature Inversion and reference inversion. Differences are expressed as percentage of PV in nature inversion. Contour interval is 10 %

Figure 5.12: *Vertical Slice of difference in Geopotential Height and Potential Vorticity on isentropic surfaces at 58°N. Note that each plot is split into two figures with different vertical spacing and different contour interval. Black shading marks the position of the ground.*

5.5.3 Importance of Middle Stratosphere

The second question in the introduction asked, "how important is the middle stratosphere in understanding the adjustment of the troposphere ?" The experiment described in this section examines this question. This experiment is similar to the one described above but compares the nature inversion to a different reference state. The new reference state has the same PV distribution as the nature inversion in the troposphere and lower stratosphere (255-700K) but has the PV distribution taken from the non-nature run in the middle stratosphere (above 700K). This reference state is

referred to as the **700K reference state.**

Comparison of the tropospheric fields in the nature inversion and the 700K reference inversion shows the influence of the middle stratospheric PV distribution on the tropospheric flow. If the middle stratospheric PV distribution has a significant impact on the tropospheric flow then the tropospheric anomalies in this comparison will be similar to those in the previous experiment.

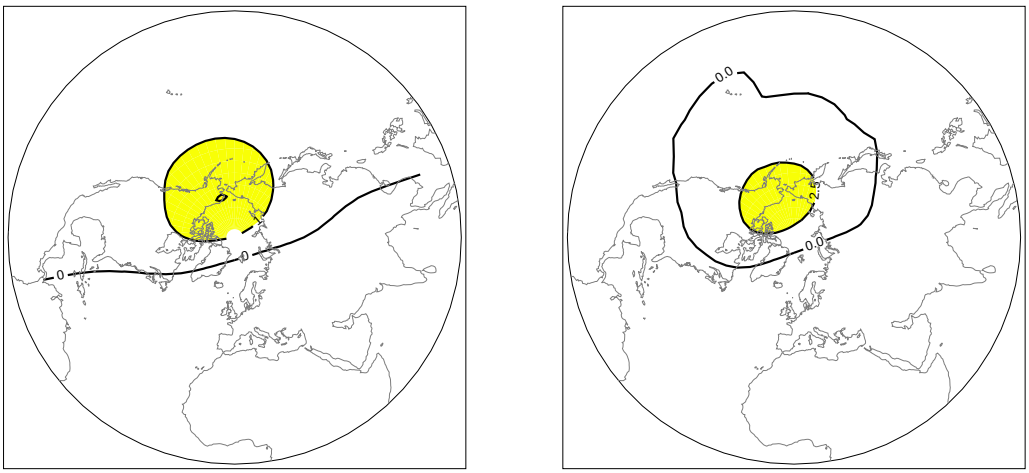

(a) Surface Pressure (b) Pressure on PV=2 surface

Figure 5.13: *Difference in tropospheric fields after inversion. Nature - 700K reference inversion.*

Figure 5.13 shows the difference to the tropospheric flow between the nature inversion and the 700K reference inversion. This figure should be compared to figure 5.11 which shows the difference between the nature inversion and the standard reference inversion. The difference to the surface pressure due to anomalies in the middle stratosphere is much smaller than the difference to the surface pressure due to all stratospheric anomalies. This suggests that differences to the tropospheric flow are due in large part to PV anomalies in the lower stratosphere. This is despite the smaller size of PV anomalies (ie differences between the nature PV distribution and the reference state PV distribution) in the lower stratosphere (typically 50PVU ($\sim 30\%$ of total PV) in the lower stratosphere and 500PVU ($\sim 50\%$ of total PV) in the middle stratosphere.)

Figure 5.14 shows a vertical slice of the differences between the nature inversion and the 700K reference inversion at 58 °N. Differences to the geopotential height below 700K are coherent in the vertical with differences to the geopotential height and PV distributions at 700K. This result

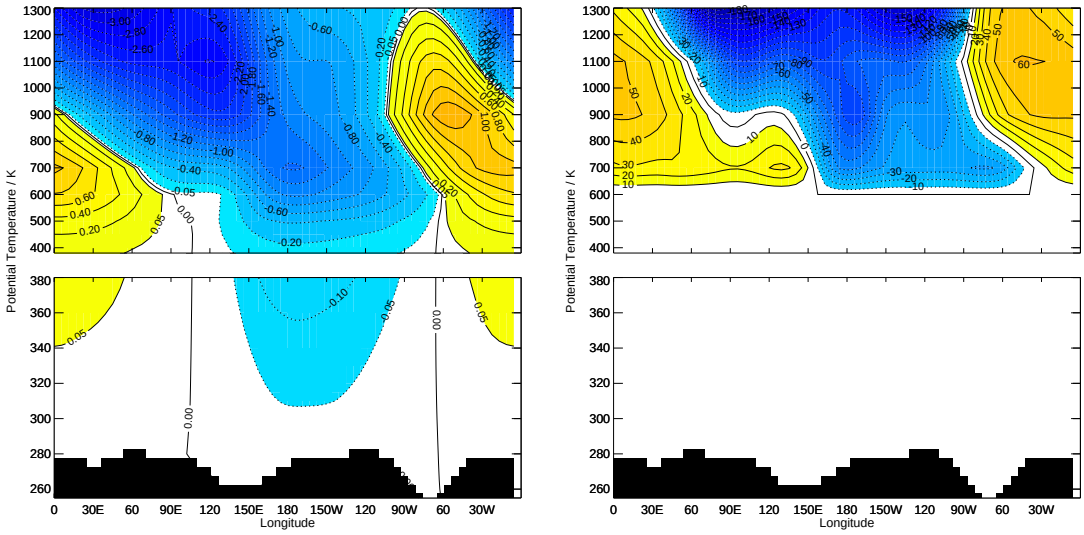

(a) Difference in Geopotential Height on isentropic surfaces between Nature Inversion and 700K reference inversion. In top panel contour spacing is 0.2km (apart from contours at -0.05 and 0.05 km). Bottom panel has different vertical spacing and contour interval of 0.05km

(b) Difference in Potential Vorticity on isentropic surfaces between Nature Inversion and 700K reference inversion. Differences are expressed as percentage of PV in nature inversion. Contour interval is 10 %

Figure 5.14: *Vertical Slice of difference in Geopotential Height and Potential Vorticity on isentropic surfaces at 58°N. Note that each plot is split into two figures with different vertical spacing and different contour interval.*

is similar to the result for the difference between the nature inversion and standard reference inversion (Fig. 5.12). This suggests that the location of the largest tropospheric adjustment to the stratospheric PV distribution is likely to be dominated by the location of large anomalies in the lower stratospheric PV distribution. In general, large departures of the lower stratospheric PV distribution occur along an axis between 90 °E and 90 °W. Adjustment of the tropospheric flow along this axis would produce tropospheric flow structures which would not map strongly onto the AO structure.

Although it appears that the tropospheric adjustment to the stratospheric PV distribution is dominated by lower stratospheric PV anomalies, this does not discount the importance of the middle stratosphere in influencing the development of PV anomalies in the lower stratosphere (Black, 2002), as the flow evolves.

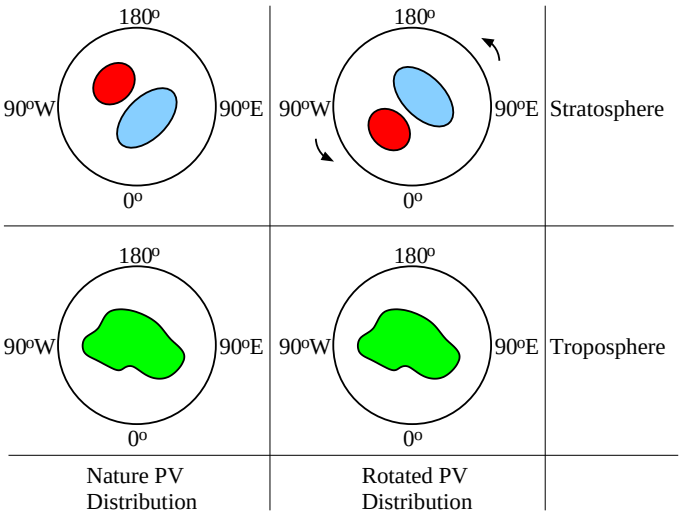

Figure 5.15: *Schematic table showing how the rotated PV distributions (see text for details) are constructed from the standard PV distributions. Circles represent polar stereographic projections of PV on stratospheric and tropospheric isentropic surfaces. Blue, red and green filled shapes represent PV structures on those isentropic surfaces.*

5.5.4 Dependence of difference on Troposphere

The third question in the introduction asked, "do particular parts of the tropospheric flow adjust preferentially to the stratospheric PV distribution ?" The experiment described in this section examines this question. It might be hypothesised that the tropospheric adjustment to the stratospheric flow was larger when the stratospheric PV anomalies are located over the centres of action of the AO.

One way of investigating this hypothesis is to change the relative position of the stratospheric and tropospheric PV distributions. This can be achieved by constructing new PV distributions in which the PV in the stratosphere (defined as before as above the 400K isentropic surface) is rotated relative to the tropospheric PV distribution. Comparing differences to the inverted tropospheric fields (relative to a zonally symmetric reference state) between a number of inversions where the stratospheric PV distribution has been rotated by different amounts shows how the influence of particular stratospheric PV anomalies changes according to the tropospheric PV distributions beneath them. The construction of additional rotated PV distributions is shown schematically in Fig. 5.15.

In this section we compare the adjustment of the tropospheric flow to PV fields in the original nature inversion and two further inversions in which the stratospheric PV fields have been rotated 90 °and 180 °to the east. The new inversions are referred to as the **Nature Rotated 90** and **Nature Rotated 180** inversions. The tropospheric adjustment to the new, rotated inversions is calculated by taking differences between the tropospheric fields in the rotated nature inversions and the standard reference state inversion used in section 5.5.2. If the tropospheric adjustment to the stratospheric PV distribution is influenced by the tropospheric flow then changing the location of the stratospheric anomaly relative to the tropospheric PV distribution will change the structure and quantitative size of the relocated tropospheric anomaly.

Figure 5.16 shows the adjustment of the tropospheric flow fields to the rotated nature inversions. This figure should be compared to the adjustment of the troposphere to the standard nature inversion (Figure 5.11). Comparison of the tropospheric adjustment between the two rotated PV distributions in Fig. 5.16 and Fig. 5.11 should take into account the rotation of the stratospheric PV distribution in these three cases, for direct comparison the differences should be rotated to the west by 90 °(Fig.5.16 (a) and (b)) and 180 °(Fig. 5.16 (c) and (d)). The adjustment of the troposphere to the both the rotated PV distributions and the standard nature PV distribution is surprisingly similar. In all three cases the structure of the adjustment to both surface pressure and pressure on the PV=2 surface has a strong wavenumber one component associated with the wavenumber one stratospheric PV differences. There is thus only a minor dependence of the tropospheric adjustment to the underlying tropospheric flow (in particular the maximum adjustment to the surface pressure is slightly greater in the two rotated cases compared to the standard nature inversion (Figure 5.11)).

If the mechanism for the impact of the stratospheric flow on the troposphere is due to a large-scale adjustment of the tropospheric flow to the stratospheric PV distribution then this mechanism must be able to explain why there is a more prominent response over the Atlantic and Pacific centres of action. This section shows that the response of the tropospheric flow to identical PV anomalies is not stronger in these regions and cannot explain the prominence of these centres of action.

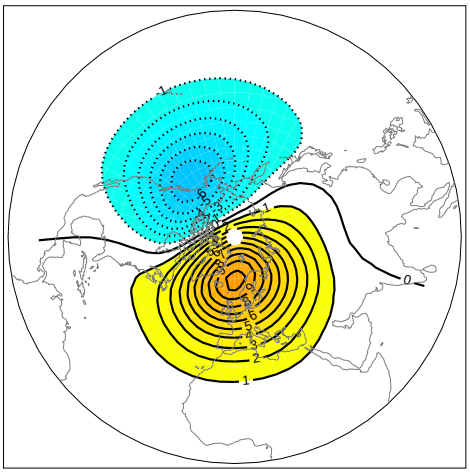

(a) Surface Pressure. Stratospheric PV rotated 90E

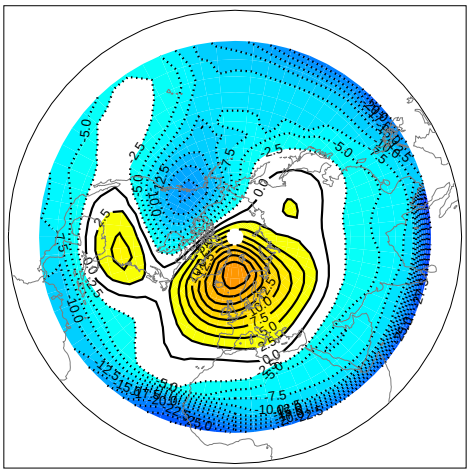

(b) Pressure on PV=2 surface. Stratospheric PV rotated 90E

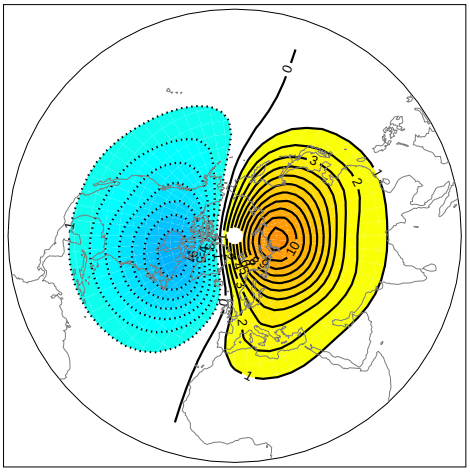

(c) Surface Pressure. Stratospheric PV rotated 180

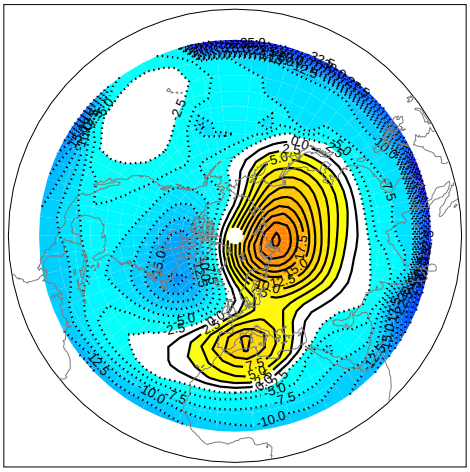

(d) Pressure on PV=2 surface. Stratospheric PV rotated 180

Figure 5.16: *Difference in tropospheric fields after inversion. Nature inversion - reference inversion*

5.5.5 Adjustment of the troposphere throughout the run

The fourth question in the introduction asked, “is there a particular time during the integration of the nature run at which the adjustment of the troposphere to the stratospheric PV distribution is

larger than at other times ?"The experiment described in this section examines this question.

To compare the adjustment of the troposphere at different timesteps during the models' nature integration a new reference state is defined at each timestep. This reference state is not taken from the non-nature run because the stratospheric PV distribution in the non-nature run after a few days is significantly zonally asymmetric. Instead, a new reference state is constructed at each timestep by rearranging the zonally asymmetric stratospheric PV distribution in the nature inversion into a zonally symmetric structure. As in the idealised studies the rearrangement is chosen to preserve the area integral of the PV distribution in the nature inversion. The following procedure is used to calculate the reference state at each timestep. The basis for the equivalent latitude diagnostics used in this procedure can be found in Butchart and Remsberg (1986).

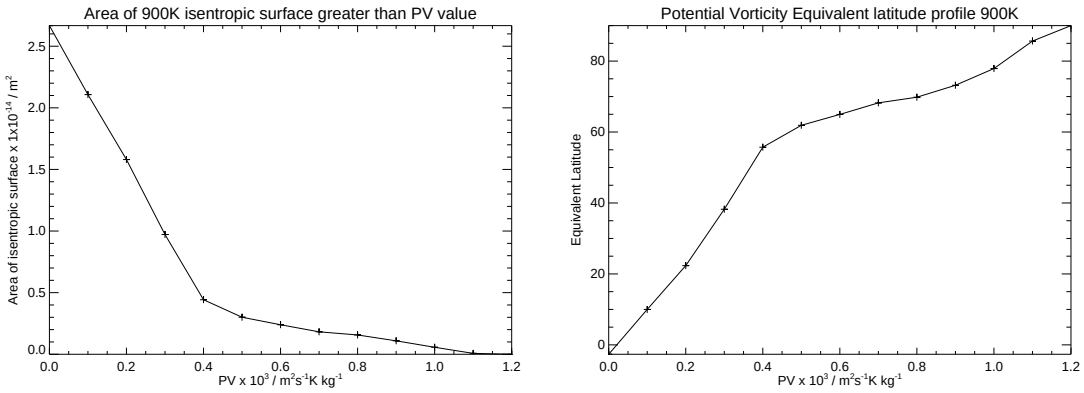

(a) Area of 900K isentropic surface with PV greater than specified value

(b) Equivalent Latitude of PV on 900K isentropic surface

Figure 5.17: *Example output of code used to calculate zonal mean reference PV distribution from nature PV distribution.*

- Define a set of PV contours.
- Calculate the area of the globe with PV greater than each contour (Figure 5.17 (a)).
- Convert each area into an equivalent latitude (Figure 5.17 (b)).
- Interpolate the equivalent latitude profile to the latitude grid used in the inverter.

This method is used to compare the adjustment of the tropospheric flow at 0, 10, 15 and 20 days into the run.

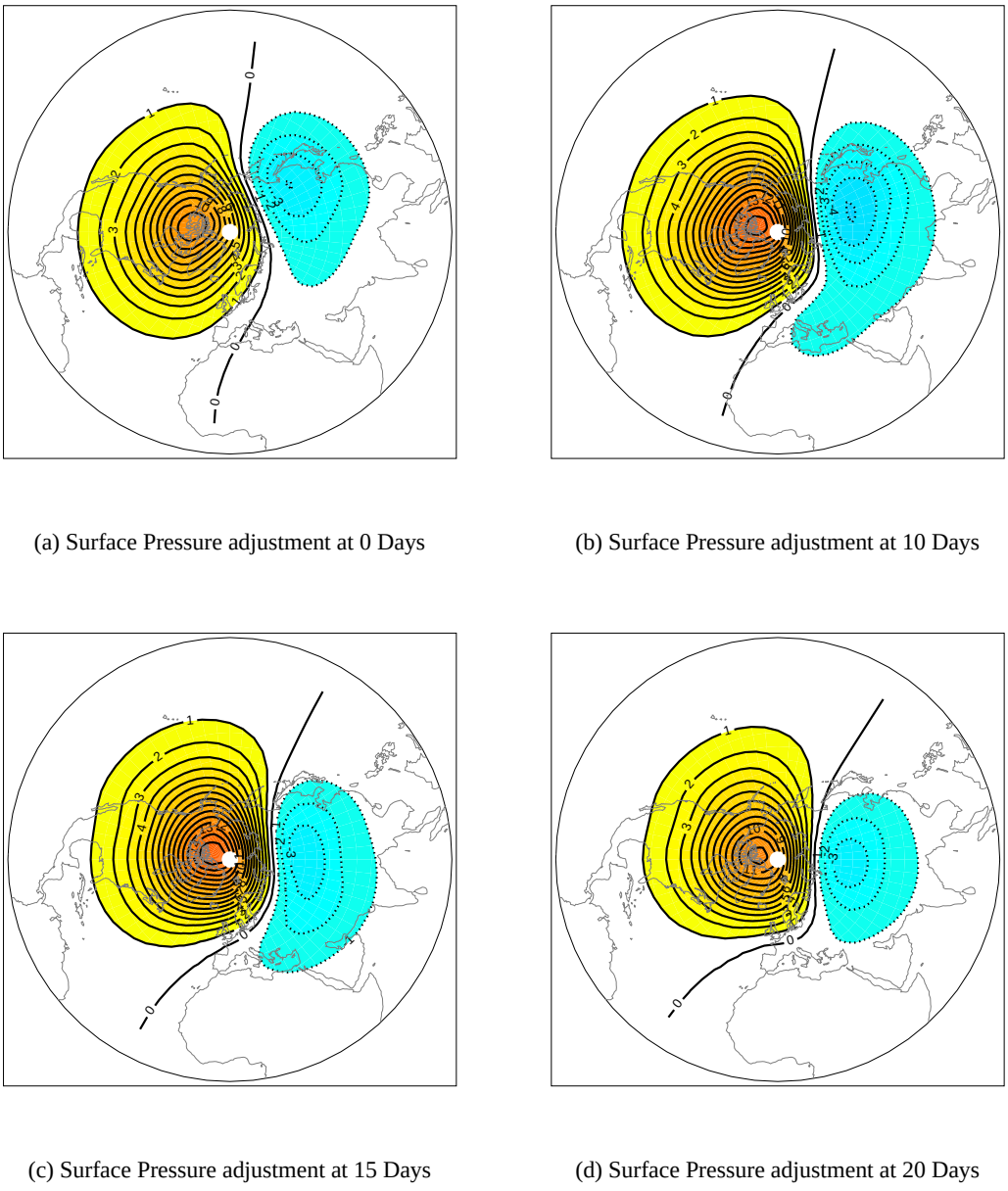

(a) Surface Pressure adjustment at 0 Days

(b) Surface Pressure adjustment at 10 Days

(c) Surface Pressure adjustment at 15 Days

(d) Surface Pressure adjustment at 20 Days

Figure 5.18: *Adjustment of tropospheric flow fields to the stratospheric PV distribution in the nature run at four times during the integration*

Figure 5.18 shows the adjustment of the surface pressure at (a) 0 days, (b) 10 days (c) 15 days and (d) 20 days into the nature run. Note that the adjustment of the nature run at 0 days is different to that shown in (Fig. 5.11) due to the differences in the reference state used.

The adjustment of the tropospheric flow to the stratospheric PV distribution is surprisingly similar

at different timesteps in the model. The adjustment of the troposphere is dominated by a large increase in height over North America and the Canadian Arctic ocean and a large decrease in height over Eastern Eurasia. The orientation of this structure along the 90 °W to 90 °E line. As shown in previous sections the adjustment of the troposphere to the stratospheric PV distribution is dominated by the PV distribution in the lower stratosphere. Although the PV distribution in the nature run changes dramatically in the middle stratosphere over the course of the model integration as the vortex splits, the structure of the PV distribution in the lower stratosphere remains dominated by a displacement of the polar vortex along the 90 °W - 90 °E line toward Eurasia. This structure can be seen in the difference between the ensemble mean PV on the 500K isentropic surface in the nature and non-nature runs of case study one (Fig. 4.12).

In the AO diagnostics of the model run (Fig. 4.2) significant differences to the tropospheric flow are indicated in the first case study after 15 days of the integration. If the mechanism for the influence of the stratosphere on the troposphere is related to the large-scale adjustment of the troposphere to the stratospheric PV distribution, then it might be expected that the structure of this adjustment maps more strongly onto the AO structure in the latter part of the run than it does in earlier part of the run. Figure 5.11 shows that while the structure of this adjustment would in part map onto the AO structure, (Fig. 1.1) due to the increase to surface pressure and geopotential height fields over the polar cap, there is no dramatic change to the structure of this adjustment over the course of the run.

As mentioned in the introduction the PV inversion procedure adopted in this chapter can only be used to determine the instantaneous, simultaneous adjustment of the stratosphere to changes to the PV distribution away from an arbitrary reference state. By comparing the adjustment the surface pressure field in the inversion experiments shown above and the differences to the surface pressure field in the model some understanding of the role of synoptic scale processes in the troposphere in the impact of the stratosphere on the troposphere can be gained.

Figure 5.19 shows differences in the surface pressure distribution taken from the first ensemble member of the two model runs. Figure 5.19 (a) shows the surface pressure difference after 12 hours of the model run. This difference should be compared to the tropospheric adjustment to the stratospheric PV distribution at 0 days into the run (Fig. 5.18 (a),the surface pressure field in the nature and non-nature ensembles is specified to be equal in the model integrations). The

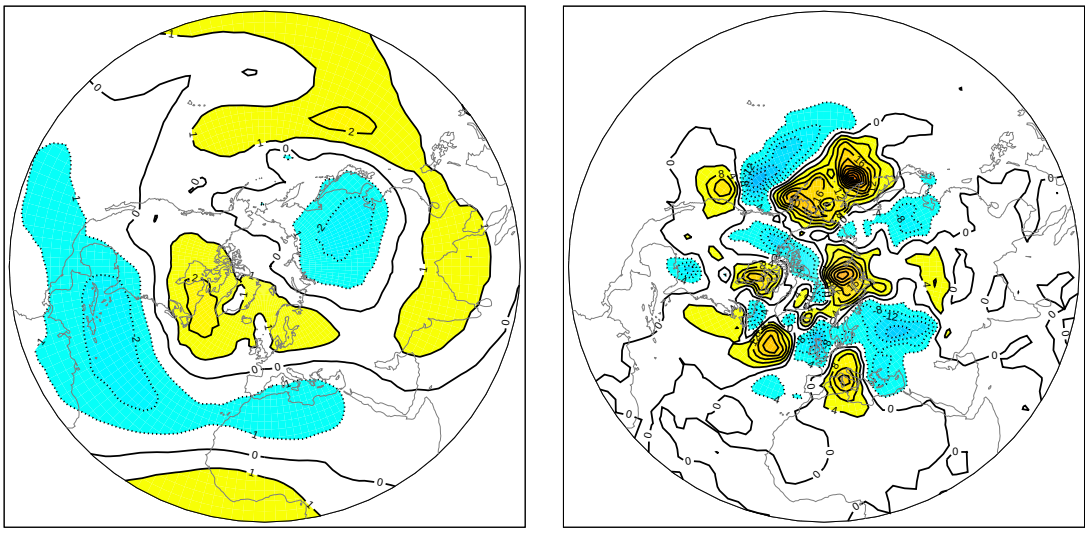

(a) Surface Pressure 12 Hours

(b) Surface Pressure 10 Days

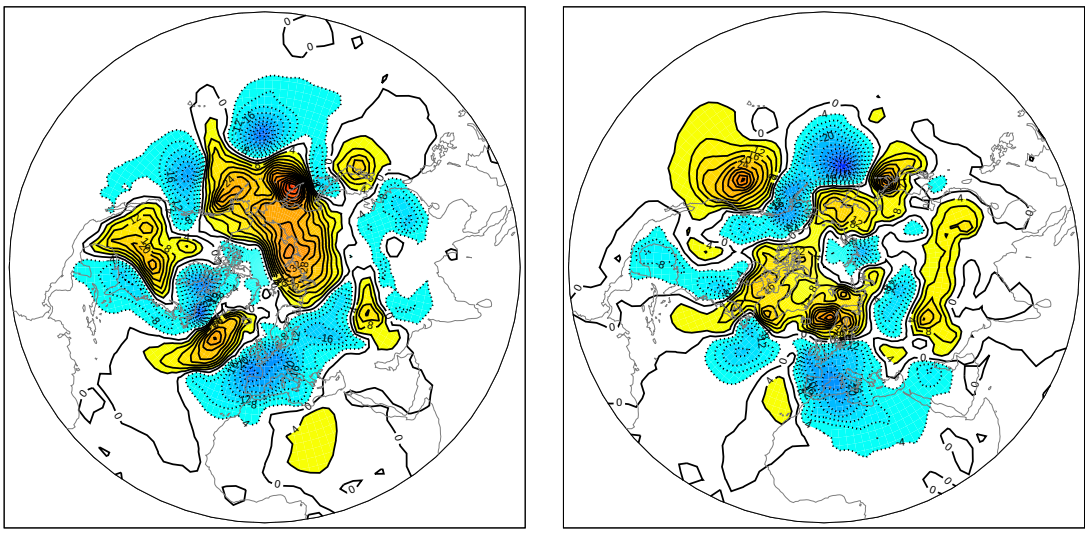

(c) Surface Pressure 15 Days

(d) Surface Pressure 20 Days

Figure 5.19: *Difference in tropospheric fields from model run. Nature - Non-Nature run. Contour interval is 4hPa in all plots apart from (a) where the contour interval is 1 hPa.*

differences here have similar longitudinal structure as the adjustment process determined from the inverter. This suggests that at the start of the model integration, differences to the tropospheric flow are dominated by large scale tropospheric adjustment. The magnitude of differences to the surface pressure are similar in the model run compared to the tropospheric adjustment derived from the inverter.

As the run progresses differences to flow fields in the troposphere are increasingly dominated by differences on the synoptic scale (as noted in section 4.3). Figure 5.19 (b), (c) and (d) shows differences in the surface pressure distribution after 10, 15 and 20 days of the model run. There is little relationship between the magnitude or spatial scale of the differences in the model run and the instantaneous adjustment calculated by the inversion procedure. However it could be suggested that these synoptic scale differences were simply noise on the large-scale adjustment features identified by the inversion procedure. Closer inspection of the differences to surface pressure field in Fig. 5.19 reveals that the largest of these differences occurs in the Atlantic and Pacific storm track regions. Differences to the surface pressure field along the 90 °W - 90 °E line are relatively modest. Comparison of the aggregated differences to the tropospheric flow in the model integrations (Fig 4.9) with the adjustment processes examined in this chapter also shows that the aggregated differences have a spatial structure which is tied to the Northern Hemisphere storm-tracks.

Comparison of differences to the surface pressure between the nature and non-nature runs and the tropospheric adjustment to the stratospheric PV distribution in the nature run show that the mechanism for the influence of the stratosphere on the troposphere cannot be understood purely in terms of a large-scale tropospheric adjustment to the lower stratospheric PV distribution. While this adjustment process occurs at every timestep of the model, it is rapidly converted into small scale differences to individual synoptic systems by the tropospheric flow. As these systems reach maturity in the tropospheric storm-track regions they impact strongly on the centres of action of the AO.

5.6 Summary of findings using PV inversion

In this chapter a new hemispheric PV inverter was used to investigate the mechanism for the impact of the stratosphere on the troposphere seen in the numerical modelling experiments of chapter 4. Its hemispheric formulation is ideally suited to studies of the impact of the stratosphere on the troposphere, as this problem is of hemispheric extent. The hypothesis that the impact of the stratosphere on the troposphere is through a large-scale geostrophic and hydrostatic adjustment of the tropospheric flow to the lower stratospheric PV distribution is tested.

The first set of experiments outlined in this chapter used an idealised distribution of PV to investigate the impact of a simple, wavenumber one perturbation to the stratospheric PV distribution on a simplified tropospheric flow. The main conclusions were

- The tropospheric flow adjusts in response to changes to the stratospheric PV distribution.
- The structure of the tropospheric adjustment is strongly related to the structure of the stratospheric perturbation. A wavenumber one perturbation in the stratosphere will have a wavenumber one response in the troposphere.
- The typical size of changes to the tropospheric flow is up to 10hPa in the surface pressure. The change to the position of the tropopause is of the order of 250m.
- For a tilted stratospheric perturbation, the change to the tropospheric flow resembles changes to the lower stratospheric PV distribution.

The second set of experiments examined the differences to the tropospheric flow related to stratospheric PV anomalies in the model run. The main conclusions of this part of the chapter answer the questions posed in the section 5.1:

- Differences to the tropospheric flow in the ensemble experiments of chapter 4 cannot be completely explained by a balanced, hydrostatic and geostrophic adjustment of the tropospheric flow to the stratospheric PV distribution. The orientation of patterns of the tropospheric adjustment is along the 90 °W - 90 °E line and is related to the PV distribution in the lower stratosphere. Differences in the ensemble experiments are concentrated in the storm-track regions.
- The adjustment of the tropospheric flow in response to the stratospheric PV distribution is dominated by PV anomalies in the lower stratosphere.
- The adjustment of the tropospheric flow in response to the stratospheric PV distribution has only a weak dependence on the tropospheric flow in the location that the adjustment occurs.
- The structure of the instantaneous adjustment of the tropospheric flow to the stratospheric PV distribution is similar over the first ten days of the model run. This is related to the

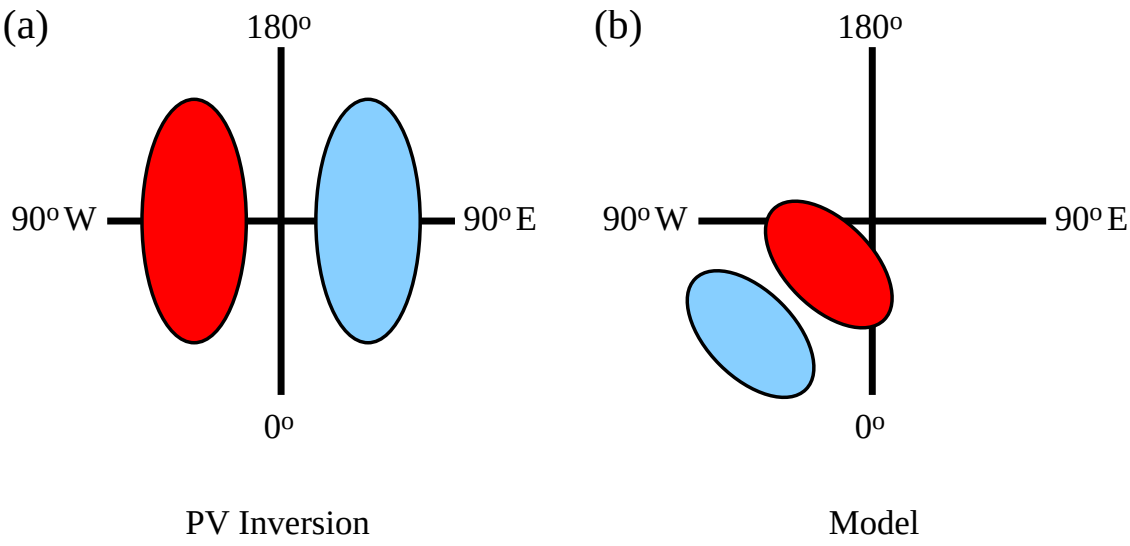

Figure 5.20: *Schematic showing the position of geopotential height differences between the nature and non-nature ensembles (a) as a result of the instantaneous adjustment of the troposphere to stratospheric PV anomalies (b) as a result of the evolution of the nature and non-nature ensembles in the numerical model. Red colours indicate an increase in geopotential height, blue colours indicate a decrease in geopotential height.*

long memory of the stratospheric flow which changes little over the ten days of the model integration examined here.

5.6.1 Problems with the large-scale adjustment hypothesis

The PV inversion experiments in this chapter identified the structure of the large-scale geostrophic and hydrostatic adjustment of the tropospheric flow to the stratospheric PV distribution. The spatial structure of this adjustment is different to the spatial structure of mean differences to the flow between the nature and non-nature ensembles in the model run.

The geostrophic and hydrostatic tropospheric adjustment to has a large scale, wavenumber one type structure. The location of these structures is shown schematically in Fig. 5.20

The instantaneous adjustment of the troposphere to the warming structure in the nature ensemble is a wave one structure with the largest increases in geopotential height over north America and a decrease in geopotential height over central Eurasia. In the numerical model the strongest signa-

ture in the tropospheric geopotential height response is a smaller scale change to the geopotential height over the Atlantic storm-track region. The aggregated impact of changes to individual synoptic scale features occurs over the storm track regions of the northern hemisphere, which correspond to centres of action of the tropospheric AO. Differences to the geopotential height distribution in these regions result in a strong signature in the AO index.

This result suggests that the interaction of the stratosphere and troposphere is a much more complicated process than a simple geostrophic and hydrostatic adjustment of the tropospheric flow to the lower stratospheric PV distribution.

5.7 Mechanism

We conclude by proposing a mechanism for the impact of the stratosphere on the troposphere, manifested for example by the apparent progression of AO index anomalies as depicted in Fig. 1.1. The mechanism is derived by considering the combined conclusions of the three studies presented in chapters 2, 4 and 5. The mechanism *does not* assume that the stratosphere is an autonomous system "forcing" the troposphere. It is well known that the stratospheric state is strongly influenced by that of the troposphere (Matsuno, 1971).

- Large-Scale anomalies in the climatological Potential Vorticity distribution in the stratosphere, the formation of which is strongly related to the underlying tropospheric circulation, occur through a large depth of the stratosphere. During sudden warmings, the anomalies may appear to descend from the upper stratosphere to the lower stratosphere. Mechanisms for this descent have been proposed by Matsuno (1971) in terms of downward propagating zero wind lines and by O'Neill and Pope (1988) in terms of "downward burrowing" of potential vorticity anomalies.

- In the lower stratosphere the signature of a stratospheric sudden warming in the PV distribution is a reduction in PV over the polar cap (north of 60N) and a corresponding (though not zonally symmetric) increase in PV in mid-latitudes (in the converse case the opposite applies).

- PV anomalies in the lower stratosphere tend to persist for 10 or more days. The impact of these large-scale PV anomalies in the lower stratosphere appear not as large-scale anomalies in the troposphere but as changes to synoptic-scale tropospheric systems generated through baroclinic instability.

- Synoptic-scale systems are closely associated with the storm tracks over the North-Atlantic and North-Pacific. By averaging in time or over a number of realisations (eg a large forecast ensemble) larger-scale geopotential height anomalies emerge. Reproducible structures emerge over the North-Atlantic sector but not over the North Pacific sector (at least for the three case studies described in this thesis).

The precise way in which PV anomalies affect synoptic-scale systems e.g. strength, tracking, lifetime has yet to be determined. Considerable further research is required to investigate this aspect. The above mechanism proposes that large-scale anomalies in the stratosphere project strongly onto the North-Atlantic Oscillation (NAO) pattern in the North Atlantic and consequently onto the AO pattern depicted in Fig. 1.1. That the tropospheric response to stratospheric PV anomalies is more coherent over the North-Atlantic sector than the North-Pacific sector is related to the latitudinal location of storm-tracks in the North-Atlantic and North-Pacific and the displacement of the lower-stratospheric polar vortex toward Eurasia during stratospheric sudden warmings. Our mechanism proposes that the impact of the stratospheric state on the troposphere must be understood in terms of local dynamics, rather than purely in terms of coupled 'Annular Modes' of variability.

CHAPTER 6

Conclusions

6.1 Background

This thesis investigated the dynamical relationship between the stratosphere and troposphere. This issue has long been of interest to dynamical meteorologists. While it is well known that the troposphere, and in particular tropospheric planetary wave activity, plays a large role in the dynamical evolution of the stratosphere (Matsuno, 1971) the relationship between the state of the stratosphere and the future state of the troposphere is less certain.

Recently the relationship between the stratosphere and troposphere has been more prominent in the atmospheric science literature, in particular since the papers of Baldwin and Dunkerton (1999, 2001) and Thompson et al. (2002). These papers stimulated a large interest in the topic in the atmospheric science and wider science community (Baldwin et al., 2003b).

Much of the previous work in this area focussed on understanding the relationship between the stratosphere in long, re-analysis datasets. Knowledge of the relationship between the stratosphere and troposphere could be summarised as:

- Large-scale atmospheric variability in the stratosphere and troposphere can be characterised by the first empirical orthogonal function of geopotential height, the Arctic Oscillation (Thompson and Wallace, 1998)
- Large variations in the amplitude of stratospheric AO appear to proceed similar variations in the tropospheric AO (Baldwin and Dunkerton, 1999).
- Composite pictures of the tropospheric flow following large departures of the stratospheric AO (Baldwin and Dunkerton, 2001) or the polar night jet (Thompson et al., 2002) from its climatological state show a large change to a number of tropospheric parameters such as

mean air temperature and the position of the mean storm track as well as the tropospheric AO.

Recently, a number of modelling studies examined the mean response of the troposphere to a change to the stratospheric circulation. In particular the studies of Norton (2003) and Polvani and Kushner (2002) showed that making changes to the mean circulation of the stratosphere through changes to the Rayleigh friction parameterisation or the equilibrium temperature profile, results in large-scale changes to the tropospheric circulation.

6.2 Aims

Currently it is widely accepted that a relationship between the stratosphere and troposphere exists, but the mechanism for this influence is not well understood. The quantitative size of the influence of the stratosphere on the troposphere is also poorly understood. In this thesis we have used data analysis and numerical modelling techniques to attempt to understand the relationship between the stratosphere and troposphere. The following questions were posed in the introduction.

- Does the stratospheric state have an influence on the tropospheric flow ?
  - What is the quantitative size of this influence ?
  - By what dynamical mechanism does the influence occur ?
- Are medium, extended and long range[1] forecasts of the tropospheric state improved by considering the stratospheric state ?

The thesis focussed on understanding the relationship between the stratosphere and troposphere in terms of its potential benefit to tropospheric forecasting. Both the data analysis and numerical modelling parts of the thesis determine the potential quantitative benefit of stratospheric information to medium, extended and long range tropospheric forecasts. Previous studies were focussed

[1] In this context the standard forecast ranges are defined as, medium-range: 72-240 Hours, extended-range:10-30 days, long-range: greater than 30 days

on identifying a relationship between the stratosphere and troposphere and were less concerned with its ultimate practical application.

6.3 Statistical Modelling Experiments

Chapter 2 presented a study which attempted to further quantify the relationship between the stratosphere and troposphere using the same dataset as that used by Baldwin and Dunkerton (1999). The methodology used was to attempt to model the data using a simple statistical model. The model aims to predict the future state of the tropospheric AO and contains two predictors representing the current state of the stratospheric and tropospheric parts of the AO. The model is summarised in Eq. 2.1 and Fig. 2.1. Chapter 2 investigated the validity of this model and found that it was suitable to describe the AO dataset.

The primary conclusions of this chapter were:

- A small but statistically significant relationship between the stratosphere and troposphere exists in the AO dataset.
- The relationship typically explains $\sim 5\%$ of the variance of the 1000hPa AO timeseries.
- The relationship is most prominent on extended and long range timescales (10-45 days)
- The relationship is largest between the 1000hPa AO timeseries and the upper troposphere / lower stratosphere region (50-250hPa).
- The relationship is strongest in the winter season and particularly in February and March.
- The relationship has approximately similar magnitudes for each decade in the data set, although the autocorrelation of the tropospheric AO is extremely variable between different decades of the timeseries, much of this variability is related to changes to the tropospheric AO persistence.

The chapter succeeded in characterising the relationship between the stratosphere and troposphere as small, but statistically significant and refined the range of atmospheric levels, timescales and seasons on which the relationship between the stratosphere and troposphere was important.

The final section of chapter 2 evaluated the forecasting skill of the statistical model developed in this chapter. By splitting the dataset into two parts the forecasting skill of such a model could be evaluated. While the forecasting skill of such a model is small on extended range timescales ($< 5\%$ skill score), the inclusion of extra stratospheric information in the model increases the skill by up to 50% to $\sim 10\%$ skill.

This result suggests that the skill of tropospheric forecasts may be improved by the inclusion of stratospheric information . While the skill scores shown in chapter 2 are small they motivate further study of the relationship between the stratosphere and troposphere as of potential benefit to tropospheric forecasts. Chapters 3,4 and 5 examined three case studies of large amplitude changes to the stratospheric circulation to try and better understand the link between the stratosphere and troposphere. While this chapter showed that the relationship between the stratosphere and troposphere is statistically linear (cf Fig. 2.2) there was also substantial noise around the relationship. To determine a significant link between the stratosphere and troposphere above this noise case studies were chosen where there was a large departure of the stratospheric state from its climatological norm (this would be toward the ends of the ellipse in Fig. 2.2 (a)) to maximise the signal to noise ratio.

6.4 Numerical Modelling Experiments

Chapters 3 and 4 presented a numerical modelling study which investigated the impact of stratospheric initial conditions on the tropospheric forecast. This methodology is different to the recent studies of Norton (2003) and Polvani and Kushner (2002) who made permanent changes to the model dynamics of the stratosphere in their models. The approach used in this thesis was more suited to investigations of the impact of the stratosphere in a transient forecasting context and is similar to the study of Kodera et al. (2000).

In this study we used a state of the art numerical weather forecasting model, the ECMWF IFS model. This model is ideally suited to the study because it has high resolution in the horizontal and the vertical, a high top (0.1 hPa) and a large number of levels (25) in the stratosphere. The ECMWF model was used for the medium-range forecast experiments outlined in chapter 3 because it performed better in a test case than the UKMO HadAM3 model.

The model is used to investigate the relationship between the stratosphere and troposphere in three case studies. In each of the case studies two 20 day ensemble forecasts were run. The first, nature, ensemble forecast used observed atmospheric initial conditions. The second, non-nature, ensemble forecast used observed atmospheric initial conditions in the troposphere and different initial conditions in the stratosphere. The non-nature stratospheric initial conditions were taken from a separate atmospheric analysis in which the stratospheric AO had the opposite sign. Differences in the tropospheric evolution of the nature and non-nature ensembles are related to the stratospheric initial conditions.

The primary conclusions of the modelling study were:

- Stratospheric initial conditions have a statistically significant impact on the tropospheric evolution.
- Significant changes to the tropospheric AO occur between 10-20 days of the run.
- Changes to the AO index in the troposphere are positively correlated with the preceding changes in the AO index in the stratosphere.
- Changes to the tropospheric flow occur on synoptic scales and represent changes to the propagation or intensity of individual synoptic systems. The typical size of these differences is 100-200m.
- Averaging the differences to individual synoptic systems over the ensemble and over a number of timesteps shows the average impact of the change to the synoptic systems on the tropospheric flow. This impact is generally on larger spatial scales and is concentrated in the oceanic storm track regions. The typical size of ensemble mean differences to the geopotential height field is 20-40m.
- The averaged differences are consistent between the three cases in the Atlantic sector and not consistent (but of similar magnitude) in the three cases in the Pacific sector. Differences in the Atlantic sector map strongly onto the AO structure but do not represent a coherent change to the hemisphere scale variability.

These results have some bearing on the current debate in the literature about the physical relevance

of the Arctic Oscillation pattern (see Section 1.3.1.1). The results in this chapter suggest that within the context of the impact of the stratosphere on the troposphere, the paradigm of a coherent hemispheric mode of variability is not valid. While the aggregated tropospheric impact of the change to the stratospheric initial conditions maps strongly onto the AO structure it does not in itself represent a coherent hemispheric scale structure. In particular in the Pacific sector the impact on the tropospheric flow is very different in the three case studies and different to the impact in the Atlantic sector. The AO paradigm may be more useful in longer term climate impact studies where a number of such events are aggregated together.

6.5 Investigating the Mechanism

Results from the numerical modelling study showed that the tropospheric response to changes to the stratospheric initial conditions is dominated by synoptic scales. This result could be interpreted in two ways.

- The troposphere adjusts geostrophically and hydrostatically, on large spatial scales to the large-scale stratospheric PV distribution. Synoptic scales in the difference field are noise on this large-scale difference
- Individual tropospheric synoptic systems respond non-linearly to the stratospheric PV distribution. This small-scale adjustment is an important intermediate step between the large-scale lower stratospheric PV anomalies and the eventual time and ensemble averaged change to the tropospheric flow.

These two possibilities were investigated by running PV inversion experiments with PV distributions taken from the model conditions. The structure of the geostrophic and hydrostatic adjustment of the troposphere to the PV distribution was calculated with the inverter. The geostrophic and hydrostatic adjustment of the troposphere to the stratospheric PV had the following features.

- The adjustment has a large-scale, wavenumber one structure similar to the structure of anomalies in the PV distribution in the lower stratosphere. The adjustment occurs along an axis between 90 °W - 90 °E.

- The adjustment of the tropospheric flow to the PV distribution in the middle stratosphere is small. The structure of the tropospheric adjustment is barotropic with PV anomalies in the lower stratosphere (500K).
- The adjustment has only a weak dependence on the tropospheric flow in the location that the adjustment occurs.
- The adjustment is similar for a number of timeslices taken from the model run. This is related to the long memory of the lower stratospheric PV distribution. There is no indication that the structure of the adjustment is different at times of the model run when statistically significant changes to the AO index occur.

The model of the impact of the stratosphere on troposphere as a large-scale adjustment of the tropospheric flow to the stratospheric PV distribution did not explain the differences to the tropospheric flow observed in the model experiments. The structure of the large-scale adjustment is different to the averaged differences to the tropospheric flow in the model runs. The large-scale tropospheric adjustment occurs along an axis between 90 °W - 90 °E, differences to the tropospheric flow in the model occur over the storm-track regions. It was proposed that synoptic scale variability plays an important role in the communication of the stratospheric differences from the northern hemisphere land masses (where the adjustment of the troposphere to the stratospheric PV distribution occurs) to the ocean basin storm track regions (where the aggregated differences to the tropospheric flow are maximised).

The mismatch between the large-scale adjustment of the troposphere to the stratospheric PV distribution and the differences in the tropospheric flow in the model runs lead us to propose the following mechanism for the influence of the stratosphere on the troposphere.

- Long-lived, large-scale anomalies occur in the stratospheric PV distribution as a result of tropospheric influence.
- Tropospheric synoptic systems respond to changes to the stratospheric PV distribution.
- Differences to synoptic systems occur preferentially in some locations. Averaging differences to synoptic systems over a range of times or a large ensemble highlights the aggregated impact of changes to individual synoptic systems.

- The largest aggregated impacts of tropospheric synoptic scale systems occur over the North Atlantic and North Pacific storm-track regions.
- There is a consistent aggregated impact of tropospheric synoptic scale systems in the North Atlantic sector which maps strongly onto the NAO structure and hence onto the AO structure.

6.6 Answers to questions posed in the introduction

Three questions were posed in the introduction of the thesis as the aims of the project. The answers to these questions are:

- Both the data analysis and modelling studies have demonstrated that the stratospheric state has an influence on the troposphere. This influence is a causal link as demonstrated by the modelling study.
  - The quantitative size of the influence of the stratospheric state on the troposphere is small. In the statistical model the lower stratospheric AO could only explain $\sim 5\%$ of the variance of the tropospheric AO timeseries. In terms of differences to individual synoptic features in the troposphere changes of $\sim 100 - 200m$ in geopotential height in individual ensemble members were present in the modelling study. This is roughly a $2 - 4\%$ change to the 1000hPa geopotential height for a change to the middle stratospheric height distribution $\sim 500 - 750m$.
  - By combining the results of the modelling experiments and some simple PV inversion experiments a mechanism for the influence of the stratosphere on the troposphere was proposed (summarised in the previous section). This mechanism involves a relationship between the lower stratospheric PV distribution and the local synoptic scale systems in the troposphere. A significant signal in the AO index is seen due to a consistent aggregated impact of differences to tropospheric synoptic systems in the North Atlantic.
- Both the data analysis and modelling chapters examined the influence on the forecasting skill of the stratospheric state. In the statistical model a gain of skill of $\sim 5\%$ on 10-45 day

timescales was achieved when stratospheric information was included in a simple statistical forecasting model. Examples of this gain in skill was also seen in the numerical modelling experiments. The anomaly correlation of both the 500hPa and 1000hPa geopotential height fields in the numerical model is increased by up to 50 % on extended range (12-20 day) timescales when the model is initialised with analysed stratospheric initial conditions.

6.7 Future Work

The mechanism proposed above requires several further experiments to fully understand the way in which the stratosphere and troposphere interact.

- **How are tropospheric synoptic systems influenced by the stratospheric PV distribution?**

  The objective storm tracking procedure described in Hoskins and Hodges (2002) can be used to analyse the trajectory and intensity of individual tropospheric synoptic systems. The track and intensity information generated by this procedure could be used to investigate the relationship between the stratospheric PV and tropospheric systems in the following ways.

  1. Statistical analysis of the relationship between the amount, intensity and propagation direction of synoptic systems and the stratospheric PV in long reanalysis datasets.
  2. Comparison of the evolution of stratospheric features in the nature and non-nature ensembles in each case study. This is a more direct investigation of the relation between tropospheric features and the stratospheric PV distribution.

- **Is the impact of the stratosphere on the troposphere similar in other, dynamically different, cases ?**

  There is also a wide scope for more experiments with a GCM similar to those described in the thesis. Running more case studies would help to further characterise the relationship between the stratosphere and troposphere. These cases might include the southern hemisphere where the stratospheric variability is very different to the northern hemisphere due to the smaller planetary wave activity. The current interest which surrounds the unprecedented southern hemisphere sudden warming in September 2002 would make it an

excellent first study. The comparison between this case study and the warming cases in the northern hemisphere would provide a good test of the mechanism proposed in this thesis.

It would also be of benefit to examine the relationship between the stratosphere and troposphere in Antarctic Oscillation Index diagnostics. A relationship between the stratosphere and troposphere in the Southern Hemisphere has recently been suggested by the papers of Gillett and Thompson (2003) and Thompson and Solomon (2002)

The methodology developed in this thesis has provided a way of further investigating the impact of the stratosphere on the troposphere in a more comprehensive study.

APPENDIX A

Mass Conservation in PV inversion

The formulation of the PV inverter in chapter 5 does not conserve mass in the following sense. One could imagine taking a particular PV distribution and rearranging the PV contours in an adiabatic sense so that the total amount of PV was preserved. If these two distributions were inverted it might be expected that the total mass in the two inversions would be constant, however in the inverter used here this would not necessarily be the case.

This appendix shows why the inverter used in chapter 5 does not have this property and makes a comparison with a much simpler inversion equation. There is no explicit constraint of total mass within PV inversion but the inversion procedure can be constructed to include such a constraint. It is easiest to see this within the equations described by Kleinschmidt and reprised by Hoskins et al. (1985)

Derivation of a simple PV inversion equation following Kleinschmidt is shown in Hoskins et al. (1985) (p900). They assume a circularly symmetric PV anomaly on some of the isentropic surfaces in the atmosphere. The balance condition is described by gradient wind and hydrostatic balance.

The PV inversion equation is:

$$\frac{\partial}{\partial r}\left[\frac{1}{r}\frac{\partial(rv)}{\partial r}\right] + g^{-1}P\frac{\partial}{\partial\theta}\left(\frac{f_{loc}}{R}\frac{\partial v}{\partial\theta}\right) = \sigma\frac{\partial P}{\partial r} \tag{A.1}$$

where:

v - is the radial velocity

r - is the distance from the centre of the anomaly

P - is the PV

θ - is potential temperature

This equation has three unknowns, P,v and σ. In order to determine the distribution of velocity the distribution of both P and σ are required. PV inversion attempts to determine the distribution of both flow and mass when only the PV is know. This means that solving Eq. A.1 requires an iterative procedure because of its two unknowns .The problem can be solved using an initial guess of the isentropic mass density σ (providing appropriate boundary conditions are known). After the velocity field has been determined by inverting Eq. A.1 a new isentropic mass density field can be determined by consideration of the balance condition. Comparison of the balanced mass distribution and the initial guess shows when the solution has converged. It is possible to include various constraints to the way in which the mass distribution is rearranged. In Hoskins et al. (1985) an explicit constraint on the mass is included in the formulation of the inversion:

$$\int\int \frac{\partial p(x,y,\theta)}{\partial \theta} dxdy = \frac{dp_{ref}(\theta)}{d\theta} \int\int dxdy \tag{A.2}$$

This condition states that the pressure distribution obtained from the inversion ($p(x,y,\theta)$) should be obtained by an adiabatic rearrangement of a pre-defined reference pressure distribution ($p_{ref}(\theta)$) which is only a function of potential temperature. It should be recognised, however that this condition is an additional constraint on the PV inversion and need not be required to solve equation 5.10.

By assuming the constraint of equation A.2 Hoskins et al. (1985) show that this implies knowledge of the mass lying between isentropic surface, which leads to a relationship between the distribution of PV anomalies ($P' = P(x,y,\theta) - P_{ref}(\theta)$) and the relative circulation around the boundary of the domain ($C_b\theta$).

$$-\int\int g^{-1}(\frac{\partial p}{\partial \theta})P'dxdy = C_b(\theta) \tag{A.3}$$

Because this relationship exists one could imagine an alternative constraint for the inversion which prescribed the relative circulation at the boundary of the domain along with the PV distribution. In this case the mass distribution would be determined by Eq. A.3 and would not necessarily be related to an assumed reference mass distribution. If one attempted to prescribe both the circulation and mass fields then the problem would become over-prescribed.

In the simple problem described above it is clear that solving a PV inversion requires an iterative procedure to produce both a mass and flow field from knowledge of the PV alone. In the PV inversion equation used in the inverter of chapter 5 this is not so clear. The inversion equation is:

$$P\,\frac{p_0}{2\Omega\sin\phi Rg}\left(\frac{\partial M/\partial\theta}{C_p}\right)^{(C_v/R)}\frac{\partial^2 M}{\partial\theta^2} + \frac{1}{\Omega^2 a^2}\left(\frac{1}{\sin^2 2\phi}\frac{\partial^2 M}{\partial\lambda^2} + \frac{1}{2\sin 2\phi}\frac{\partial}{\partial\phi}\left(\frac{cos\phi}{\sin\phi}\frac{\partial M}{\partial\phi}\right)\right) = -1 + R_d \tag{A.4}$$

For ease of computation the inversion equation is written in terms of Montgomery Streamfunction, M. In Eq. A.4 this means that the inversion equation has only two unknowns P and M. However, to solve this equation an iterative procedure similar to the one described for the Kleinschmidt problem above is required. An initial guess of M is needed for the inversion to be solved. The formulation of the inverter using M makes it more difficult to see that the inversion procedure has to solve for both mass and velocity. However, because Montgomery Streamfunction represents neither the mass or velocity fields further calculations (namely hydrostatic and geostrophic balance in this case) are required to extract the mass and flow fields from the final M distribution.

The inverter is formulated in this way because it simplifies many of the procedures required to solve the inversion equation over the hemisphere and in three dimensions. This means, however that an additional constraint on either the mass or the flow field (similar to that of Eq. A.2 in the Kleinschmidt example) cannot be included in this inverter. It would only be possible to constrain the rearrangement of M in this case and this would constrain neither the flow or mass fields.

The inverter used in the experiments of chapter 5 is formulated in such a way that it does not explicitly preserve the total mass field. Our interest in performing these experiments is to examine

the longitudinal structure of the adjustment of the tropospheric response to the stratospheric PV distribution. The quantitative size of this adjustment is of lesser importance. The conclusions of chapter 5 are not affected by the non-conservation of mass of the inverter.

Bibliography

M H P Ambaum and B J Hoskins. The NAO troposphere-stratosphere connection. *J. Clim.*, 15: 1958–1969, 2002.

M H P Ambaum, B J Hoskins, and D B Stephenson. Arctic Oscillation or North Atlantic Oscillation. *J. Clim.*, 14:3495–3507, 2001.

D G Andrews, J R Holton, and C B Leovy. *Middle Atmosphere Dynamics*. Academic, 1987.

A Arakawa and V R Lamb. Computational Design of the Basic Dynamical Processes of the UCLA General Circulation Model. *Methods in Computational Physics*, 17:174–267, 1977.

J Austin. A Three-Dimensional Coupled Chemistry-Climate Model Simulation of Past Stratospheric Trends. *J. Atmos. Sci.*, 59:218–232, 2002.

J Austin and N Butchart. The influence of climate-change and the timing of stratospheric warmings on arctic ozone depletion. *J. Geophys. Res.*, 99:1127–1145, 1994.

M P Baldwin, X Cheng, and T J Dunkerton. Observed correlations between winter-mean tropospheric and stratospheric circulation anomalies. *Geophysical Research Letters*, 21:1141–1144, 1994.

M P Baldwin and T J Dunkerton. Propogation of the Arctic Oscillation from the stratosphere to the troposphere. *J. Geophys. Res.*, 104:30,937–30,946, 1999.

M P Baldwin and T J Dunkerton. Stratospheric Harbingers of Anomalous Weather Regimes. *Science*, 294:581–584, 2001.

M P Baldwin, D B Stephenson, D W J Thompson, T J Dunkerton, A J Charlton, and A O'Neill.

Stratospheric Memory and Skill of Extended-Range Weather Forecasts. *Science*, 301:636–640, 2003a.

M P Baldwin, D W J Thompson, E F Shuckburgh, W A Norton, and N P Gillett. Weather from the Stratosphere ? *Science*, 301:317–319, 2003b.

R X Black. Stratospheric forcing of Surface Climate in the Arctic Oscillation. *J. Clim.*, 15: 268–277, 2002.

R Bleck. Numerical forecasting experiments based on the conservation of potential vorticity on isentropic surfaces. *J. Appl. Met.*, 12:737–752, 1973.

B A Boville. The Influence of the Polar Night Jet on the Tropospheric circulation in a GCM. *J. Atmos. Sci.*, 41:1132–1142, 1984.

B A Boville and D P Baumhefner. Simulated Forecast Error and Climate Drift Resulting from the Omission of the Upper Stratosphere in Numerical Models. *Mon. Wea. Rev.*, 118:1517–1530, 1990.

B A Boville and X Cheng. Upper boundary effects in a General Circulation Model. *J. Atmos. Sci.*, 45:2591–2605, 1988.

G Branstator. Circumglobal Teleconnections, the Jet Stream Waveguide, and the North Atlantic Oscillation. *J.Clim*, 15:1893–1910, 2002.

R Buizza, T Petroliagis, T Palmer, J Barkmeijer, M Hamrud, A Hollingsworth, A Simmons, and N Wedi. Impact of model resolution and ensemble size on the performance of an Ensemble Prediction System. *Q. J. Roy. Met. Soc.*, 124:1935–1960, 1998.

R Buizza, D S Richardson, and T N Palmer. Benefits of increased resolution in the ECMWF ensemble system and comparison with poor-man's ensembles. *Q. J. Roy. Met. Soc.*, 129:1269–1288, 2003.

N Butchart and E E Remsberg. Area of the stratospheric polar vortex as a diagnostic for tracer transport on an isentropic surface. *J. Atmos. Sci.*, 43:1319–1339, 1986.

B A Cash, P J Kushner, and G K Vallis. The Structure and Composition of Annular Modes in an Aquaplanet General Circulation Model. *J. Atmos. Sci.*, 59:3399–3414, 2003.

J M Chambers, W S Cleveland, B Kleimer, and P A Tukey. *Graphical Methods for Data Analysis*. Wadsworth, Belmont, California, 1983.

A J Charlton, A O'Neill, D B Stephenson, W A Lahoz, and M P Baldwin. Can knowledge of the state of the stratosphere be used to improve statistical forecasts of the troposphere? *Q. J. Roy. Met. Soc.*, 595:3205–3225, 2003.

C Chatfield. *The analysis of Time Series*. Chapman and Hall, London, 1996.

B Christiansen. A model study of the dynamical connection between the Arctic Oscillation and stratospheric vacillations. *J. Geophys. Res.*, 105(D24):29,461–29,474, 2000.

M J P Cullen. The unified forecasting/climate model. *Meteor. Mag.*, 122:81–94, 1993.

R Daley. *Atmospheric Data Analysis*. Cambridge University Press, 1991.

C Deser. On the teleconnectivity of the Arctic Oscillation. *Geophysical Research Letters*, 27(6): 779–782, 2000.

S J Eichelberger and J R Holton. A mechanistic model of the northern annular mode. *J. Geophys. Res.*, 107, 2002. doi:10.1029/2001JD001092.

A Eliassen and E Palm. On the transfer of energy in stationary mountain waves. *Geofys. Publikasjoner*, 12:1–23, 1961.

J K Gibson, P K Kalberg, S Uppala, A Noumara, A Hernadez, and E Serrano. ERA Description. Re-Analysis Project Report Series 1, ECMWF, Reading, UK, 1997.

N P Gillett, M R Allen, and K D Williams. The role of the stratospheric resolutionin simulating the Arctic Oscillation response to greenhouse gases. *Geophysical Research Letters*, 29, 2002. doi:10.1029/2001GL014444.

N P Gillett, M R Allen, and K D Williams. Modelling the atmospheric response to doubled CO_2 and depleted ozone using stratosphere-resolving coupled models. *Q. J. Roy. Met. Soc.*, 29: 947–966, 2003.

N P Gillett, M P Baldwin, and M R Allen. Evidence for nonlinearity in observed stratospheric circulation changes. *J. Geophys. Res.*, 106:7891–7902, 2001.

N P Gillett and D W J Thompson. Simulation of recent Southern Hemisphere Climate Change. *Science*, 302:273–275, 2003.

K Hamilton. The GFDL SKYHI general circulation model: some results of relevance for numerical weather prediction. In *Stratosphere and Numerical Weather Prediction*. ECMWF Workshop Proceedings, 1993.

D E Hartley, J T Villarin, R X Black, and C A Davis. A new perspective on the dynamical link between the stratosphere and troposphere. *Nature*, 391:471–473, 1998.

D L Hartmann, J M Wallace, V Limpasuvan, D W J Thompson, and J R Holton. Can ozone depletion and global warming interact to produce rapid climate change ? *Proc. Nat. Acad. Sci.*, 97:1412–1417, 2000.

Y Hayashi. Space-Time Spectral Analysis and its Applications to Atmospheric Waves. *J. Met. Soc. Japan*, 60:156–171, 1982.

P H Haynes, C J Marks, M E McIntyre, T G Shepherd, and K P Shine. On the "Downward Control" of Extratropical Diabatic Circulation by Eddy-Induced Mean Zonal Forces. *J. Atmos. Sci.*, 48:651–678, 1991.

E J Highwood, B J Hoskins, and P Berrisford. Properties of the Arctic tropopause. *Q. J. Roy. Met. Soc.*, 126:1515–1532, 2000.

J R Holton. *An Introduction to Dynamic Meteorology*. Academic Press, 1992.

J R Holton and C Mass. Stratospheric Vacillation Cycles. *J. Atmos. Sci.*, 33:2218–2225, 1976.

M Hortal and A J Simmons. Use of reduced Gaussian grids in spectral models. *Mon. Weather Rev.*, 119:1057–1074, 1991.

B J Hoskins. Towards a PV-Theta view of the general circulation. *Tellus*, 43:27–35, 1991.

B J Hoskins and K I Hodges. New Prespectives on the Northern Hemisphere Winter Storm Tracks. *J. Atmos. Sci.*, 59:1041–1061, 2002.

B J Hoskins, M E McIntyre, and A W Robertson. On the use and significance of isentropic potential vorticity maps. *Q. J. Roy. Met. Soc.*, 111:877–946, 1985.

I T Jolliffe and D B Stephenson, editors. *Forecast Verification: A Practioner's Guide in Atmospheric Science*. Wiley and Sons, 2003.

I T Kindem and B Christiansen. Tropospheric Response to Stratospheric Ozone Loss. *Geophysical Research Letters*, 28:1547–1550, 2001.

K Kodera and M Chiba. Tropospheric circulation changes associated with stratospheric sudden warmings : A case study. *J. Geophys. Res.*, 100:11,055–11,068, 1995.

K Kodera, M Chiba, K Yamazaki, and K Shibata. A possible influence of the polar night stratospheric jet on the subtropical tropospheric jet. *Journal of the Meteorological Society of Japan*, 69:715–720, 1991.

K Kodera and Y Kuroda. A mechanistic model study of slowly propogating coupled stratosphere-troposphere variability. *J. Geophys. Res.*, 105:12,361–12,370, 2000.

K Kodera, Y Kuroda, and S Pawson. Stratospheric sudden warmings and slowly propogating zonal-mean zonal-wind anomolies. *J. Geophys. Res.*, 105:12,351–12,359, 2000.

K Kodera, K Yamazaki, M Chiba, and K Shibata. Downward propogation of upper stratospheric mean zonal wind pertubation to the troposphere. *Geophysical Research Letters*, 17:1263–1266, 1990.

K Labitzke. On the Mutual Relation between Stratosphere and Troposphere during periods of Stratospheric Warmings in Winter. *J. Atmos. Sci.*, 4:91–99, 1965.

W A Lahoz. Northern Hemisphere stratospheric variability in the Met. Office Unified Model. *Q. J. Roy. Met. Soc.*, 126:2605–2630, 2000.

T Matsuno. A dynamical model of stratospheric warmings. *J. Atmos. Sci.*, 28:1479–1494, 1971.

M E McIntyre and T N Palmer. The "Surf Zone" in the stratosphere. *J. Atmos. Terr. Physics*, 46: 825–849, 1984.

S Miyahara, Y Hayashi, and J D Mahlman. Interaction between Gravity Waves and Planetary Scale Flow simulated by the GFDL "SKYHI" General Circulation Model. *J. Atmos. Sci.*, 43: 1844–1861, 1986.

F Molteni, R Buizza, T N Palmer, and T Petroliagis. The ECMWF Ensemble Prediction System: Methodology and Validation. *Q. J. Roy. Met. Soc.*, 122:73–119, 1996.

W A Norton. Sensitivity of Northern Hemisphere surface climate to simulation of the stratospheric polar vortex. *Geophysical Research Letters*, 30:1627, 2003. doi:10.1029/2003GL016958.

A O'Neill. *The Stratosphere and its role in the Climate System*, chapter Observations of Dynamical Processes, pages 59–82. Springer-Verlag, 1995.

A O'Neill. Stratospheric Sudden Warmings. In J R Holton, John A Pyle, and J A Curry, editors, *Encyclopedia of Atmospheric Sciences*. Elsevier, 2003.

T N Palmer and D T Anderson. The prospects for seasonal forecasting - A review paper. *Q. J. Roy. Met. Soc.*, 120:755–793, 1994.

J Perlwitz and H F Graf. The Statistical connection between Tropospheric and Stratospheric Circulation of the Northern Hemisphere in Winter. *J. Clim.*, 8:2281–2295, 1995.

J Perlwitz and N Harnik. Observational Evidence of a Stratospheric Influence on the Troposphere by Planetary Wave Reflection. *J. Clim.*, in press, 2003.

R A Plumb. The interaction of two internal gravity waves with the mean flow; implications for the theory of the quasi-biennial oscillation. *J. Atmos. Sci.*, 34:1847–1858, 1977.

R A Plumb and K Semeniuk. Downward migration of extratropical zonal wind anomalies. *J. Geophys. Res.*, 108:4223, 2002. doi:2002JD002773.

L M Polvani and P J Kushner. Tropospheric response to stratospheric perturbations in a relatively simple general circulation model. *Geophysical Research Letters*, 29:14284–14287, 2002.

R S Quiroz. The association of stratospheric warmings with tropospheric blocking. *J. Geophys. Res.*, 91:5277–5285, 1986.

M L Salby. *Fundamentals of Atmospheric Physics*. Academic Press, 1996.

A A Scaife and I N James. Response of the stratosphere to interannual variability of tropospheric planetary waves. *Q. J. Roy. Met. Soc.*, 126:275–297, 2000.

R Scherhag. Die explosionsartigen Stratosphärenerwärmungen des Spätwinters 1951-52. *Ber. deut. Wetterd (US Zone)*, 6:51–63, 1952.

D T Shindell, R L Miller, G A Schmidt, and L Pandolfo. Simulation of recent northern winter climate trends by greenhouse-gas forcing. *Nature*, 399:452–455, 1999.

K P Shine, M S Bourqui, P M de Forster, S H E Hare, U Langematz, P Braesicke, V Grewe, M Ponater, C Schnadt, C A Smith, J D Haigh, J Austin, N Butchart, D T Shindell, W J Randel, T Nagashima, R W Portmann, S Solomon, D J Seidel, J Lanzante, S Klein, V Ramaswamy, and M D Schwarzkopf. A comparison of model-simulated trends in stratospheric temperatures. *Q. J. Roy. Met. Soc.*, 129:1565–1588, 2003.

A J Simmons, D M Burridge, M Jarraud, C Girard, and W Wergen. The ECMWF medium-range prediction models: development of the numerical formulations and the impact of increased resolution. *Meteorol. Atmos. Phys.*, 40:28–60, 1989.

A J Simmons and D S Burridge. An energy and angular momentum conserving vertical finite difference scheme and hybrid vertical coordinates. *Mon. Weather Rev.*, 109:758–766, 1981.

M Taguchi, T Yamaga, and S Yoden. Internal Variability of the Troposphere-Stratosphere Coupled System Simulated in a Simple Global Circulation Model. *J. Atmos. Sci.*, 58:3184–3203, 2001.

M Taguchi and S Yoden. A Parameter sweep experiment on the Annular Variability with a simple Global Circulation Model. *J. Met. Soc. Japan*, 80:1077–1088, 2002.

C Temperton. Implicit Normal Mode Initialization. *Monthly Weather Review*, 116:1013–1031, 1988.

D W J Thompson, M P Baldwin, and J M Wallace. Stratospheric connection to Northern Hemisphere wintertime weather: implications for prediction. *J. Clim.*, 15:1421–1428, 2002.

D W J Thompson and S Solomon. Interpretation of Recent Southern Hemipshere Climate Change. *Science*, 296:895–899, 2002.

D W J Thompson and J M Wallace. The Arctic Oscillation signature in the wintertime geopotential height and temperature fields. *Geophysical Research Letters*, 25:1297–1300, 1998.

D W J Thompson and J M Wallace. Annular modes in the extratropical circulation. Part I: Month-to-month variability. *Journal of Climate*, 13:1000–1018, 2000a.

D W J Thompson and J M Wallace. Regional Climate Impacts of the Northern Hemisphere Annular Mode. *Science*, 293:85–88, 2001.

D W J Thompson, J M Wallace, and G C Hegerl. Annular modes in the extratropical circulation. Part II: Trends. *Journal of Climate*, 13:1000–1036, 2000b.

J E Walsh, W L Chapman, and T L Shy. Recent decrease of Sea Level Pressure in the Central Arctic. *J. Clim*, 9:480–486, 1996.

D. S. Wilks. *Statistical Methods in the Atmospheric Sciences*. Academic Press, 1995.

S Zhou, A J Miller, J Wang, and J K Angell. Downward-Propagating Temperature anomalies in the Preconditioned Polar Stratosphere. *J.Clim*, 28:4107–4110, 2002.